Alma Mater Studiorum – Università di Bologna

DOTTORATO DI RICERCA IN

Scienze Chimiche

Ciclo XXVII

Settore Concorsuale di afferenza: 03/B1

Settore Scientifico disciplinare: CHIM/03

Development of synthetic methods of silicon nanocrystals functionalized with photoactive molecules

Presentata da: Mirko Locritani

Coordinatore Dottorato

Prof. Aldo Roda

Relatore

Prof. Paola Ceroni

Esame finale anno 2015

Contents

Part III

Chapter 3 Techniques for the characterization of silicon nanocrystals

3.1 Introduction

3.2 X-ray diffraction (XRD)

3.3 ATR-FTIR spectroscopy

3.4 X-ray photoelectronspectroscopy (XPS)

3.5 Nuclear magnetic resonance analysis (NMR)

3.6 Trasmission electron microscopy (TEM)

3.7 Photophysical Techniques

Part IV

Chapter 4 Silicon nanocrystals functionalized with pyrene units: efficient light-harvesting antennae with bright near-infrared emission

4.1 Introduction

4.2 Synthesis of oxide-embedded silicon nanocrystals of different sizes

4.3 Liberation of hydride-terminated-SiNCs from silica matrix

4.4 Covalent functionalization of SiNCs with pyrene units

4.5 Results and discussion

4.6 Conclusion

Part V

Chapter 5 Interaction between pyrene-functionalized Silicon nanocrystals and carbon allotropes

5.1 Introduction

5.2 Thermal hydrosililation of SiNCs with 1-(allyloxymethyl)pyrene (C_3) and 1-((undec-10-en-1-yloxy)methyl)pyrene (C_{11})

5.2.1 Experimental details

5.3 Material characterization

Preface

The object of this thesis is the development of a synthetic method for the synthesis of silicon nanocrystals and covalent functionalization with chromophores. Part of the work concerns the photophysical and photochemical investigation of semiconductor nanocrystals.

The thesis is divided in different parts.

Chapter 1 introduces the basic properties of semiconductors and the effect of quantum confinement effect on optical properties reducing the size of semiconductors.

Chapter 2 describes different synthetic methods for the synthesis of silicon nanocrystals available in literature.

Chapter 3 illustrates techniques used to characterize and investigate the systems reported in this thesis.

Chapter 4 focuses on the synthetic method for the synthesis of silicon nanocrystals developed in University of Texas at Austin in collaboration with Professor Brian A. Korgel.

In Chapter 5 is reported the interaction of functionalized silicon nanocrystal with carbon allotropes.

Chapter 6 concerns the interaction of silicon nanocrystals with zinc porphyrin.

Chapter 7 describes the functionalization of silicon nanocrystals with thiadiazole.

The research project was financed by European Research Council by ERC Starting Grant: PhotoSi and University of Bologna.

ALMA MATER STUDIORUM
UNIVERSITÀ DI BOLOGNA

European Research Council
Established by the European Commission
Supporting top researchers from anywhere in the world

List of abbreviations

CVD: chemical vapor deposition
CB: conduction band
cSi: crystalline silicon
d: diameter
FS-nc-Si: free standing nanocrystalline silicon
FWHM: full width half maximum
HPLC: high performance liquid chromatography
HR-TEM: high resolution trasmission electron microscopy
HSQ: hydrogen silsesquioxane
porSi: porous silicon
PL: photoluminescence
QD: quantum dots
QY: quantum yield
SAED: selection area electron diffraction
Si: silicon
SiNCs: silicon nanocrystals
SiQDs: silicon quantum dots
SWCNT: single wall carbon nanotube
τ: lifetime
TEM: trasmission electron microscopy
VB: valence band
XRD: x-ray diffraction

Chapter 1 Introduction

1.1 Silicon

Silicon (Si) is a chemical element with atomic number 14 present in the IVA group of the periodic table, along the bold line that separates metals from non-metals (Figure 1.1). It belongs to the p-block with configuration ($1s^2 2s^2 2p^6 3s^2 3p^2$), can donates or shares four valence electrons to form bonds like carbon and manifests sp^3-hybridization.

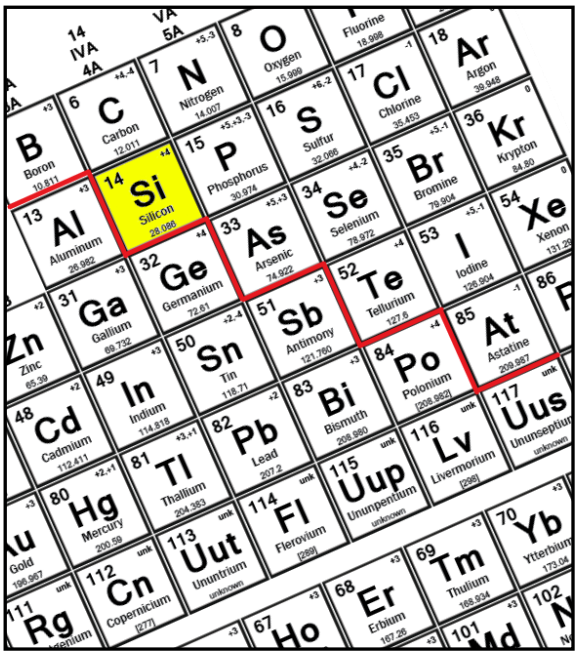

Figure 1.1

It was discovered by Antoine Lavoisier[1] in 1787 but the present name was coined by Thomas Thomson[2], he believed that silicon was a nonmetal similar to boron and carbon.

After the oxygen, silicon is the most abundant element in the Earth's crust, it is widely distributed in dusts, sands and planets as various forms of silicon dioxide (silica) or silicates.

It is the raw material to produce glass, cement, ceramics and synthetic polymers as silicones.

---

[1] Lavoisier, Traité Élémentaire de Chimie, (Paris, France: Cuchet, **1789**), vol. 1, page 17.

[2] Thomas Thomson, A System of Chemistry in Four Volumes, 5th ed., **1817**, vol. 1.

Silicon has a big impact on the modern world economy for its properties as semiconductor in fact it is at the basis of the microelectronic industry that requires a high degree of purity.

Silicon is a classic example of indirect semiconductor with band gap of 1.12 eV at room temperature.

At present, single-crystal silicon (mc-Si) is the main material of microelectronic technology, is used to produce a variety of semiconductor devices from diodes and transistors to extremely complex integrated circuits and processors.

In addition, the high photosensitivity of silicon (the change of electrical conductivity under illumination) is widely used, which allows one to convert light energy into electrical energy. This effect is used in silicon solar cells and photodetectors.

However, the reverse process, for instance efficient conversion of electrical energy into visible light in silicon devices has so far failed. This is connected with the peculiarities of the electronic properties of silicon.

1.2 Semiconductors from point of view of band theory

From to the study of Ashcroft and Mermin[3], solid-state materials can be classified as electrical conductors (usually metals), semiconductors and insulators according to the nature of electrical conductivity.

The electronic structure of these "bulk" materials, can be described using the band theory. An electronic band is defined as a combination of atomic orbitals that constituted the material.

This band can be visualized as dense series of molecular orbitals, generated by linear combination of atomic orbital.

A simple way to explain the above concept is to consider a solid material as an indefinitely large assembly of atoms.[4]

An atom is described by molecular orbitals (Figure 1.2 a): HOMO (highest occupied molecular orbital) and LUMO (lowest unoccupied molecular orbital).

A small cluster of several atoms of a semiconductor (Figure 1.2 b), is characterized by a combination of atomic orbitals, with a series of occupied low-energy levels and empty high-energy levels for excited electrons.

When increases the number of atoms in the cluster, the discrete orbitals overlap forming two bands structure that represent a continuum (Figure 1.2 c).

Valence band (VB) is formed by bonding molecular orbitals (HOMO) and conduction band (CB) is constituted by non-bonding molecular orbitals (LUMO).

[3] N. W. Ashcroft, N. D. Mermin, Solid State Physics, **1976**.

[4] V. Balzani, P. Ceroni, A. Juris, Photochemistry and Photophysics, **2014**, Wiley.

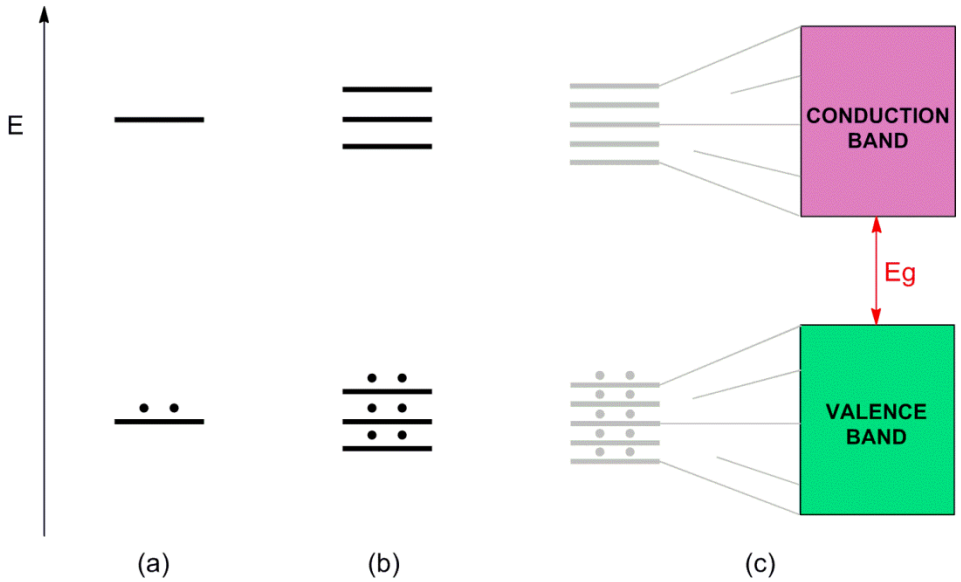

Figure 1.2

The energy difference between VB and CB is called energy gap E_g. The materials are classified conductors, semiconductors and insulator as a function of this energy gap (Figure 1.3).

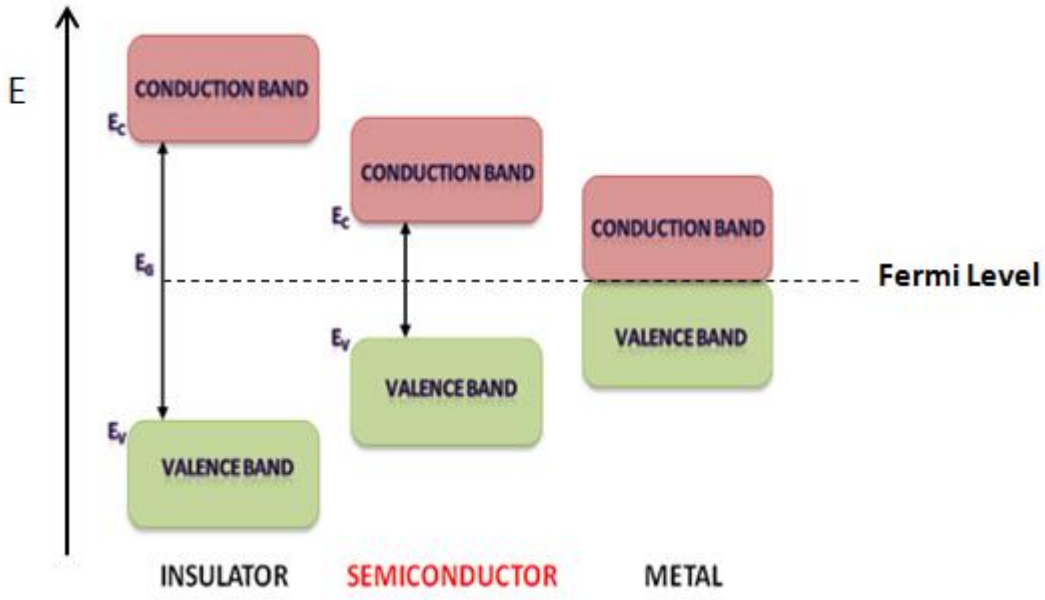

Figure 1.3

To understand the properties of these materials is essential to evaluate the Fermi level[5] usually denote by μ or E_F. For an intrinsic semiconductor, the Fermi level can be considered as an

[5] Kittel, Charles. Introduction to Solid State Physics, **1980**, 7th Edition. Wiley.

hypothetical energy level of electron, such that at thermodynamic equilibrium this energy level have a 50 % probability of being occupied.

The location of Fermi level in the band structure of material is important to determine the electrical behavior.

In an insulator, μ lies within a large band gap, far away from any levels while in a metal μ lies within a delocalized band.

In a semiconductor the Fermi level is located between the uppermost level of the valence band and the lowest level of the conduction band.

1.3 Doping of semiconductors

The Fermi level is also involved in the doping of semiconductors, a process of controlled addition of impurities (defects) that changes the electrical conductivity.

There are two types of dopants:

- donors that generate free electrons in a crystal and lead to **n-type** semiconductors;
- acceptors that create holes with formation of **p-type** semiconductors.

For instance, when trivalent boron replaces a silicon atom in the crystal, a vacant state "hole" is created, which can move around the lattice and functions as a charge carrier. This is a p-doped silicon.

In the case of n-doped silicon, the energy needed to move the extra electron to the conduction band (0.045eV) is comparable to k_bT at room temperature.

Therefore, thermal energy will be capable of ionizing the impurity, thereby causing an increase in the electron density in the CB, so that the Fermi level moves closer to the CB.

The doping of semiconductors finds application in the solar cell[6], where electrons flow toward the holes at the interface between n-type and p-type materials (Figure 1.4).

[6] V. Balzani, P. Ceroni, A. Juris, Photochemistry and Photophysics, **2014**, p. 402, Wiley.

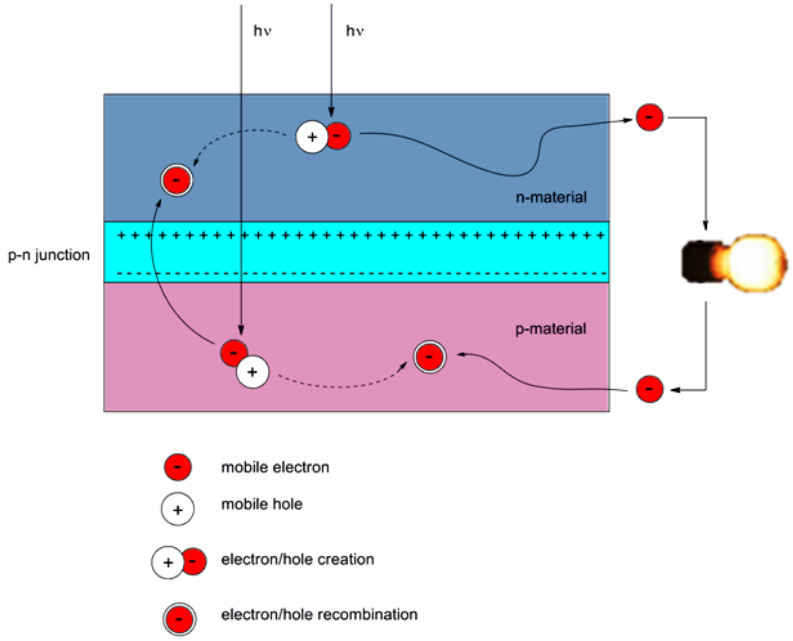

Figure 1.4 Conversion of light into electrical energy in a photovoltaic cell.[7]

As a result of electron migration on the p-n junction, the positively charge p-doped material becomes negative, counterbalanced by an inverse charge on the n-doped material.

This spontaneous process creates an electrical field that, at a given point, will prevent more electrons from crossing the junction and filling all the holes in the p-side.

1.4 Optical properties of semiconductors

The properties of semiconductors are connect to the nature of the chemical bonding between the atoms and crystallographic structure that define the type of band gap and effective mass of charge carriers.

Absorption of light can promote the transition of an electron from the valence band to the conduction band (Figure 1.5). To induce such transition, a photon must have energy higher or equal than the band gap.

[7] V. Balzani, P. Ceroni, A. Juris, Photochemistry and Photophysics, **2014**, cap 14, p. 402, Wiley.

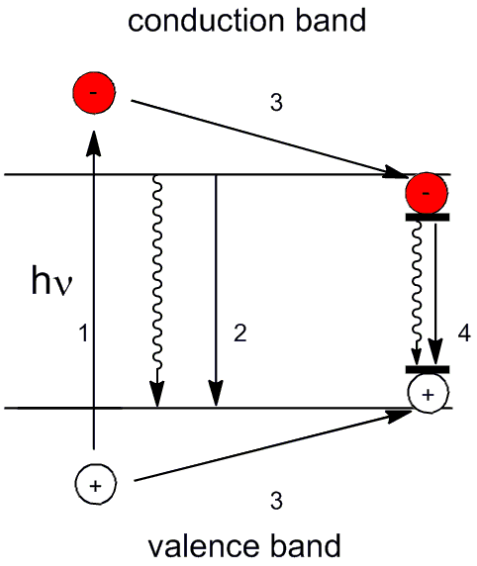

Figure 1.4 Principal electronic processes: 1 excitation, 2 radiative or non radiative decay of free carriers, 3 charge trapping, 4 radiative and nonradiative recombination of trapped charge carriers. Reproduced from Ref.[8]

The result is the electron-hole pair, called exciton,[9] a bound state due to the electrostatic Coulomb force between the electron and the hole.

After thermal relaxation into free electrons and holes, these charge carriers can either recombine by nonradiative or radiative processes or can be trapped by defects present in the crystal structure.

The width of the intrinsic band gap in the semiconductor (undoped), is very important because it allows to observe the luminescence, preventing the rapid deactivation of the electron-hole charge carriers.

As for molecules, the photon absorption is regulated by selection rules, in particular the law of conservation of momentum.

According to this law, only those transition in which the quasi-momentum (p)[10] of the final state is equal to the quasi-momentum of the initial state are allowed.

---

[8] V. Balzani, P. Ceroni, A. Juris, Photochemistry and Photophysics, **2014**, cap 3, p. 98, Wiley.

[9] Exciton is an electrically neutral quasiparticle that exists in insulators, semiconductors and in some liquids. The exciton is regarded as an elementary excitation of condensed matter that can transport energy without transporting net electric charge. An exciton can form when a photon is absorbed by a semiconductor. This excites an electron from the valence band into the conduction band. In turn, this leaves behind a positively-charged electron hole. The electron in the conduction band is then effectively attracted to this localized hole by the repulsive Coulomb forces. Frenkel J., **1931**, "On the Transformation of light into Heat in Solids. I". Physical Review.

In the case of solid, the radiative process should conserve the electron momentum, as the photon momentum is small compared to the crystal momentum.

In analogy with molecular photophysics, where the excited state can be distorted with respect to the ground state, in a semiconductor, the minimum of the conduction band and the maximum of the valence band can have the same value of electrical momentum (**direct**) or a different value (**indirect semiconductor**), Figure 1.5.

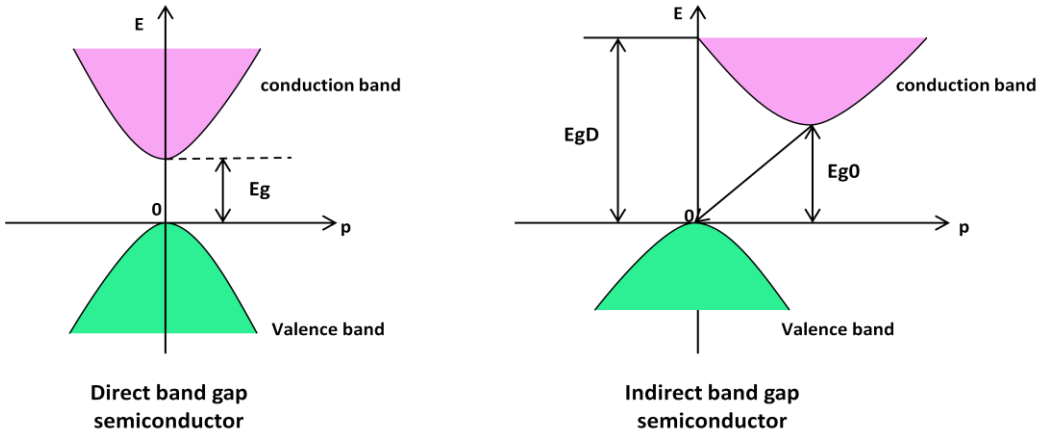

Figure 1.5 Energy diagram as a function of the electron momentum p, E_{gD} energy gap in direct transition, E_{g0} energy gap in indirect transition.

Direct-band gap semiconductor as GaAs, absorbs efficiently the light when the energy of photon overtake the band gap, as a consequence the transition from the VB to CB produces free charge carriers.

This implies the formation of the electron with momentum p_c in the conduction band and hole remaining in the valence band with momentum p_v.

When the excited electron/hole carriers return to the ground state, a reverse transition from the CB to VB is observed with the emission of a photon (Figure 1.6). This process, in which the electron of the CB annihilates the hole in the VB by radiative recombination, releases the excess of energy by photoluminescence.

[10] In solid-state physics, crystal momentum or quasi-momentum p is a momentum-like vector associated with electrons in a crystal lattice. It is defined by the associated wave vectors k of this lattice , according p = ħk. Where ħ is the reduced Planck's costant.

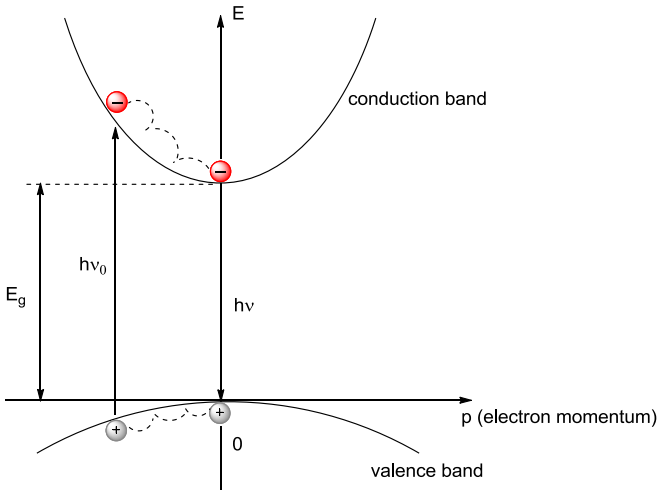

Figure 1.6 Energy diagram as a function of the electron momentum p, $h\nu_0$ - energy of the exciting photon; hν - energy of the emitted photon.

The emission probabilities are high for direct-band gap semiconductors, therefore are used as light-emitting diodes.

In **indirect-band gap** semiconductors such as silicon, the minimum of CB is shifted compared to the maximum of VB, hence the selection rule is not respected (Figure 1.5). To conserve the electron momentum, the radiative processes must be coupled to a phonon[11] or a defect in the crystal structure.

The involvement of the phonon makes this process much less likely to occur in a given span of time. As a consequence, the radiative recombination is far slower in indirect band gap materials than direct band gap ones.

1.5 Defects in the crystal structure of semiconductors

Radiative transitions can also occur by electron-hole recombination in donor-acceptor sites of dopant or defects (process 4, Figure 1.4).

[11] In physics, a phonon is a collective excitation in a periodic, elastic arrangement of atoms or molecules in condensed matter, such as solids and some liquids.
The concept of phonon was introduced in 1932 by Russian physicist Igor Tamm, it represents an excited state in the quantum mechanical quantization of the modes of vibrations of elastic structures in which a lattice of atoms or molecules uniformly oscillates at a single frequency.

Impurities or defects can be “deep” or “shallow” centers of electron localization near the middle of the band gap or the allowed bands. In these points electrons and holes can be considered “fixed” compared with the electrons and holes in the conduction and valence band that transport electrical current.

There are several defects in the crystal lattice of semiconductors as chemical impurities, vacant lattice sites and atom embedded in the interstitials that can bind and release electrons.

In the ideal case, the chemical impurities such as atoms can be removed from the crystal while the vacancies and interstitials are thermodynamically inevitable.

In the case of vacancies, the absence of an atom leads the formation of dangling bonds while the interstitial defects insert an excess of the silicon atoms in the unit cell (Figure 1.7).

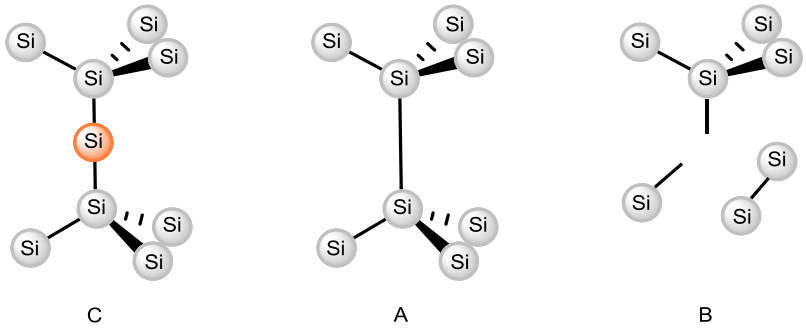

Figure 1.7 A- no defects in the silicon structure, B- vacancy, C- interstitial atom.

The presence of defects can be due to the internal factors like the intrinsic properties of the atom or external factors, however also in the ideal case, a perfect crystal presents some defects that alter the internal energy of the crystal. The free electrons may be trapped by defects.

Some linear and planar defects like twins, dislocations and stacking faults are the result of formation process of crystalline silicon.

1.6 Silicon nanocrystals or Silicon Quantum dots

The reduction of the semiconductor dimensions to nanoparticles with diameters of a few nanometers leads to the world of quantum dots (QDs).

A quantum dot is a nanocrystal made of semiconductor materials, the first example was discovered in a glass matrix by Alexey Ekimov[12] at first in 1981.

The term **quantum dot** was coined by Mark Reed[13] at Texas Instruments, to describe a form of particle size where the excited electrons and holes are spatially confined in three dimensional space; hence the electronic and optical properties are the result of limitations of the excitons to a finite number of available quantum states.

In these systems the motion of the electrons, is associated to the quanto-mechanical model of a particle in a box[14], hence the electronic properties are strictly correlated with the size of the material.

In QDs, a quantum confinement regime is reached when the size of the semiconductor nanocrystal is below the Bohr radius and optical properties become size dependent. The Bohr radius is characteristic of a given material and is a measure of the extension of the exciton wavefunction over the crystal lattice.

Similar to a molecule, a quantum dot has both a quantized energy spectrum and a quantized density of electronic states near the edge of the band gap.

Decreasing of nanocrystals size causes an increase in the band-gap energy (Figure 1.8) and consequently variation in the electronic properties.

[12] Ekimov AI, Onushchenko AA, **1981**, Soviet Physics Semiconductors-USSR 16 (7): 775–778.

[13] M. A. Reed, J. N. Randall, A. E. Wetsel, Phys. Rev. Lett. 60, 535, **1988**.

[14] Efros, A. L., Rosen, M. Annu. Rev. Mater. Sci. **2000**, 30, 475–521.

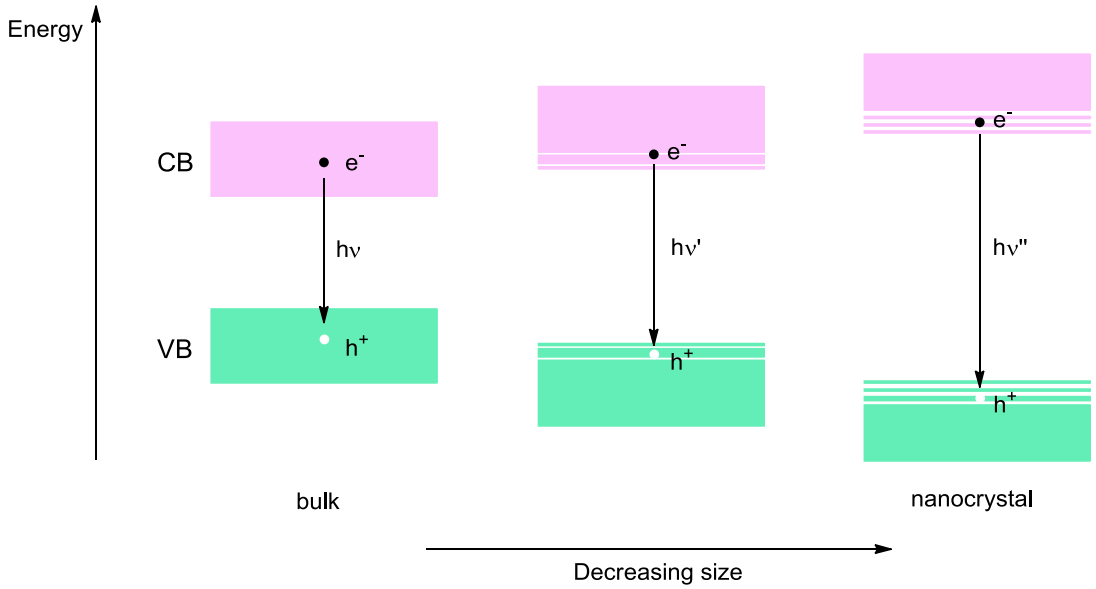

Figure 1.8 Effect of the quantum confinement on the emission energy of bulk and nanocrystal semiconductors

The electronic properties of QDs are dependent on the size and shape of the material. For example, the band gap in a quantum dot which determines the frequency range of emitted light, is inversely related to its size[15] (Figure 1.9) .

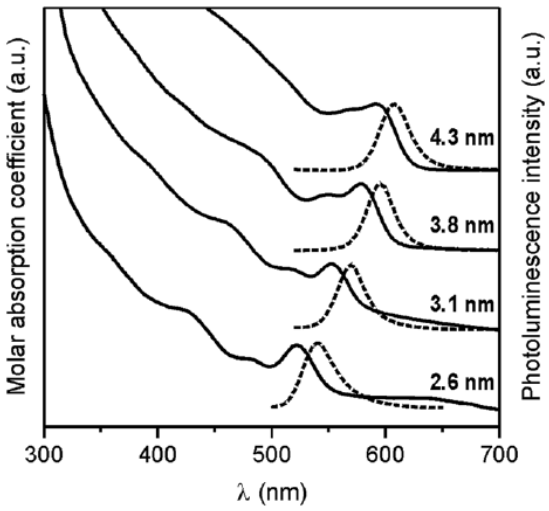

Figure 1.9 Effect of the quantum confinement reproduce from ref. [16] Absorption (left) and emission spectra (right) of CdSe Qds, λ_{ex} = 480 nm.

QDs exhibit unique photophysical properties that are not observed in their bulk-counterpart. The main properties of direct band gap semiconductor nanocrystals are:

[15] Hessel C. M., Korgel B. A., et al. Chem. Mater. **2012**, 24, 393-401.

[16] A. Credi, New J. Chem. **2012**, 36, 1925-1930.

- large molar absorption coefficients in the UV-visible region and intense emission bands;

- high emission quantum yield[17] due to the strong overlap between the electron and hole wave functions in the confined structure;

- tunable emission wavelength[18] that can be tuned from the blue to the NIR spectral region adjusting the size of the nanocrystal;

- long fluorescence lifetime[19] of the order of tens of nanoseconds;

- high photostability[20] compared to classical fluorophores that allow applications as in vivo imaging.

Also in silicon nanocrystals or silicon quantum dots, the strong quantum-confinement effect play an important role to determine the electronic and optical properties.

Figure 1.10 reports an example[21] of quantum size effect, that causes a shift of photoluminescence band toward higher energy reducing the size of SiNC and an enhancement of the spontaneous emission rate.

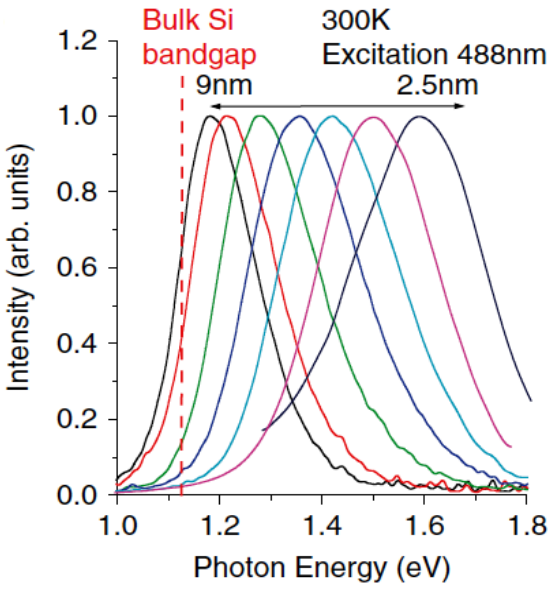

Figure 1.10 PL spectra of SiO_2-embedded SINCs at room temperature reproduced from ref.[22]

[17] Mattoussi H., Mauro J. M., Bawendi, M. G., J. Am. Chem. Soc. **2000**, 122, 12142–12150.

[18] Smith A.M., Nie S., Acc. Chem. Res. **2010**, 43, 190-200.

[19] Lounis B., Bechtel H. A., Gerion D., Alivisatos A. P., Moerner W. E., Chem. Phys. Lett. **2000**, 329, 399–404.

[20] Jaiswal. J. K., Simon S. M., Nat. Biotechnol. **2003**, 21, 47–51.

[21] L. Pavesi, R. Turan, "Silicon Nanocrystals:Fundamentals, Synthesis and Application", **2010**, Wiley-Vch.

[22] S. Takeoka, M. Fujii, S. Hayashi, Phys. Rev. B, **2000**, 62, 16820-16825.

Chapter 2

Synthetic methods

2.1 Techniques for the synthesis of silicon nanocrystals

The current knowledge of the properties of SiNCs is due to the pioneering study[23] on first luminescence nanoporous silicon (porSi) prepared by electrochemical etching of Si wafer. The sample manifested electroluminescence and size-tunable luminescence but the great size and shape distribution led to a complex analysis of results.

Another factor to consider in the interpretation of experiments is the enormous surface area-to-volume ratio; for instance a compact icosahedral silicon structure with a diameter of 2.0 nm have about 280 Si atoms[24], of which 120 (43%) on the surface of the particle while a larger icosohedral structure with 600 total Si atoms has 200 surface atoms (33%).

For that reason, the surface influences the characteristics of the material.

Computationally, it has been predicted that surface chemistry will influence the lowest unoccupied molecular orbital energy (LUMO) and hence the optical band gap of SiNCs[25].

It is evident the importance to develop methods of synthesis that allow to realize a good control of optical properties of SiNCs by an efficient surface passivation, functionalization and size separation. Only in this way it is possible to have a clear distinction between effects related to size, surface and collective behavior.

Synthetic techniques for the preparation of SiNCs (Figure 2.1) can be classified according to various parameters[26]:

- type of synthetic approach (top-down and bottom-up);
- nature of resulting material: SiNCs in solid state matrices and colloidal SiNCs;

[18] L. T. Canham, Appl. Phys. Lett., **1990**, 57, 1046-8.

[24] F. Hua, M. T. Swihart, E. Ruckenstein, Langmuir, **2005**, 21, 6054-6062.

[25] J. Zou, R. K. Baldwin, K. A. Pettigrew, S. M. Kauzlarich, Nano Lett., 2004, 4, 1181-1186.

[26] K. Dohnalovà, T. Gregorkiewicz, K. Kusovà, J. Phys., Condens. Matter, **2014**, 26, 1-28.

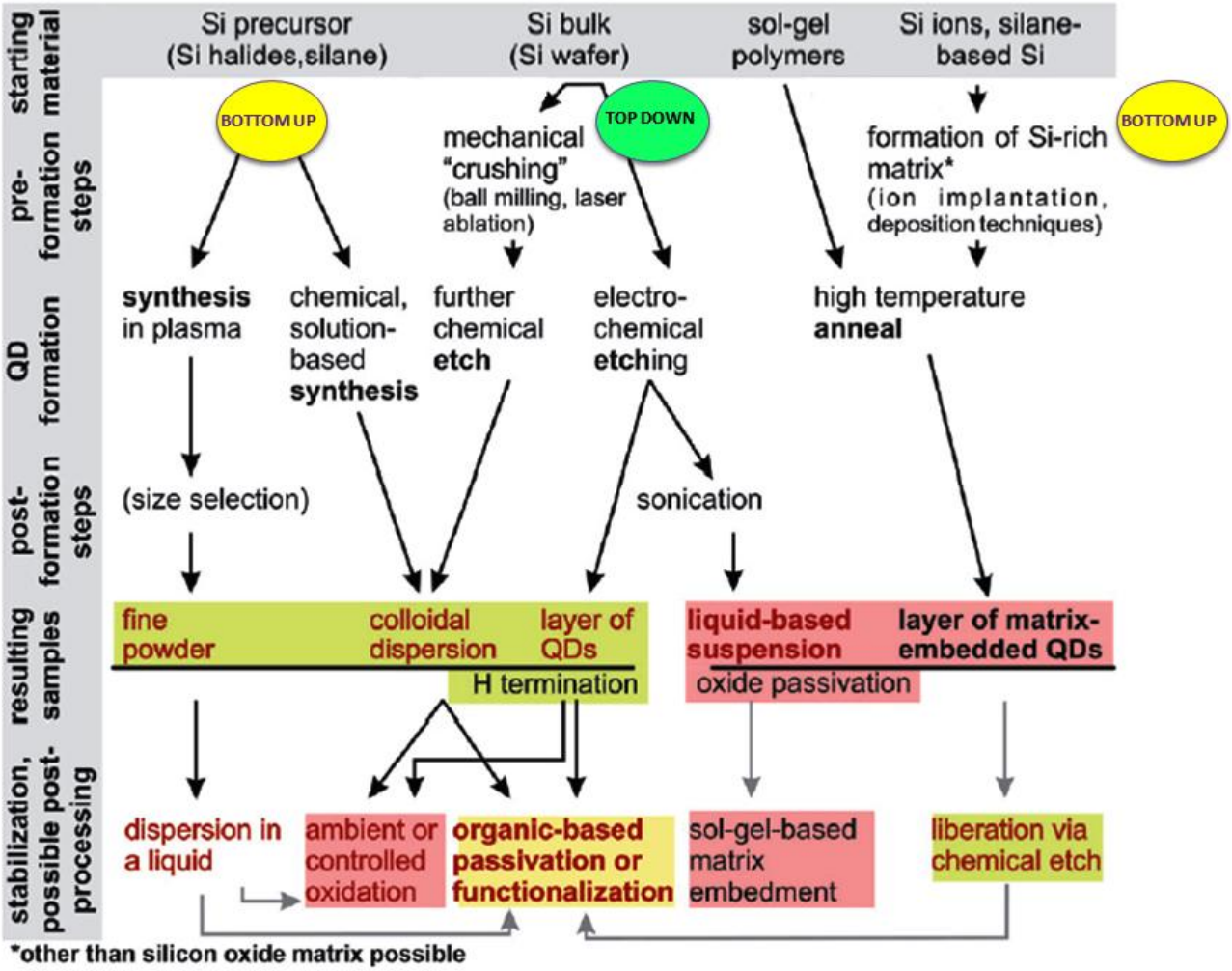

Figure 2.1 A general overview[27] of the most common sequence steps in the preparation of matrix-embedded and free-standing SiNCs.

2.2 SiNCs in solid matrices

SiNCs in solid matrices (e.g. oxide matrix) are good starting materials to obtain narrow size distribution and dense packing. The control of the density and size can be realized by different method:

- ion implantation of silica;
- plasma enhanced chemical vapor deposition (CVD);
- sputtering;
- molecular beam deposition.

[27] K. Dohnalovà, T. Gregorkiewicz, K. Kusova, J. Phys. Condens. Matter 26, **2014**, 173201-173229.

One of the major drawbacks of these techniques is low production yield and requirement of high temperatures for the annealing step.

2.3 Colloidal SiNCs

For free-standing SiNCs we can use different synthetic approaches.

Top-down techniques as laser ablation in inert atmosphere and ball milling followed by etching and ultrasonication.

The most common bottom-up procedures are synthesis in plasma, laser pyrolysis and chemical solution-based synthesis.

Free-standing SiNCs are useful for a great variety of deposition processes such as drop casting, ink-jet printing, spraying, stamping and roll-to-roll.

2.4 Production methods

Current synthetic methods are divided into three big categories: chemical, physico-chemical and physical.

Here, the main synthetic strategies know in the literature will be presented, providing an overview of the relationship between the method of the synthesis and SiNCs optical and chemical properties (Table 2.1).

table 2.1

Chemical	Physico-chemical
Chemical solution-based synthesis	Laser-induced dissociation of silane
Thermal degradation in supercritical fluids	
Nanosilicon from SiO_x	

2.5 Chemical methods

2.5.1 Chemical solution-based synthesis

These procedures have attracted much attention since they allow to control the surface chemistry and particles size. In the 1992 Heath[28] proposed a system consisting of a high-pressure bomb reactor to reduce a mixture of silicon tetrachloride and n-octyltrichlorosilane with sodium dispersion (Figure 2.2).

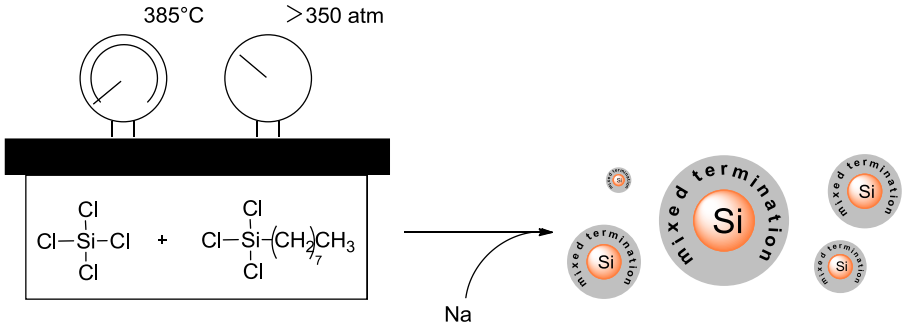

Figure 2.2

The process (with an yield lower than 10 %) provided polydisperse silicon nanoparticles (d = 2-9 nm) that showed Si-O, Si-Cl, and Si-H bonds on their surface from the FT-IR analysis. According to the authors, the absence of alkyl chains on the surface was linked to the covalent nature of Si-C bond and surface chemistry.

Another possible strategy to obtain SiNCs is the use of Zintl salts as (A_xSi; A: Na, K, Mg), prepared by reacting Mg in a 1 % excess with Si powder at 700°C for 3 days in a sealed Nb tube, according to a literature method.[29]

Kauzlarich et al.[30] exploit the high reactivity of Zintl phase to prepare alkyl-capped SiNC with various groups: methyl, ethyl, n-butyl and n-octyl (Figure 2.3).

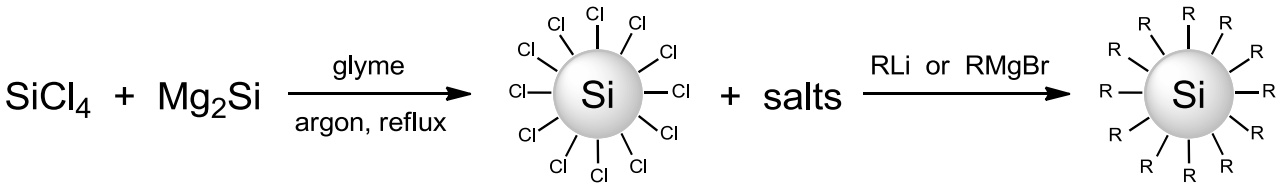

Figure 2.3

[28] J. R. Heath, Science, **1992**, 258, 1131-1133.

[29] G. H. Li, H. S. Gill, A. R. Varin, Metall. Trans. A **1993**, 24, 2383-2391.

[30] C. S. Yang, R. A. Bley, G. R. Delgado, S. M. Kauzlarich, J. Am. Chem. Soc. **1999**, 121, 5191-5195.

This reaction produces crystalline nanoparticles (d = 2-5 nm) with versatile surfaces but low yield. The average cluster size depends on the reflux time of Mg_2Si with $SiCl_4$. The presence of crystalline nanoclusters is confirmed by HR-TEM; SAED and lattice fringes are consistent with diamond-structured Si (Figure 2.4).

FT-IR shows the ν(C-H) stretching at 2900 cm^{-1} and δ(C–H) bending at 1400 cm^{-1} due to the surface alkyl group, no evidence of Si-O stretching is present (Figure 2.4).

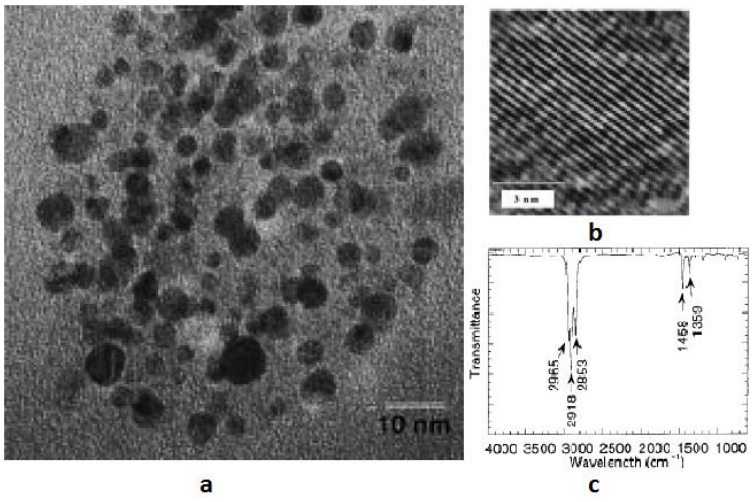

Figure 2.4 a) TEM image of a large number of silicon naocluster. b) Rotationally filterd image of $(Si)_x$-CH_3, D-spacing of these lattice fringes are consistent with the {111} silicon crystal plane (3.14 $\dot{A}$). c) FT-IR spectra for Si nanocluster terminated with n-butyl group reproducedfrom ref.[30]

PL spectra of nanoclusters show a strong UV-blue PL between 315 and 520 nm, and its intensity depends linearly on the excitation power density and cluster size (Figure 2.5).

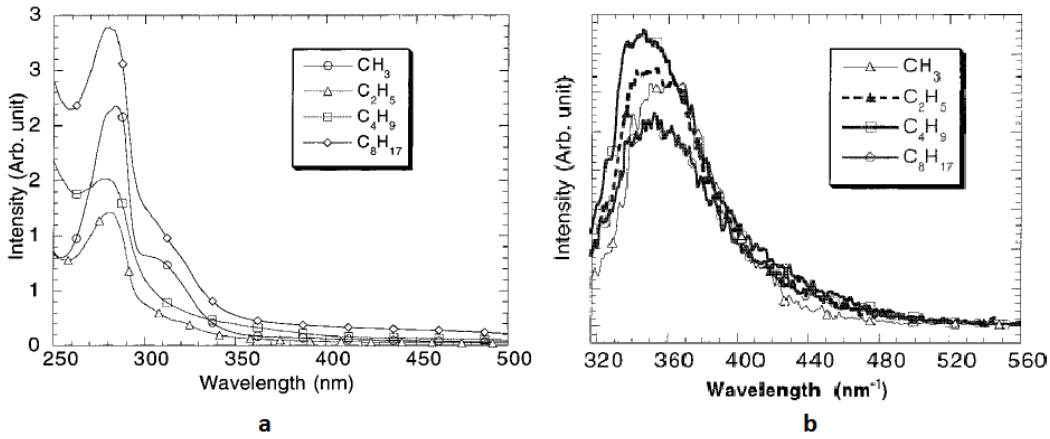

Figure 2.5 a) Absorbance spectra. b) PL spectra with an excitation bandwidth of 2.5 nm and λ_{exc} = 310 nm from ref.[30]

[30] C. S. Yang, R. A. Bley, G. R. Delgado, S. M. Kauzlarich, J. Am. Chem. Soc. **1999**, 121, 5191-5195.

In other contribution[31], alkyl capped SiNCs have been prepared via oxidation of magnesium silicide with bromine (Figure 2.6) and subsequent coverage of the surface with alkyl-lithium reagent.

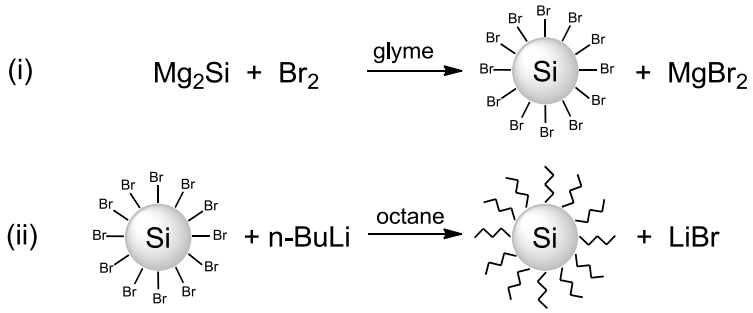

Figure 2.6

HR-TEM confirms the crystalline nature of nanoparticles with an average diameter of 4.5 nm. The control over the size is possible varying the silicon:bromine ratio. Fluorescence spectroscopy indicates an ultraviolet-blue photoluminescence (Figure 2.7) which is attributed to both quantum confinement and surface termination.

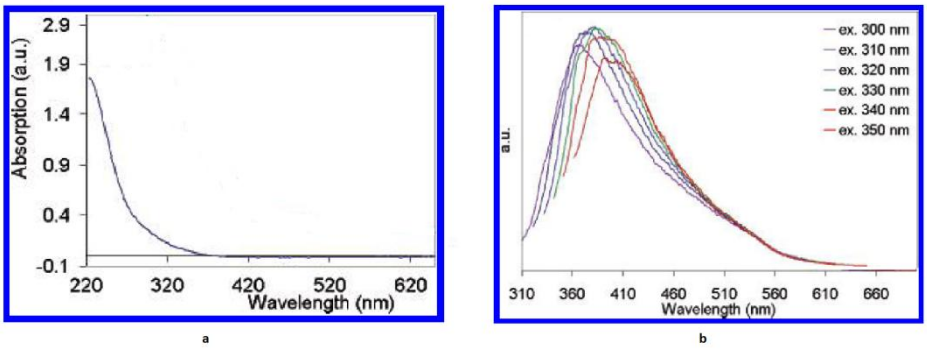

Figure 2.7 a) UV-visible spectra of silicon nanoparticles b) PL spectra reproduced from ref.[31]

[31] K. A. Pettigrew, Q. Liu, P. P. Power, S. Kauzlarich, Chem. Mater., **2003**, 15, 4005-4011.

Homogeneous solution reactions have also found application in preparing FS-SiNCs.

Some methods exploit the reduction of $SiCl_4$[32] with the production of pyrophoric silanes (Figure 3.7).

$$SiCl_4 + LiAlH_4 \xrightarrow{\text{ether}} LiCl + AlCl_3 + SiH_4$$

Figure 2.8

For example, Wilcoxon and Samara[33] use inverse micelles as reaction vessels, to grown Si nanocrystals in the size range 1.8-10 nm. Quaternary ammonium cationic salts or aliphatic polyethers are employed as surfactants. An anhydrous compound (SiX_4, X= Cl, Br, I) is dissolved in the hydrophilic interior of micelles in octane. They next reduce Si(IV) to Si(0) using an anhydrous metal hydride (usually 1 M $LiAlH_4$ in THF).

Products are further size selected using HPLC separation.

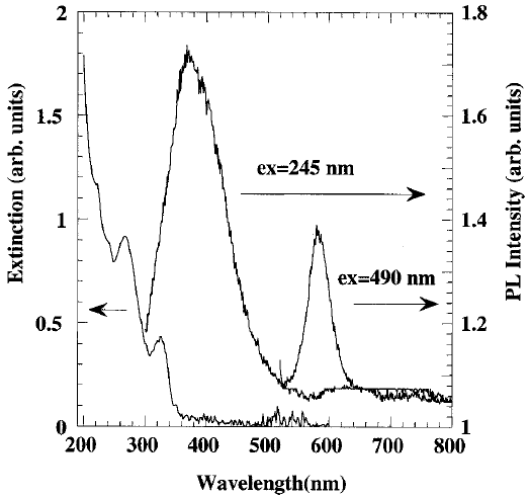

Figure 2.9 Absorbance and PL spectra of SiNC with d= 2nm reproduced from ref.[33]

The major PL peak (λ_{exc}= 245 nm) centered at 365 nm (3.40 eV) is attributed to direct electron-hole recombination (Figure 2.9) .

The radiative lifetime is 1 ns and quantum efficiency (QE) of the PL is 4 %.

The second PL peak at 580 nm (2.14 eV) is due to surface or defect recombination.

[32] A. E. Finholt, A. C. Bond, H. I. Schlesinger, J. Am. Chem. Soc., **1947**, 69, 1199-1203.

[33] J. P. Wilcoxon, G. A. Samara, App. Phys. Lett., **1999**, 74, 3164-3166.

Tilley at al.[34] later reported a variation of this method to obtain hydrophilic or hydrophobic silicon nanocrystals with good monodispersion (1-2 nm). Tetraoctylammonium bromide is used as the surfactant and the hydride reducing agent produces hydrogen-terminated particle surfaces. The SiNCs are capped with either allylamine or 1-heptene (Figure 2.10) by platinic-acid catalyzed-hydrosilylation.

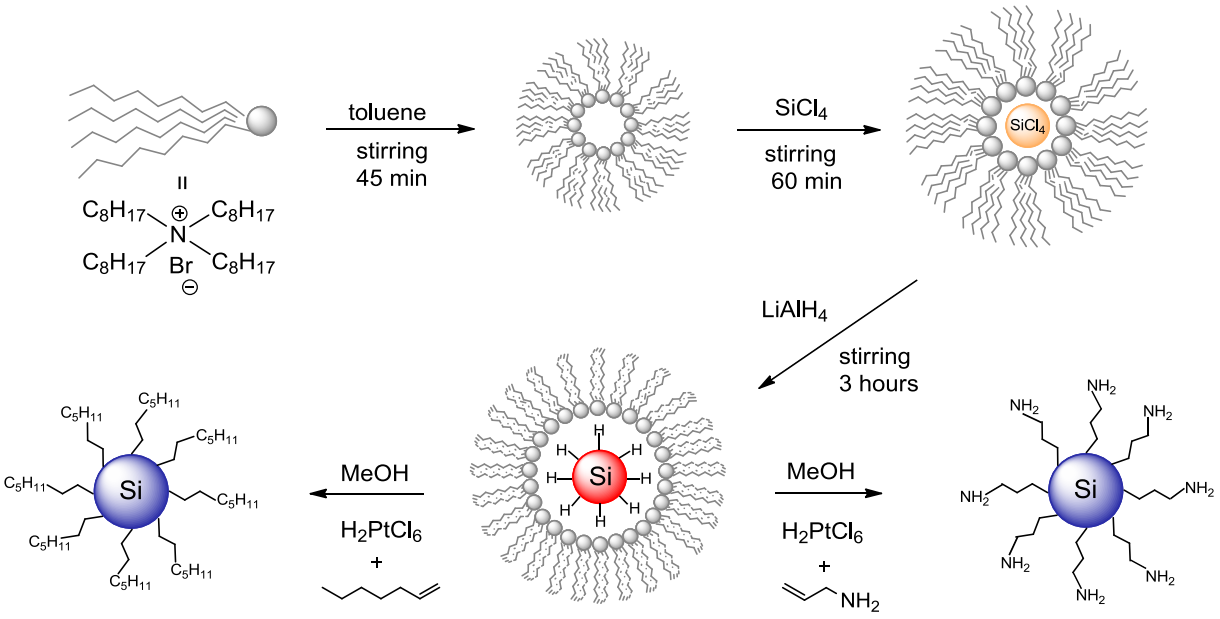

Figure 2.10 Scheme of the synthesis

Optical characterization is performed on colloidal solutions with two types of surface-capped SiNCs with identical size distribution. Allylamine-SiNC shows an absorption profile with a greater spectral range than 1-heptene-SiNCs (Figure 2.11); in addition there is a shoulder at 340 nm that can be due to the direct band gap transition.

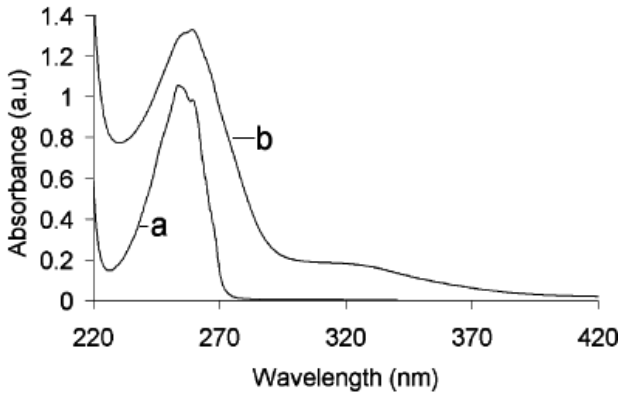

Figure 2.11 Absorption of a) 1-heptene-SiNCs, b) allylamine-SiNCs reproduced from ref.[34]

[34] J. H. Warner, H. Rubinsztein, R. D. Tilley, J. Phys. Chem. B, **2005**, 109, 19064-19067.

From the analysis of PL properties (Figure 2.12) there are two differences:

- allylamine-SINCs exhibit a major red shif in the PL peak position than 1-heptene SiNCs;

- 1-heptene-SiNCs display emission with higher energy than the allylamine-SiNC for the same excitation wavelength.

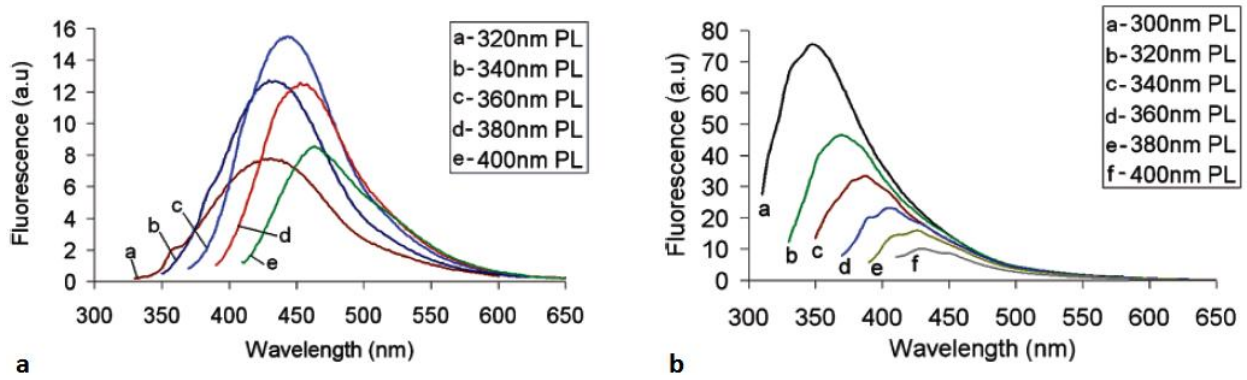

Figure 2.12 PL spectra of a) allylamine-SiNCs, b) 1-heptene-SiNCs

These results demonstrate the effect of the ligand on the SiNCs optical properties and its role in the radiative recombination mechanisms.

Sodium naphtalide has also proven useful in preparing FS-SiNCs of varied sizes and surface chemistry. In this context, Baldwin and co-workers[35] describe the preparation of air and moisture stable octanol derivatized crystalline silicon nanoparticles by room temperature sodium naphtalenide reduction of silicon tetrachloride (Figure 2.13).

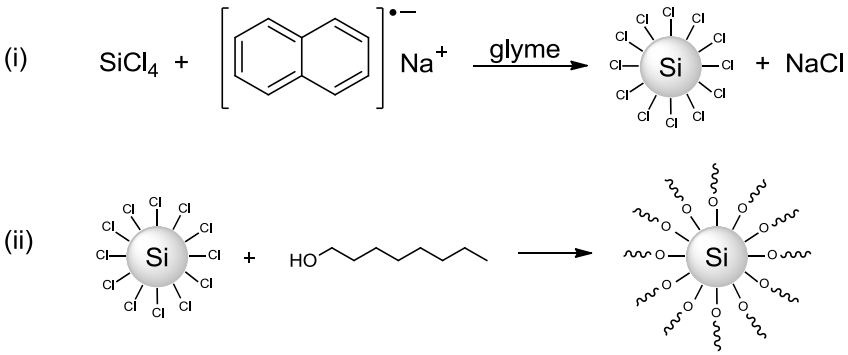

Figure 2.13

[35] R. K. Baldwin, K. A. Pettigrew, E. Ratai, M. P. Augustine, S. M. Kauzlarich, Chem. Commun., **2002**, 1822-1823.

The mean diameter is 5.2 ± 1.9 nm and lattice fringe spacing (0.314) is consistent with <111> plane of diamond crystalline silicon (Figure 2.14).

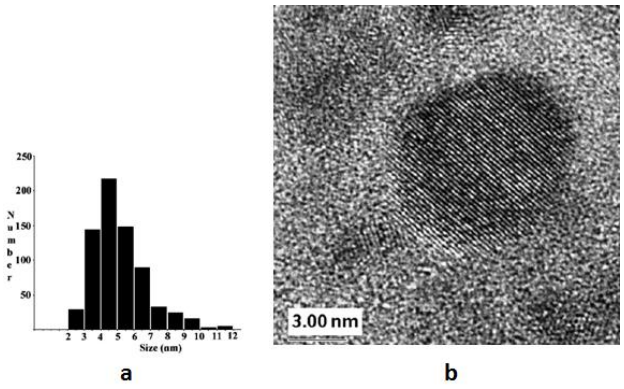

Figure 2.14 a) histogram of particle size, b) HR-TEM image of octanol-cappend SiNCs reproduced from ref.[35]

2.5.2 Thermal degradation in supercritical fluids

Precursor thermal decomposition is an attractive method for preparing semiconductors nanoparticles. In 2001, Korgel and coworkers[36] have developed a method to produce highly crystalline, organic-monolayer passivated SiNCs by thermal degradation of diphenylsilane (Si precursor) in supercritical solvent mixtures of octanol and hexane (Figure 2.15).

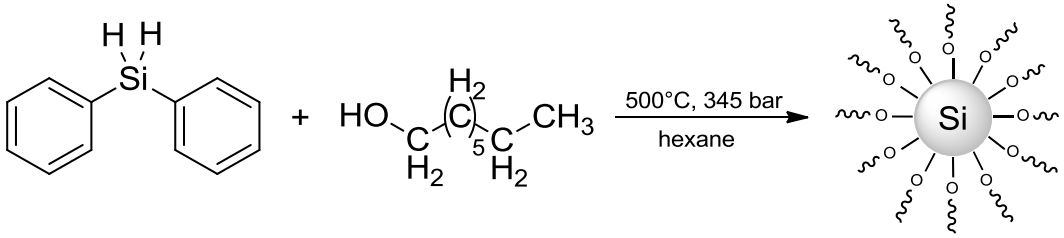

Figure 2.15

The high temperature is necessary to induce Si crystallization.

The advantage of a supercritical solvent is the high diffusion coefficient, on the order of 10^{-3} to 10^{-4} cm^2 s^{-1}, that enables the rapid reactant diffusion necessary to achieve diffusion-limited growth for the narrowest particle size distributions.

Relatively size-monodisperse SiNCs, with a diameter range from 15 to 40 Å are obtained with yields 0.5 – 5 %, they show a crystalline core with a lattice spacing of 3.1 Å, consistent with the (111) separation in the Si diamond-like structure (Figure 2.16).

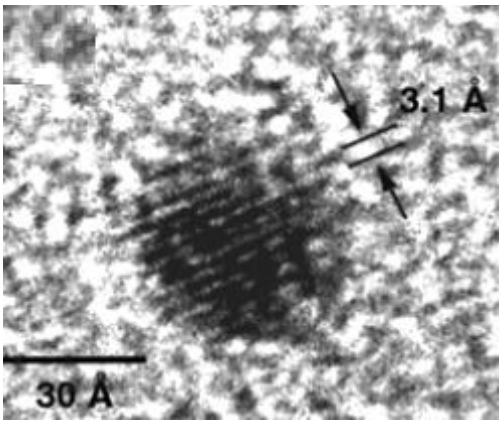

Figure 2.16 HR-TEM image of a 40 Å diameter SiNC reproduce from ref.[36]

[36] J. D. Holmes, K. J. Ziegler, R. C. Doty, L. E. Pell, K. P. Johnston, B. A. Korgel, J. Am. Chem. Soc. **2001**, 123, 3743-3748.

Control over the particles size is realized through systematic variation of the octanol: Si ratio. Silicon nanocrystals exhibit a significant blue shift in optical properties from the bulk band gap energy of 1.2 eV due to quantum confinement effects.

As shown in Figure 2.17, the smaller SiNCs emit in the UV region and the larger exhibit a green PL with quantum yields of 20 % at room temperature.

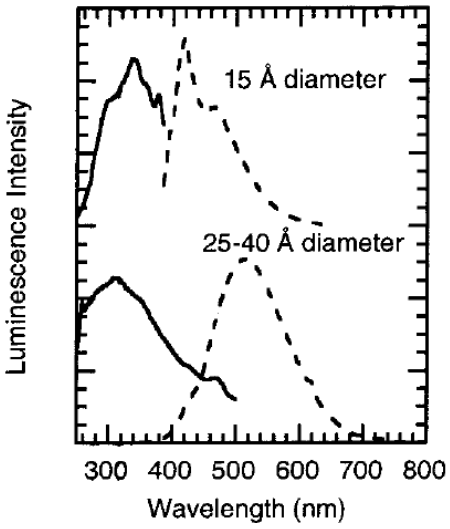

Figure 2.17 Absorbance (solid lines) and PL spectra of SiNCs at room temperature reproduced from ref.[31]

2.5.3 Silicon nanopowder from SiO_x

Si-rich silicon suboxide (SROs) films have been used as semi-insulating polysilicon films in Si-based electronic devices. Such films are generally annealed in the course of their processing and formation of Si clusters during annealing has been reported in the past decades.[37]

Inspired by these processes, Liu and Kimura[38] have synthesized silicon nanopowder with a narrow size distribution by high temperature annealing of commercially available SiO_x ($x < 2$) powder, followed by etching with HF and HNO_3.

The high temperature leads to the phase separation (Figure 2.18).

$$SiO_x \longrightarrow \frac{x}{2} SiO_2 + \left(1 - \frac{x}{2}\right) Si$$

Figure 2.18

X-ray diffraction is used to follow the transformation of the sample during the annealing. As shown in Figure 2.19, the annealing process at 1100°C results in deep oxidation of SiO_x powder, in fact the XRD patterns for three samples are dominated by the SiO_2 amorphous phase.

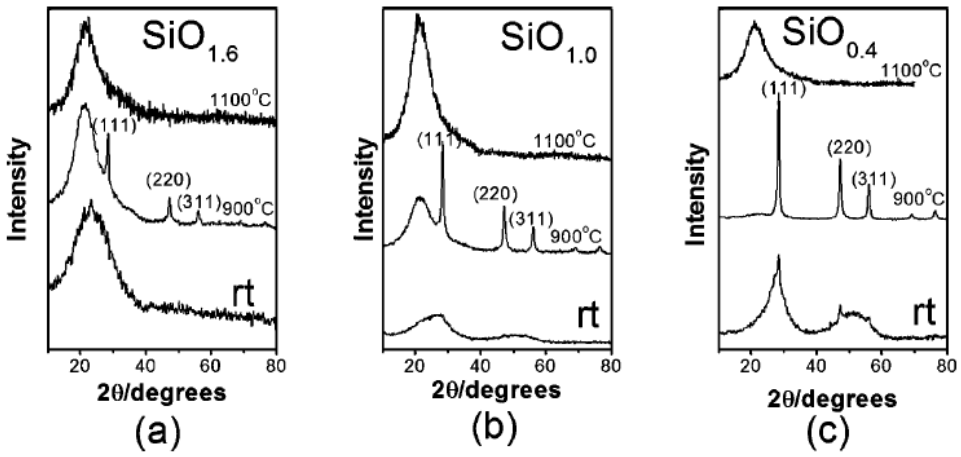

Figure 2.19 XRD reproduced from ref.[38]

From the XRD analysis it is evident that the annealing at a lower temperature (900°C) induces the phase separation with the formation of crystallized Si particle and amorphous SiO_2.

[37] L. A. Nesbit, Appl. Phys. Lett, **1985**, 46, 38.

[38] S-M Liu, S. Sato, K. Kimura, Langmuir, **2005**, 21, 6324-6329.

Also the effect of HF etching process is studied by XRD (Figure 2.20).

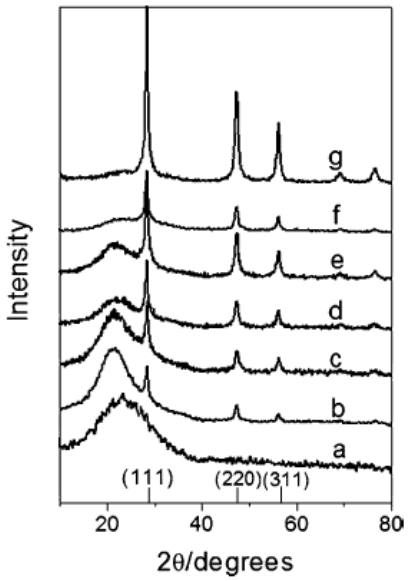

Figure 2.20 The change of XRD patterns during HF etching process. Curves a and b were measured on $SiO_{1.6}$ starting material and 900 °C annealed sample, respectively. Curves c-g were obtained after etching for (c) 1 h, (d) 2 h, (e) 3 h, (f) 4 h, and (g) 6 h reproduced from ref.[38]

From pattern a → g, the oxide phase (wide diffraction peak at 2θ of 21°) decrease with the etching time and disappears after 6 hours. The formation of Si nanoparticles is confirmed by HR-TEM, the average size of particle is 4.2 nm with polydispersity of 12 %.

Freshly etched sample shows two emission bands at 520 nm and 397 nm (Figure 2.21).

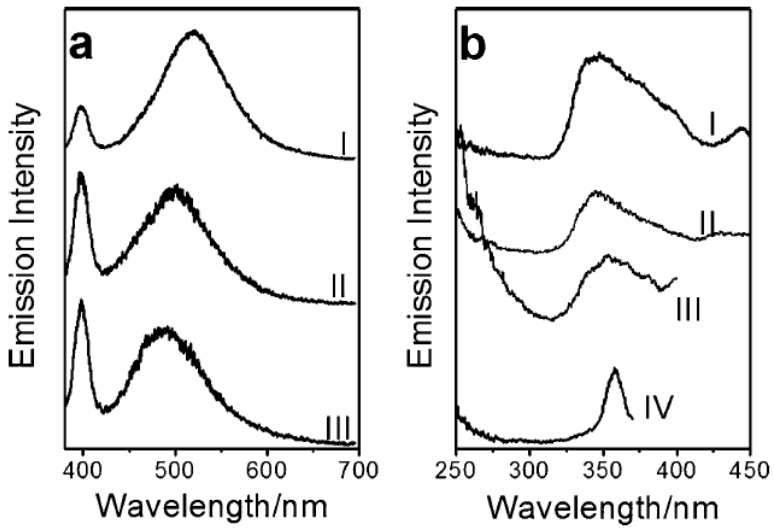

Figure 2.21 (a) PL spectra of sample after HF etching for (I) 3 h, (II) 6 h, and (III) 1 day recorded by excitation at 355 nm wavelength; (b) PLE spectra recorded at detection wavelength of (I) 520 nm, (II) 502 nm, (III) 487 nm, and (IV) 400 nm. Spectra I and IV were recorded on sample after HF etching for 3 h, spectra II and III were recorded on sample after HF etching for 6 h and 1 day, respectively. Reproduced from ref.[38]

After 1 day, the PL band at 520 nm blue-shifts to 487 nm while the high energy emission stays at 397 nm. The emission band at 520 nm is ascribed to the radiative recombination of electron-hole pairs. These results are consistent with the PL bands observed by Korgel[39] and Kauzlarich[40] from organic-passivated SiNCs with an average size of 2-5 nm.

Hessel and Veinot[41], take advantage of commercially available hydrogen silsesquioxane (HSQ) as molecular precursor to produce SiO_2-embedded SiNCs by reductive thermal annealing (Figure 2.22).

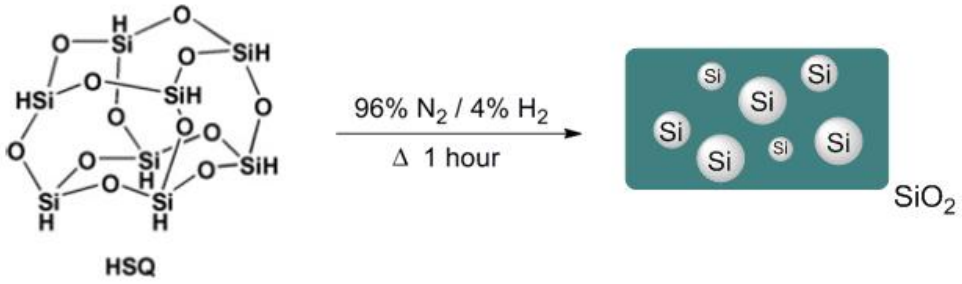

Figure 2.22

During thermal process HSQ undergoes some transformations related to cage rearrangement as the temperature increases.

The temperature at 900°C induces the crystallization growth.

X-ray diffraction shows a broad peak associated to the SiO_2 like-matrix for the sample processed at 800°C (Figure 2.23) without reflections of the diamond lattice Si.

[39] J. D. Holmes, K. J. Ziegler, R. C. Doty, L. E. Pell, K. P. Johnston, B. A. Korgel, J. Am. Chem. Soc. **2001**, 123, 3743-3748

[40] C. Yang, R. A. Bley, S. M. Kauzlarich, H. W. H. Lee, G. R. Delgado, J. Am. Chem. Soc., **1999**, 121, 5191

[41] C. M. Hessel, E. J. Henderson, G. C. Veinot, Chem. Mater. **2006**, 18, 6139-6146

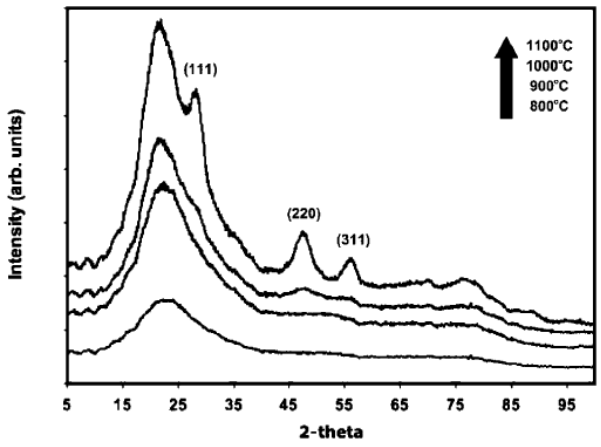

Figure 2.23 XRD of the sample during thermal processing reproduced from ref.[41]

At higher temperatures, characteristic (111), (220) and (311) reflection signals are observed as a consequent of short-range crystalline order. X-ray photoelectron spectroscopy confirm the presence of silicon and oxygen (Figure 2.24).

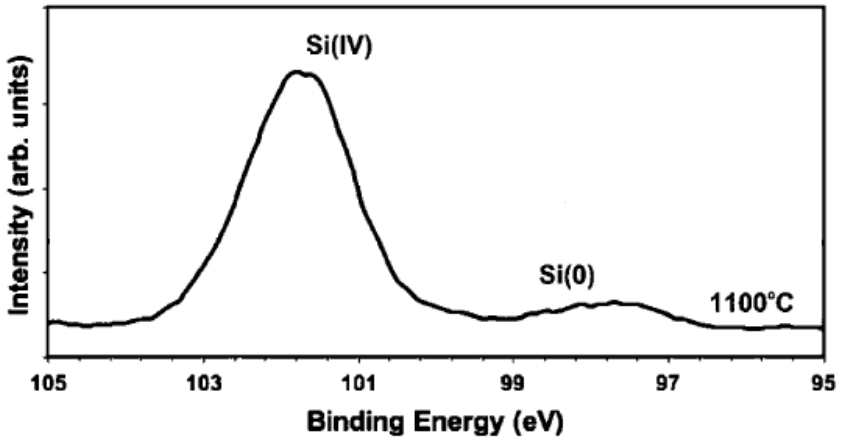

Figure 2.24 Xps of the Si 2p spectral region of composite at 1100°C. The two peaks at 101.9 and 98.1 eV are associate to oxide silicon and elemental silicon. Reproduced from ref.[41]

However, the formation mechanism of the silicon nanocrystals remain unclear.

Freestanding hydride-terminated SiNCs are obtained by etching of a solution of hydrofluoric acid, ethanol and water necessary to remove the silica matrix. The dimension and related photoluminescence of hydride-terminated SiNCs can be controlled varying the etching time (Figure 2.25).

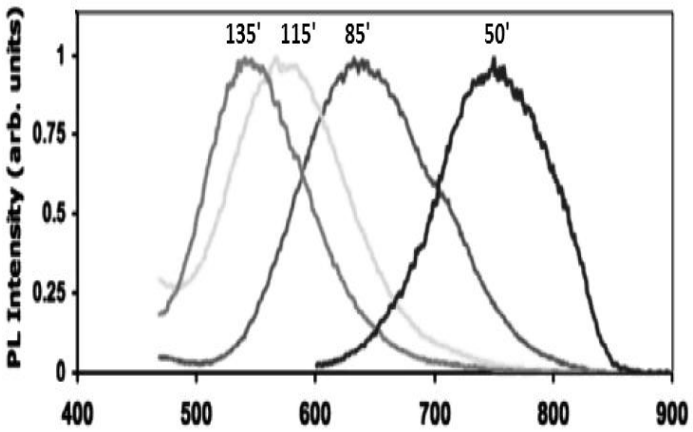

Figure 2.25 PL spectra of samples dispersed in pentane upon standard UV light.

The PL maximum shifts from red to green emission.

2.6 Physico-chemical methods

2.6.1 Laser induced SiH_4 pyrolysis

One of most effective physico-chemical method is the decomposition of silane in a CO_2 laser. Swihart and coworkers[42] have reported the use of laser induced SiH_4 pyrolysis as an efficient method for preparing macroscopic quantities of Si nanoparticles.

Crystalline nanoparticles with sizes ranging from 5 to 10 nm are prepared by silane dissociation through heating with a CO_2 laser beam in an aerosol reactor[43] and etching with a mixture of $HF/HNO_3/H_2O$ to reduce the size.

The color of the photoluminescence changes from red to green as the etching proceeded.

However the particles are instable to air in fact their emission intensity decreases due to the surface oxidation. To stabilize the optical properties they carried out the photoinitiated hydrosilylation in a UV reactor (Figure 2.26). Different compound with terminal double bond are used for the coverage of hydride-terminated silicon nanoparticles.

[42] F. Hua, M. T. Swihart, E. Ruckenstein, Langmuir, **2005**, 21, 6054-6062

[43] X. Li, Y. He, S. S. Talukdar, M. T. Swihart, Langmuir, **2003**, 19, 8490

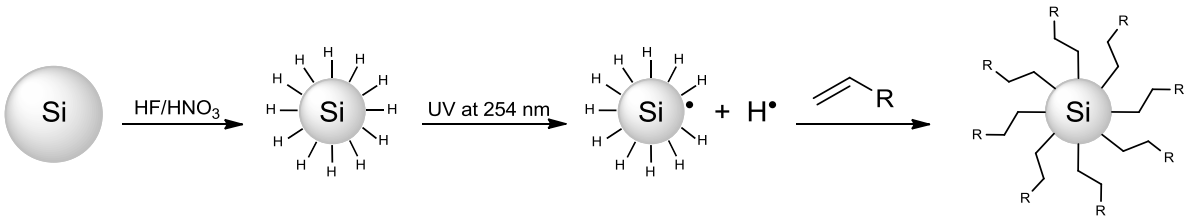

Figure 2.26

Figure 2.27 shows the PL of nanoparticles with maximum emission at 570 nm in different solvents.

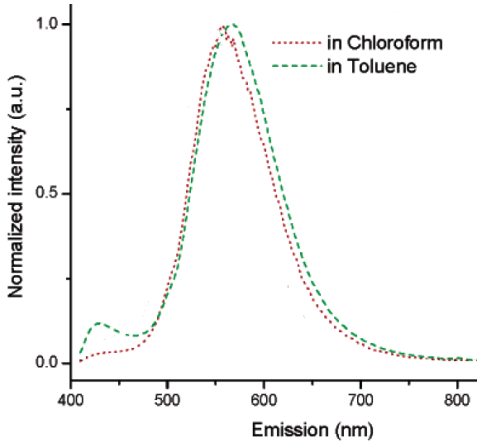

Figure 2.27 Reproduced from ref.[42]

Chapter 3

Techniques for the characterization of silicon nanocrystals

3.1 Introduction

The small size and complex surface chemistry of SiNCs require the use of different analytical techniques such as X-ray diffractometry (XRD), Fourier transform infrared spectroscopy (FTIR), X-ray photoelectron spectroscopy (XPS), nuclear magnetic resonance spectroscopy (NMR), transmission electron microscopy (TEM), and photoluminescent spectroscopy (PL).
This set of techniques offer a concrete characterization of SiNCs in order to have a good understanding of their properties.

3.2 X-ray diffraction (XRD)

XRD data were obtained with Si nanocrystals (5 mg) on quartz substrates using a Bruker-Nonius D8 Advance diffractometer. Scans of 2θ° were performed from 10–90° in 0.02 (2θ°) increments at a scan rate of 12.0° min^{-1} for 6 h.
XRD data for freshly etched Si nanocrystals were collected immediately after removing the nanocrystals from the etching solution to minimize oxidation of the nanocrystals prior to the measurement.

3.3 ATR-FTIR spectroscopy

ATR-FTIR spectra (400–4000 cm^{-1}) were acquired using a Thermo Mattson Infinity Gold FTIR with an ATR (attenuated total reflectance) stage. Samples were prepared by drop casting from chloroform dispersions after a 20 min ambient clean up in glass centrifuge tubes

3.4 X-ray photoelectronspectroscopy (XPS)

XPS was performed on a Kratos photoelectron spectrometer equipped with a charge neutralizer and 180° hemispherical electron energy analyzer. XPS samples were prepared by dropcasting Si nanocrystals (≈ 5 mg) onto indium tin oxide- (ITO) coated glass substrates and degassed at 10^{-7} Torr for 1 day prior to analysis. XPS data were internally standardized with respect to the O 1s peak position (530 eV).

3.5 Nuclear magnetic resonance analysis (NMR)

^{1}H-NMR and ^{13}C-NMR spectra were recorded on Varian INOVA 400 (400 MHz) spectrometers. Chemical shifts are reported in ppm using tetramethylsilane as the internal reference standard. Data are reported as follows: chemical shift, multiplicity (s = singlet, d = doublet, t = triplet, q = quartet, br = broad, m = multiplet), coupling constants (Hz). LC-electrospray ionization mass spectra were obtained with an Agilent Technologies MSD1100 single-quadrupole mass spectrometer. Chromatographic purification was performed on 240-400 mesh silica gel. All reactions were carried out under a nitrogen atmosphere in flame-dried glassware using standard inert techniques for introducing reagents and solvents.

3.6 Transmission electron microscopy (TEM)

TEM imaging was performed on a FEI Tecnai Biotwin TEM operated at 80 kV accelerating voltage. TEM samples were made by drop casting toluene dispersions onto carbon-coated 200 mesh copper TEM grids (Electron Microscopy Science).

3.7 Photophysical Techniques

Absorption measurements

UV-visible absorbance spectra reported in Chapter 4 and 5, were recorded with a Perkin Elmer λ40 spectrophotometer (Figure 3.1) in the 190-1100 nm range at room temperature, using quartz cells with 1.0 cm and 5.0 cm path length Hellma®.

The precision on the wavelength values was ± 2 nm. Molar absorption coefficient values were determined using the Lambert–Beer law; the experimental error, mostly due to weighting error, can be estimated to be around ± 5%.

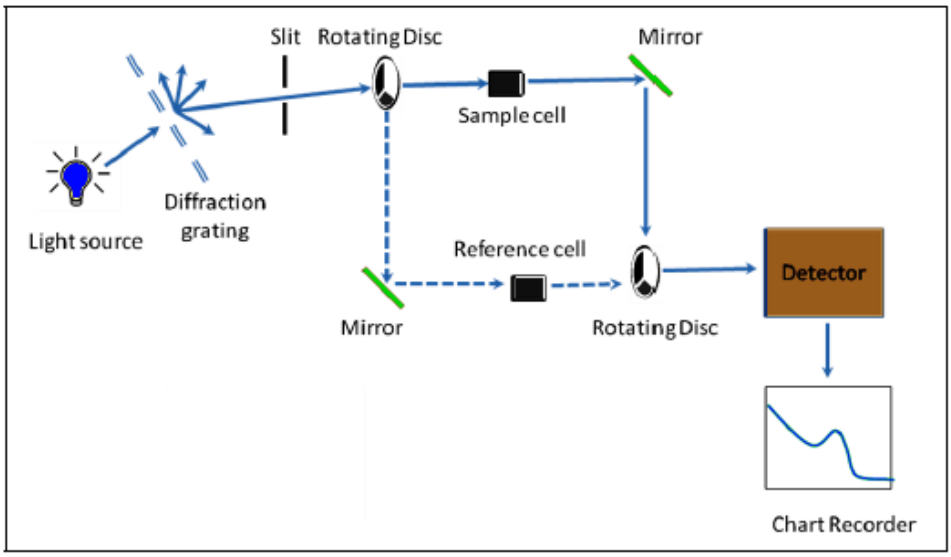

Figure 3.1 Schematic view of standard double-beam spectrophotometer.

Luminescence measurements

When necessary, solutions were deaerated by freeze-pump-thaw cycles. Emission spectra and excitation spectra in the range 250-900 nm, were obtained with a Perkin Elmer LS-50 spectrofluorometer, equipped with a Hamamatsu R928 phototube (Figure 3.2), or an Edinburgh FLS920 spectrofluorometer equipped with a Ge-detector for emission in the NIR spectral region. Correction of the emission spectra for detector sensitivity in the 650-900 nm spectral region was performed.[44]

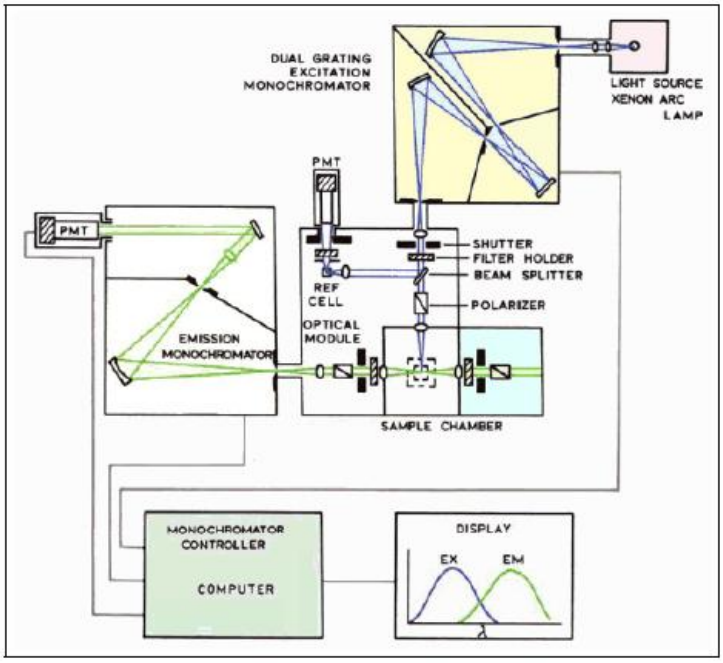

Figure 3.2 Schematic view of standard spectrofluorimeter.

Luminescence quantum yield measurements

Luminescence quantum yields were determined on solution samples at room temperature referring to the relative method optimized by Demas and Crosby.[45]

The quantum yield is expressed as:

$$\Phi_S = \Phi_R (A_s/A_R)(n_S/n_R)^2$$

[44] The Exploration of Supramolecular Systems and Nanostructures by Photochemical Techniques, P. Ceroni Ed., Springer, Lecture Notes in Chemistry, Vol. 78, Heidelberg, Germany, **2012**.

[45] Demas J. N., Crosby G. A., J. Phys. Chem. **1971**, 75, 991-1024.

Where Φ, A, *n* indicate the luminescence quantum yield, the area subtended by the emission band (in the intensity versus frequency spectrum) and the refractive index of the solvent used for the preparation of the solution, respectively; the subscripts S and R stand for sample and reference, respectively.

A_S and A_R must be obtained using the appropriate luminescence standard and under the same instrumental conditions; furthermore the sample and the reference must exhibit the same absorption at the excitation wavelength. Different standards were selected depending on the spectral region of interest.

In the Chapter 4, standard used are: naphthalene in deaerated cyclohexane solution,[46] quinine sulfate in H_2SO_4 0.5 M, 1,1',3,3,3',3'-hexamethylindotricarbocyanine iodide (HITCI) in ethanol.[47,48]

In the Chapter 5, the standard used are: $[Ru(bpy)_3]Cl_2$ in air-equilibrated water Φ_{PL}=0.040,[49] 1,1',3,3,3',3'-hexamethylindotricarbocyanine iodide (HITCI) in air-equilibrated ethanol Φ_{PL}=0.30).[50]

Luminescence lifetime measurements

PL lifetime measurements in the range 0.5 ns to 1 µs were performed by an Edinburgh FLS920 spectrofluorometer equipped with a TCC900 card for data acquisition in time-correlated single-photon counting experiments (0.2 ns time resolution) with a 340 nm pulsed diode and a LDH-P-C-405 pulsed diode laser. PL lifetime measurements in the range 10 µs to 1 s were performed on a Perkin Elmer LS-50 spectrofluorometer equipped with a pulsed Xe lamp. The estimated experimental errors is 5%.

[46] Montalti M., Credi A., Prodi L., Gandolfi M. T., Handbook of Photochemistry, ed. Taylor & Francis, London, 3rd edn., **2006**, ch. 10.

[47] Würth C., Pauli J., Lochmann C., Spieles M., Resch-Genger U., Anal. Chem. **2012**, 84, 1345-1352.

[48] Würth C., Grabolle M., Pauli J., Spieles M., Resch-Genger U., Nature Prot. **2013**, 8, 1535-1550.

[49] K. Suzuki, A. Kobayashi, S. Kaneko, K. Takehira, T. Yoshihara, H. Ishida, Y. Shiina, S. Oishi, S. Tobita, Phys. Chem. Chem. Phys. **2009**, 11, 9850.

[50] C. Würth, M. Grabolle, J. Pauli, M. Spieles, U. Resch-Genger, Nat. Protoc. **2013**, 8, 1535.

Laser flash-photolysis experiments

The experiments of ns-transient absorption spectroscopy on Silicon nanocrystals were performed by an Ultrafast Systems apparatus equipped with a Hamamatsu R928 phototube connected to a Tektronix TDS380 (400 MHz) oscilloscope and a Continuum Surelite I-10 Nd:YAG laser source (λ_{ex} = 532 nm).

Chapter 4

Silicon nanocrystals functionalized with pyrene units: efficient light-harvesting antennae with bright near-infrared emission

4.1 Introduction

Silicon nanocrystals exhibit interesting optical and electronic properties related to the quantum confinement effect. They can be efficient light emitters, with emission wavelength that can be tuned by size from the near-infrared (NIR) into the visible range.[51]

The indirect bandgap of Si, however, still makes light absorption relatively weak compared to quantum dots of direct band gap semiconductors, especially at wavelengths near the absorption edge.[52]

To circumvent this drawback, we exploited the covalent functionalization of SiNCs surface with a ligand (pyrene) capable of strong light absorption and efficient energy transfer to the SiNCs.

The aim of this work is to increase the optical absorption of SiNCs by molecular antennae while retaining their emission properties.

Two families of SiNCs with different average diameters 3.0 and 5.0 nm have been studied.

4.2 Synthesis of oxide-embedded silicon nanocrystals of different sizes

Silicon nanocrystals were synthesized by the method developed by Hessel et al.[53] The process use hydrogen silsesquioxane (HSQ) as precursor. This compound belongs to the silsesquioxane family,

[51] Brus L. E., Szajowski P. F., Wilson W. L., Harris T. D., Schuppler S., Citrin P. H., J. Am. Chem. Soc. **1995**, 117, 2915–2922.

[52] Hessel C. M., Reid D., Panthani M. G., Rasch M. R., Goodfellow B. W., Wei J., Fujii H., Akhavan V., Korgel B. A., Chem. Mater. **2012**, 24, 393–401.

a class of molecules composed of silicon-oxygen framework with empirical formula ($RSiO_{1.5}$) where R = hydrogen, alkyl, silyl and aromatic.

HSQ ($H_8Si_8O_{12}$) has been investigated as model silica surface,[54] catalytical support[55] and luminescent material.[56]

In a typical synthesis, 40 mL of Fox-16 (purchased from Dow Corning, 16wt% hydrogen silsesquioxane (HSQ) in isobutyl methyl ketone and toluene) is dried under vacuum on a schlenk line for 6 hours. The resulting white solid is placed in a quartz crucible and transferred to a tube furnace (Figure 4.1).

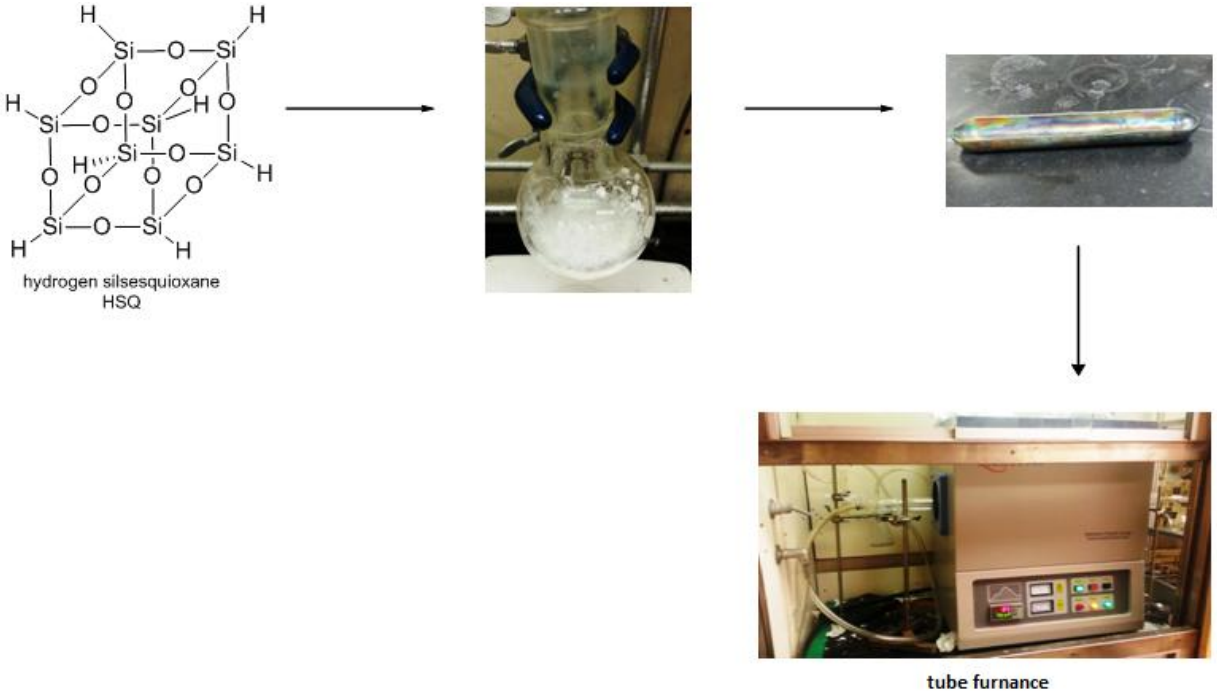

Figure 4.1 Steps for the tube furnance.

After purging with forming gas (93% N_2, 7% H_2), the tube furnace is heated to 1100^{o}C (2.6 nm diameter) or 1200^{o}C (5.0 nm diameter) at a heating rate of 18^{o}C/min and then held at that temperature for an hour.

The accepted stages[57] of HSQ thermal processing are summarized in (Figure 4.2) and are attributed to:

---

[53] Hessel C. M., Henderson E. J., Veinot J. G. C., Chem. Mater. **2006**, 18, 6139-6146.

[54] Feher F. J., Budzichowski T. A., Blanski R. L., Weller K. J., Ziller J. W., Organometallics **1991**, 10, 2526.

[55] Tour, J. M.; Pendalwar, S. L.; Cooper, J. P. Chem. Mater. **1990**, 2, 647.

[56] Azinovic D., Cai J., Eggs C., Konig H., Marsmann H. C., Veprek S. J. Lumin. **2002**, 97, 40.

- solvent losses at T < 200°C;
- cage network redistribution with associated loss of SiH_4 at 300°C;
- Si-H thermal dissociation accompanied by loss of SiH_4 and H_2 about 450°C;
- collapse of the pore structure > 500°C;
- induced crystallization above 800°C.

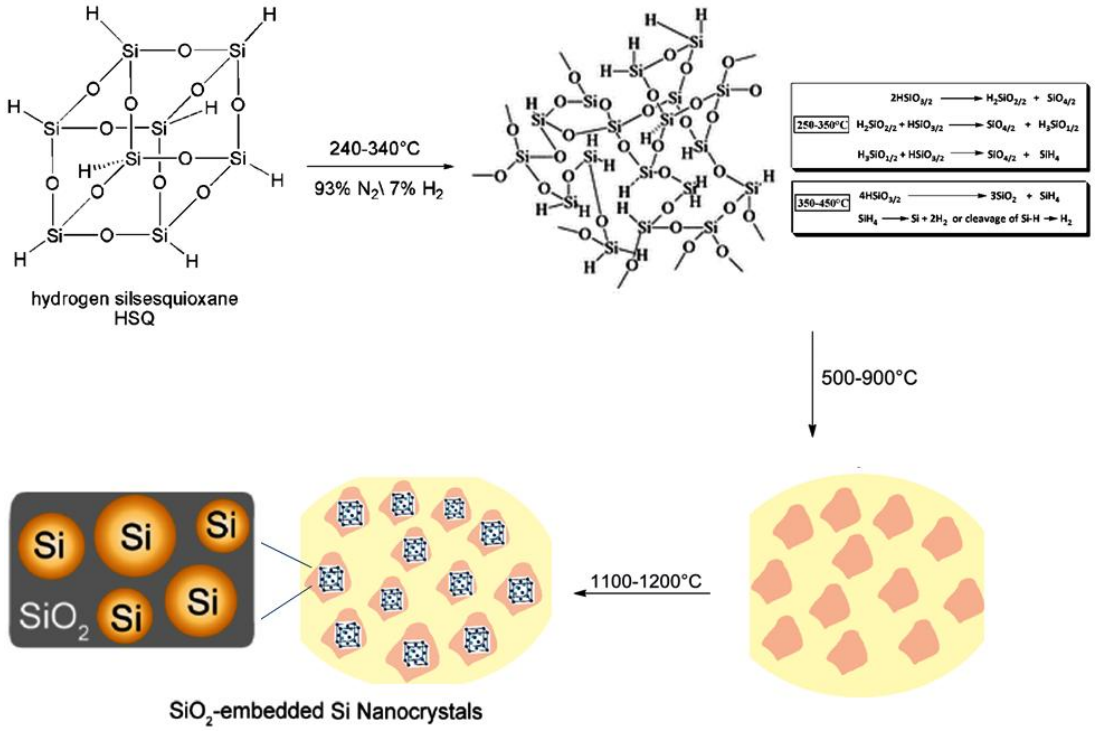

Figure 4.2 Stages of HSQ thermal degradation in an inert atmosphere.

After cooling to room temperature, the annealed material is removed and mechanically ground in a mortar and pestle to yield a fine powder (Figure 4.4). To reduce the gain size of the powder to around 200 nm, a wrist action shaker with 30 g of 3 mm diameter borosilicate glass beads is used.

[57] Detailed literature studies of HSQ thermal properties report on thermal processing of partially cross-linked HSQ gels and thin films, accounting for small differences in the present DSC temperature ranges. Yang, C.-C.; Chen, W.-C. J. Mater. Chem. **2002**, 12, 1138.

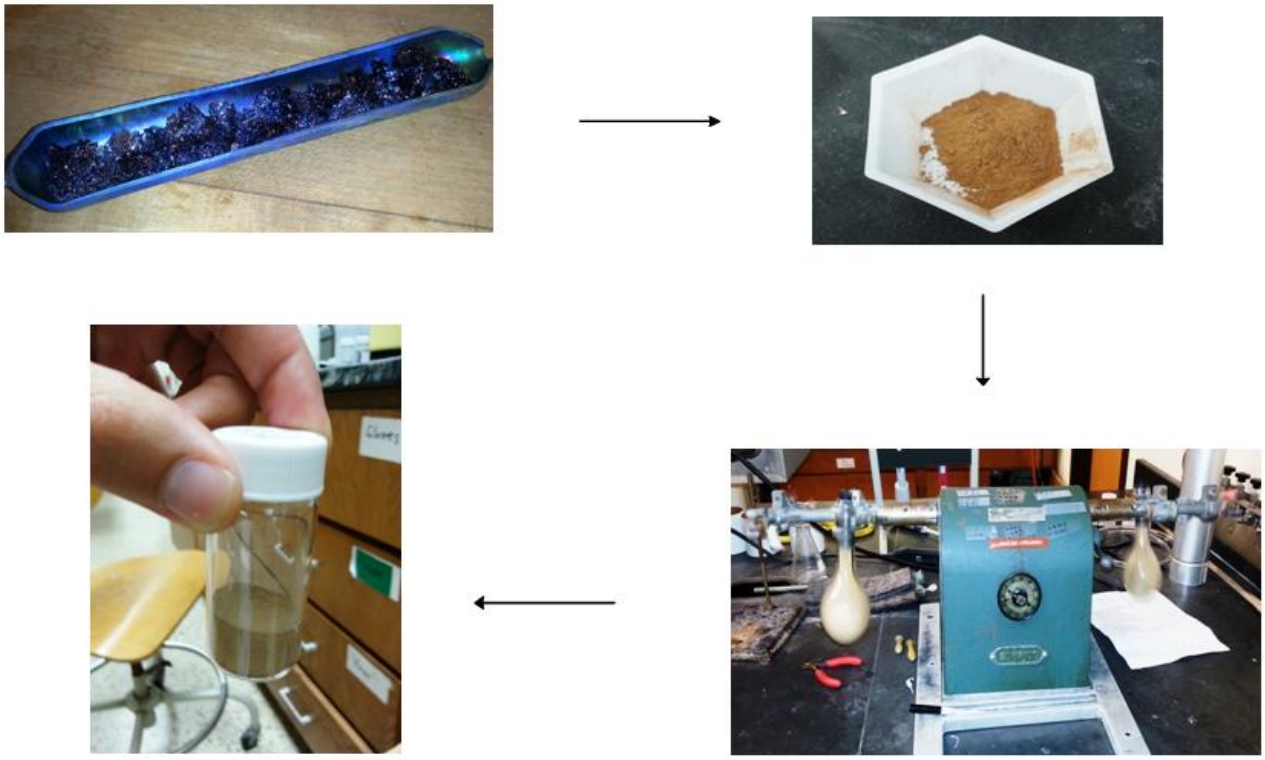

Figure 4.4

The final sample has been characterized with different techniques.

4.2.1 Material characterization

X-ray diffraction

The crystallization of matrix-embedded SiNCs was confirmed by X-ray power diffraction. When the sample is thermally processed at 1100°C, (220), (311), (111) reflection peaks increase in intensity and narrow. The position and intensities of these peaks (Figure 4.3) are consistent with diamond lattice Si.

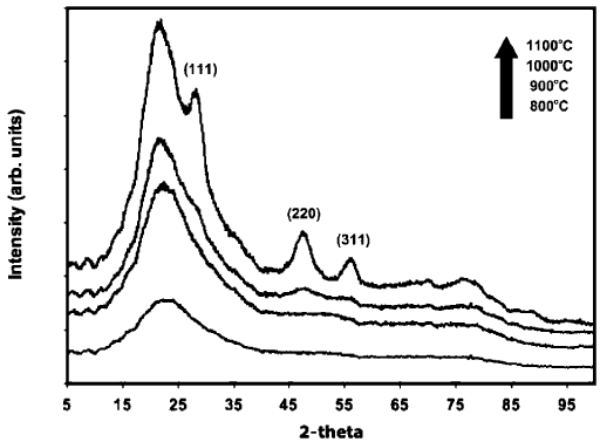

Figure 4.3 X-ray power diffraction of SiO_2/SiNCs at different temperatures.[46]

ATR-FTIR spectroscopy

ATR-FTIR spectroscopy (Figure 4.5) shows a characteristic strong absorption at 1090 cm^{-1} assigned to ν(Si–O) stretching due to the SiO_2 matrix and ν(Si–O-Si) stretching at 1048 cm^{-1} related to the interactions at the interface SiO_2/SiNCs.

The presence of Si-H bond is evidenced by weak ν(Si–H) stretching at 2035 cm^{-1} and δ(Si–H) bending at 800 cm^{-1}.

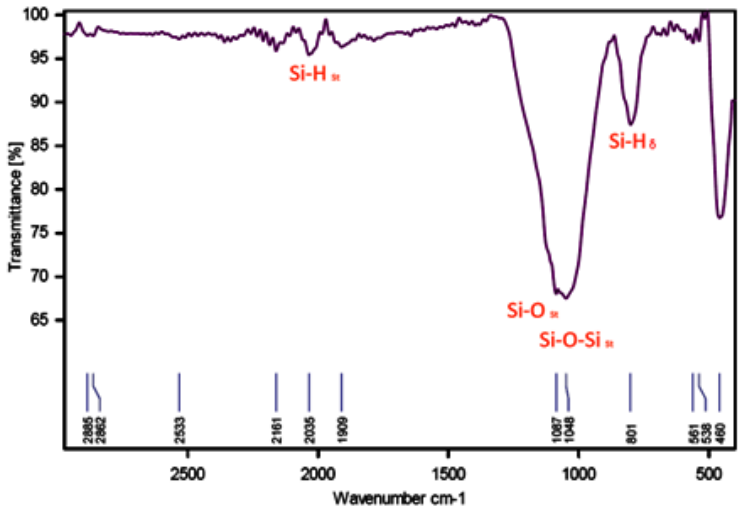

Figure 4.5 ATR-FTIR spectra of oxide-embedded SiNCs.

X-ray photoelectron spectroscopy

XPS of the oxide-embedded nanocrystals (Figure 4.6) exhibits peaks of elemental Si and SiO_2 at 99.4 eV and 103.5 eV respectively.[58] There is minimal suboxide (Si^{+1} and Si^{+2}) present, indicating that there is an abrupt interface between silicon nanocrystals and the SiO_2 matrix.[59]

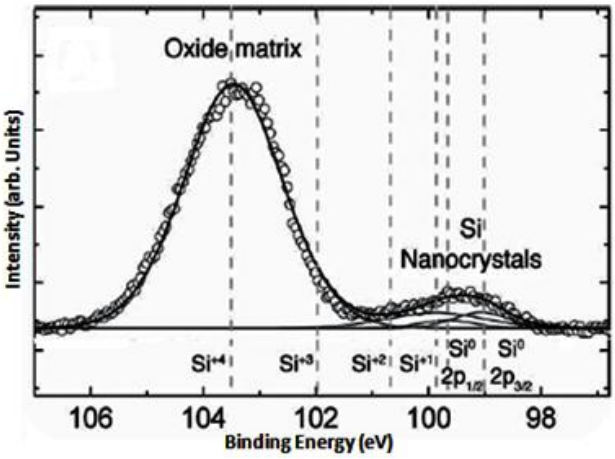

Figure 4.6 XPS of oxide-embedded SiNCs reproduced from ref.[51]

Optical properties

Figure 4.7 shows the photoluminescence spectra of SiO_2/SiNCs. Under excitation with the 325 nm line of He-Cd laser, emission at 800 nm from solid film is observed.[60]

[58] C. M. Hessel, E. J. Henderson, J. G. C. Veinot, J. Phys. Chem. C **2007**, 111, 6956.

[59] D. A. Luh, T. Miller, T. C. Chiang, Phys. Rev. Lett. **1997**, 79, 3014.

[60] Hessel C. M., Henderson E. J., Veinot J. G. C., Chem. Mater. **2006**, 18, 6139-6146.

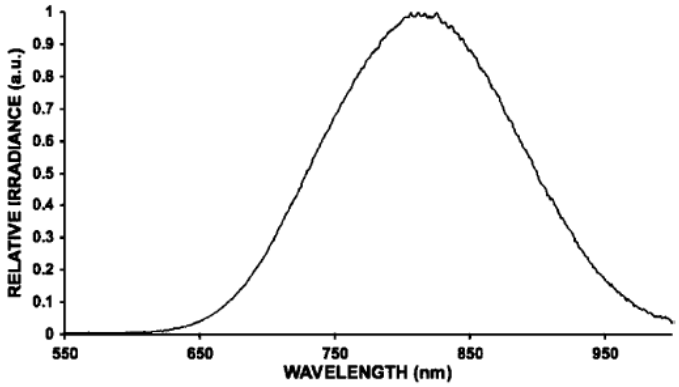

Figure 4.7 Photoluminescence spectrum from a pentane suspension of the finely ground powder from annealing at 1100°C, reproduced from ref.[53]

4.3 Liberation of hydride-terminated-SiNCs from silica matrix

The Si nanocrystals are liberated from the SiO_2 matrix by etching with a solution of 48% HF and 37.5% HCl (10:1 v/v) in the dark for 4-6 hours (Figure 4.8). During the oxide removal process the solution progresses from a dark brown to light yellow color as the nanocrystal size decrease.

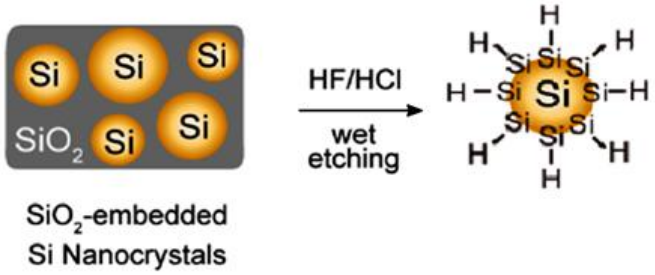

Figure 4.8

HF etches both Si and SiO_2, but the SiO_2-etching is much faster due to the polarity difference between Si-Si and Si-O bonds.[61] Hydride-terminated SiNCs are isolated as wet powder by centrifugation and rinsed once with deionized (DI) water, twice with ethanol, and once with chloroform.

To monitor changes in the surface chemistry after chemical treatment, freshly HF-etched sample has been characterized with XPS and PL spectroscopy (Figure 4.9). After HF etching, there is only a

[61] K. R. William, K. Gupta, M. Wasilik, J. Microelectromech. Syst. **2003**, 12, 761.

single XPS peak at 99.2 eV (Figure 4.9 a) associated to elemental Si, proving the removal of the entire matrix.[62]

(Figure 4.9 b) shows the optical properties of SiNCs before and after HF-etching. The as-prepared oxide-embedded Si nanocrystals exhibit a PL peak at 780 nm. HF etching shifts the PL to lower wavelength (600 nm).

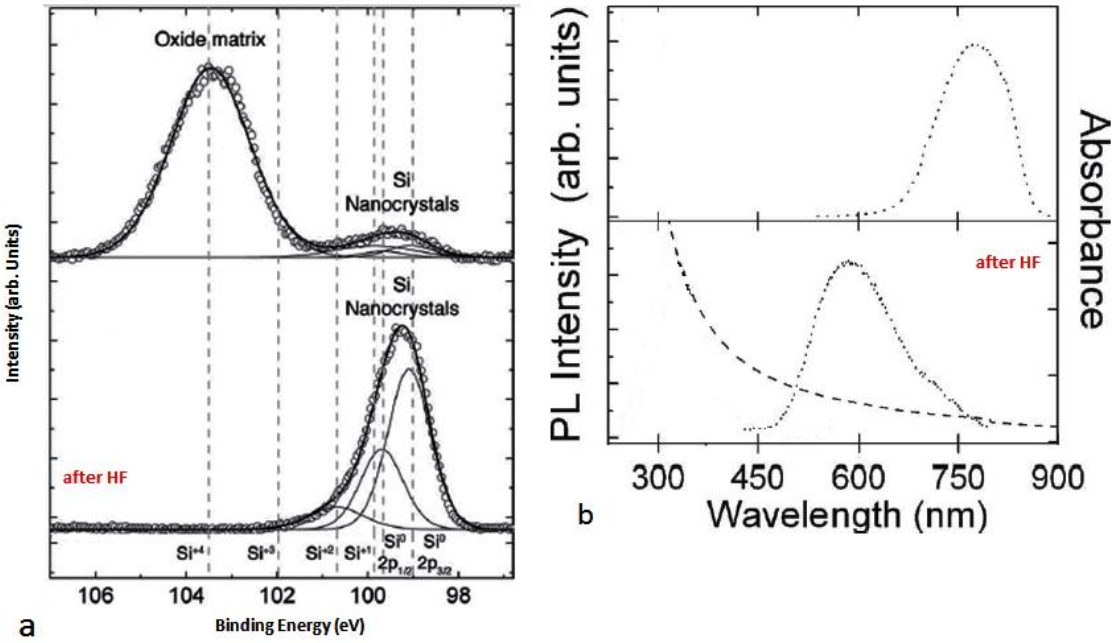

Figure 4.9 a) XPS of oxide embedded SiNCs before and after HF-etching, b) room temperature PL emission (dotted line), PLE (solid line) and UV-Vis absorbance spectra (dashed line) of SiNCs dispersed in $CHCl_3$ before and after etching with λ_{exc} = 320. Reproduce from ref.[55]

[62] C. M. Hessel, M. R. Rasch, J. L. Hueso, B. W. Goodfellow, V. A. Akhavan, J. W. Tunnel, B. A. Korgel, Small **2010**, 18, 2026-2034.

4.4 Covalent functionalization of SiNCs with pyrene units

The freshly hydride-terminated SiNCs are passivated with a mixed ligand layer of 1-dodecene and 1-(allyloxymethyl)pyrene (**Py**). For comparison, SiNCs are also passivated only with 1-dodecene (**SiNC**). In Figure 4.10 the synthesis for **SiNC** and **SiNC-Py** is depicted.

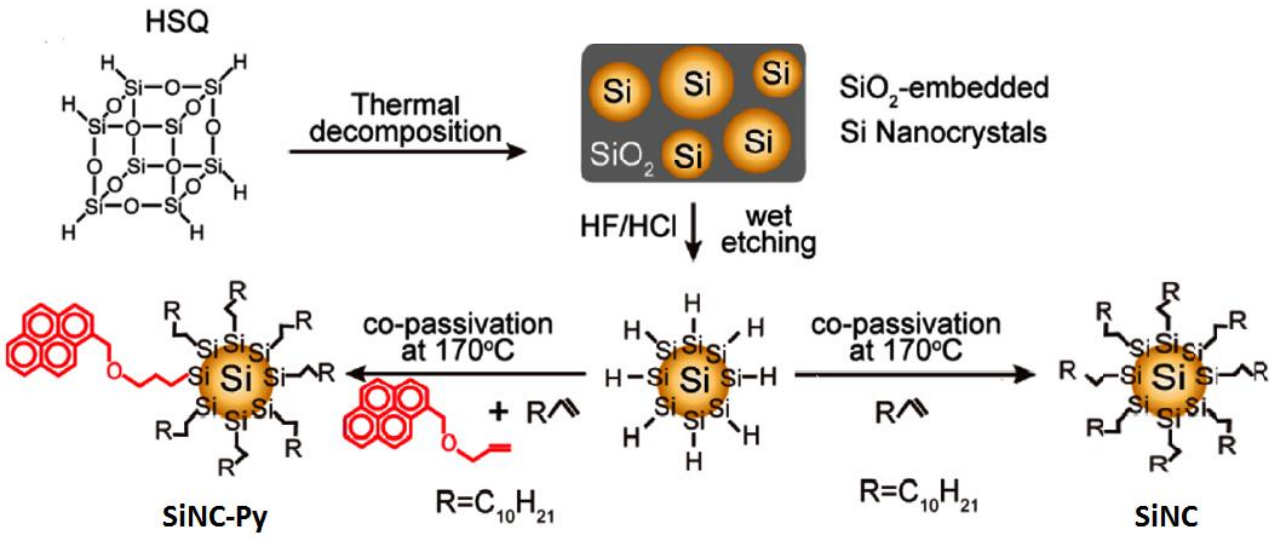

Figure 4.10 Thermal decomposition of HSQ followed by etching and covalent passivation of SiNCs.

4.4.1 Experimental details

1-(allyloxymethyl)pyrene (Py) synthesis: Sodium hydride (0.124 g, 5.16 mmol, 1.2 eq) was added to a mixture of 1-pyrenemethanol (1.00 g, 4.30 mmol, 1eq), propargyl bromide (0.645 g, 5.33 mmol, 1.24 eq) in CH_3CN (25 mL) at 70°C. The reaction mixture was stirred vigorously for 24 h at 70°C. After completion of the reaction, three drops of H_2O were added to the reaction mixture to quench the reaction. The mixture was extracted into chloroform (3 x 5 mL). The chloroform layer was dried over $MgSO_4$ and the solvent was removed under reduced pressure to give the crude product. The resulting residue was purified by silica column chromatography (Hexane/ EtOAc 8:2), to give the product as a yellow solid (750 mg, yield = 66 %).

^{1}H-NMR (400 MHz, $CDCl_3$) δ:8.38 (d, J = 9.2 Hz, 1H); 8.23-8.20 (m, 2H); 8.17-8.13 (m, 2H); 8.08-8.03 (m, 4H); 6.21-6.14 (m, 1H); 5.51 (dd, J1 = 1.6 Hz, J2 = 1.6 Hz, 1H); 5.39 (dd, J1 = 1.6 Hz, J2 = 1.6 Hz, 1H); 5.24 (s, 2H); 4.25-4.23 (m, 2H).

^{13}C-NMR (100 MHz, $CDCl_3$) δ:134.9, 131.4; 131.3; 131.2; 130.8; 129.2; 127.6; 127.4; 127.3; 126.8; 125.8; 125.2; 125.1; 124.9; 124.7; 124.5; 123.3; 117.3; 71.2, 70.6.ESI-MS : 232 $[M- C_3H_5]^+$

SiNC and SiNC-Py Synthesis: The nanocrystals are dispersed in either 5 mL of 1-dodecene, or 5 mL of 1-dodecene with 165 mg of 1-(allyloxymethyl)pyrene (1:36 pyrene:dodecene molar ratio) or 490 mg of 1-(allyloxymethyl)pyrene (1:12 pyrene:dodecene molar ratio). The initially turbid dispersions are put through three freeze-pump-thaw cycles, and then heated to 170°C under N_2 flow for 12 hours. Over time, the dispersions become optically clear, indicating that passivation of Si nanocrystals has occurred. The nanocrystals are then purified by transfer to a glass centrifuge tube and centrifugation at 8000 rpm for 5 min. Poorly-capped nanocrystals precipitate from the mixture and are discarded. The supernatant is transferred to another glass centrifuge tube and washed with four consecutive centrifugation/precipitation cycles using toluene/ethanol solvent/antisolvent pair. The final SiNC and SiNC-Py samples were dispersed in toluene at a concentration of 5 mg/mL until further characterization

NMR spectral characterization

Covalent pyrene functionalization of the **SiNC-Py** is confirmed by ^{1}H and ^{13}C NMR spectroscopy. Figures 4.11-4.14 show ^{1}H and ^{13}C NMR spectra of **Py**, **SiNC**, and **SiNC-Py**. ^{1}H NMR spectra of **SiNC** and **SiNC-Py** (Figure 4.13) with an average diameter of 3.0 nm (Py:dodecene ratio of 1:36 used in the passivation) dispersed in $CDCl_3$ at room temperature provide evidence of a covalently linked surface layer. The ^{1}H NMR spectra of **SiNC** show a uniform chemical environment for the alkyl chains with a single methyl resonance and several distinct methylene resonances. The ^{1}H NMR spectrum of **SiNC-Py** shows additional signals compared to **SiNC** attributable to pyrene moieties. The molar ratio of pyrene appended groups and dodecene alkyl chains on the Si nanocrystals determined by integration of the relevant resonances in the ^{1}H NMR spectra was 1:20, which is close to the Py:dodecene molar ratio (1:36) used in the passivation step.

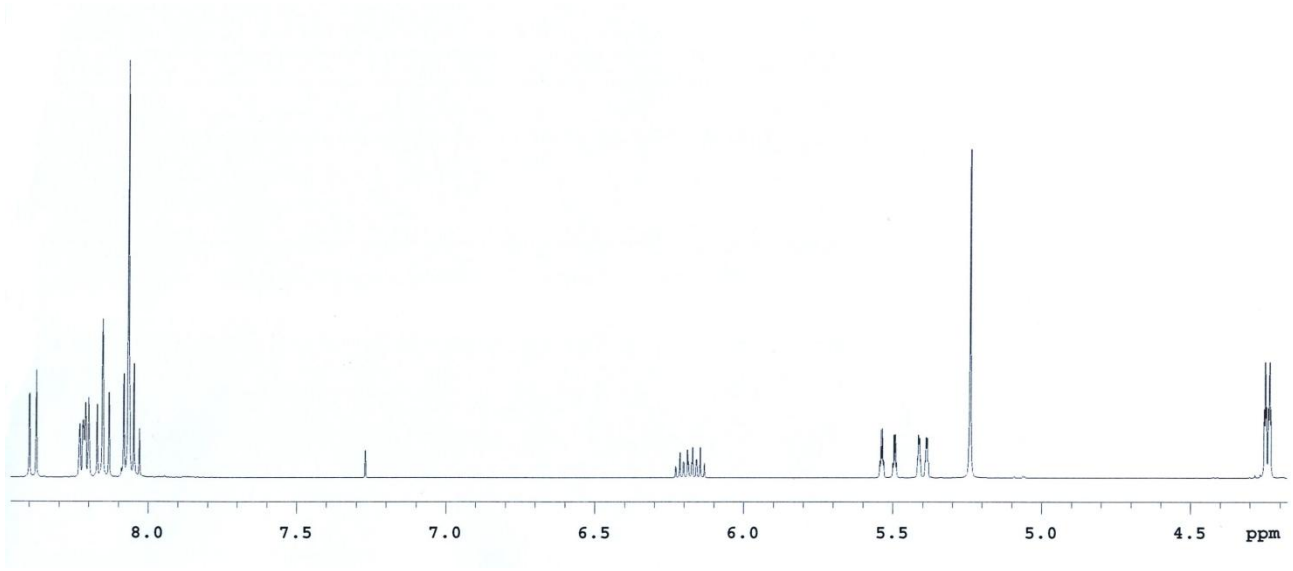

Figure 4.11 ^{1}HNMR ($CDCl_3$): 1-(allyloxymethyl)pyrene

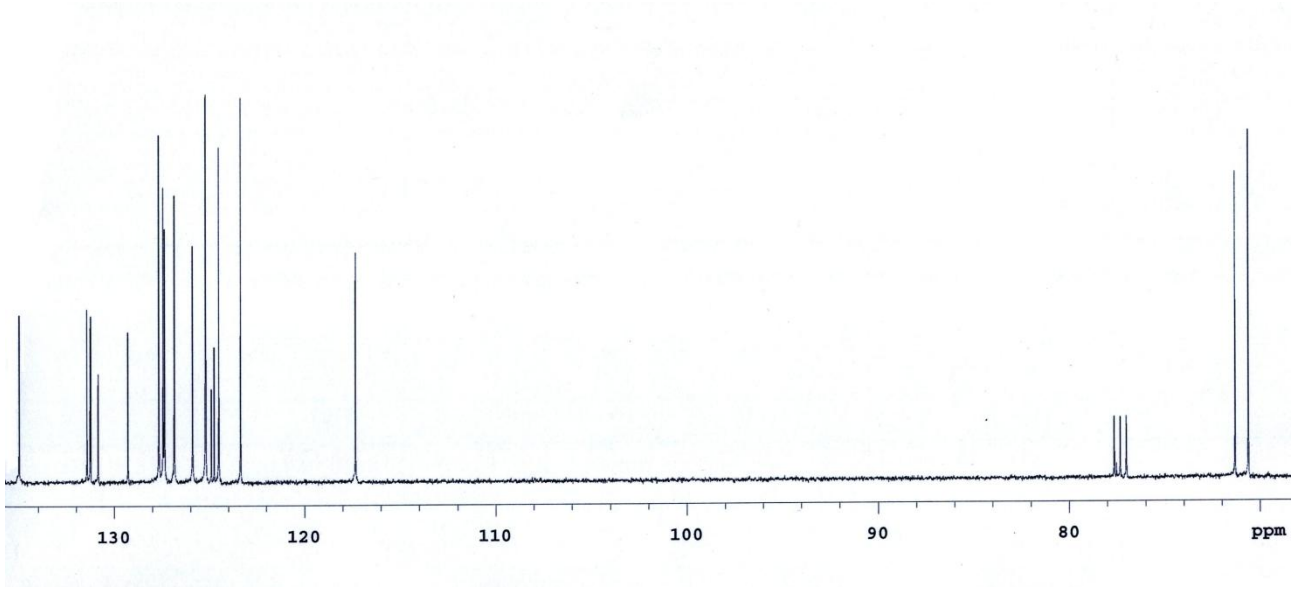

Figure 4.12 ^{13}C NMR ($CDCl_3$): 1-(allyloxymethyl)pyrene

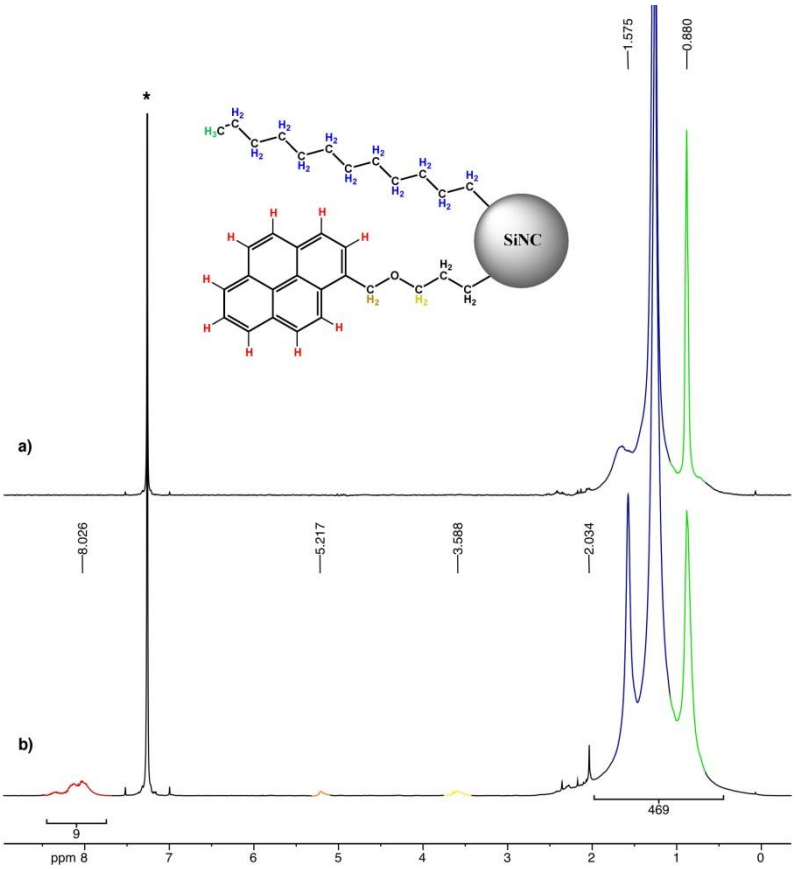

Figure 4.13 ^{1}H NMR spectra (400 MHz, $CDCl_3$, RT) of a) 3.0nm **SiNC** and b) 3.0 nm **SiNC-Py**. Asterisk indicate solvent signal.

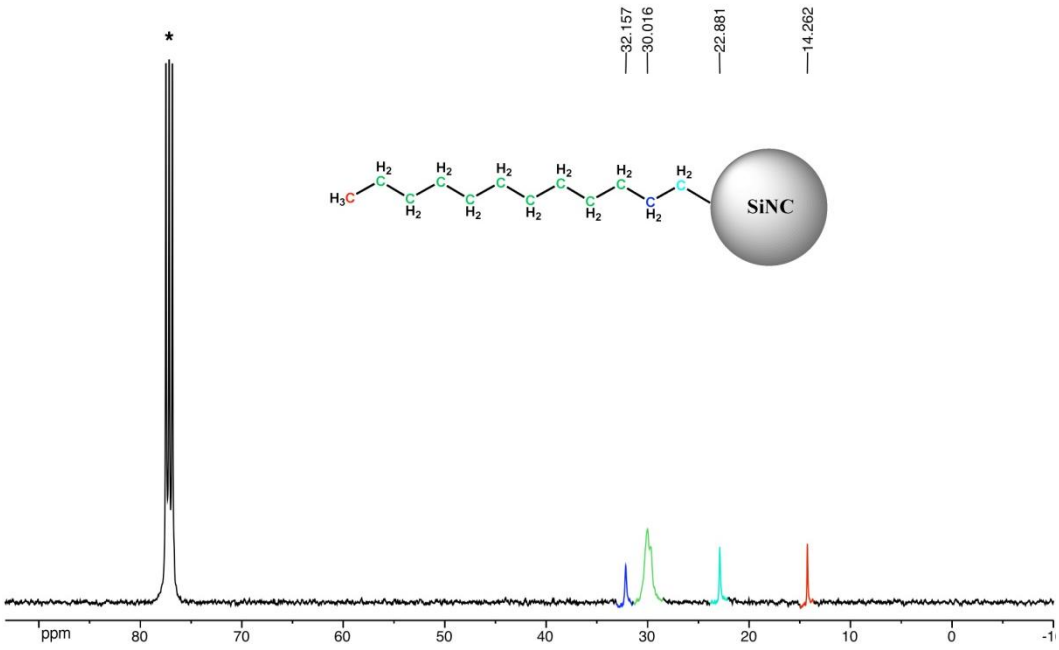

Figure 4.14 ^{13}C NMR spectra (101 MHz, $CDCl_3$, RT) of a) 3.0 nm **SiNC**. Asterisk indicate solvent signal

Transmission electron spectroscopy (TEM) characterization

The average Si core diameter of the nanocrystals was determined by TEM.

Figures 4.15-4.18 show additional TEM images of the 3.0 nm and 5.0 nm diameter **SiNC** and **SiNC-Py** samples used in the studies. There is no significant difference in size upon Py functionalization.

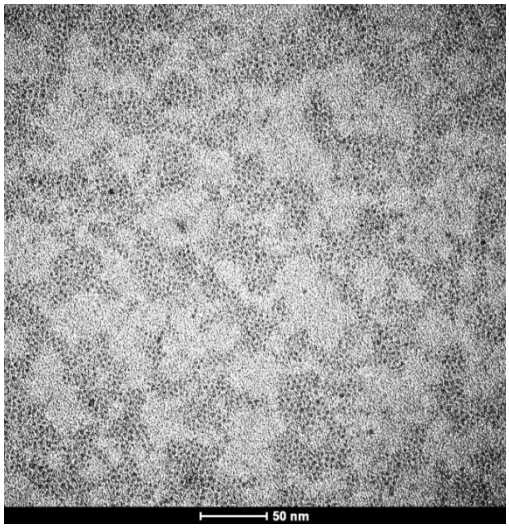

Figure 4.15 TEM image of 3.0 nm diameter **SiNC-Py**.

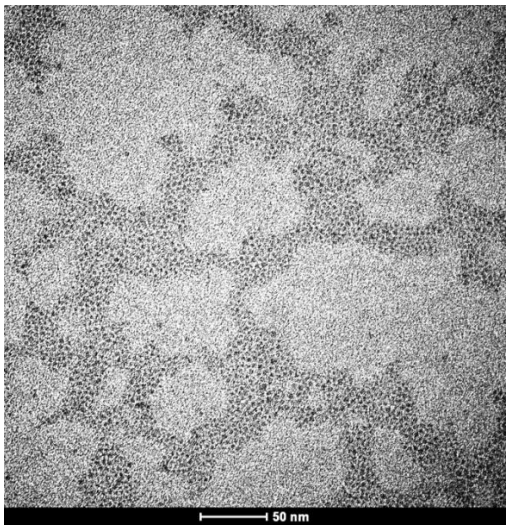

Figure 4.16 TEM image of 3.0 nm diameter **SiNC.**

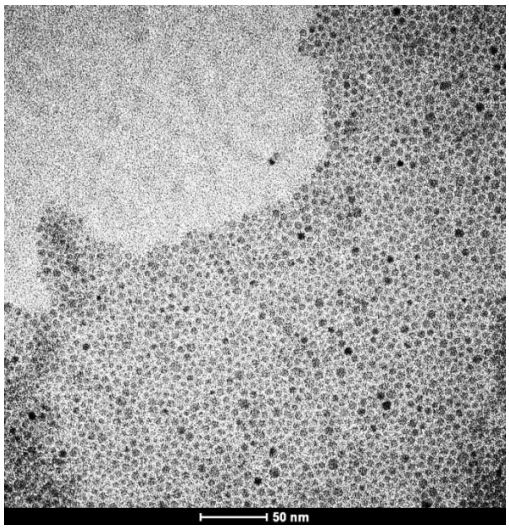

Figure 4.17 TEM image of 5.0 nm diameter **SiNC-Py**.

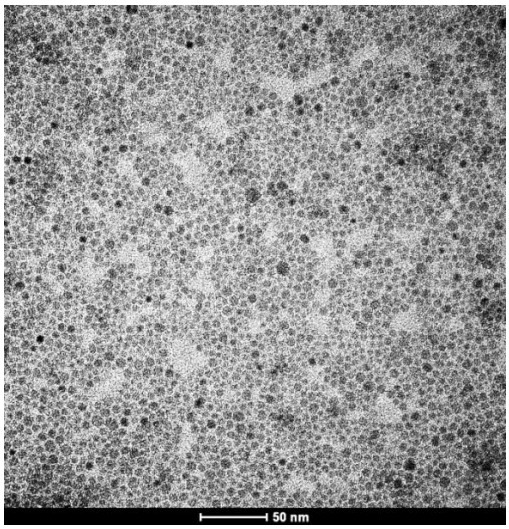

Figure 4.18 TEM image of 5.0 nm diameter **SiNC**.

4.5 Results and Discussion

Optical properties of functionalized SiNCs

Figure 4.19 shows the comparison of optical properties between **SiNC** and **SiNC-Py** of 3.0 nm in toluene dispersion.

The sample control **SiNC** (without pyrene derivatization) exhibits an unstructured absorption profile that tails past 500 nm that is characteristic of SiNCs (blue curve in Figure 4.19 a).[63]

The free chromophore **Py** (dotted line 4.19 a) has a structured absorption band with three distinctive peaks in the 300–350 nm region. The contribution of pyrene is highlighted by the presence of peaks in the **SiNC-Py** absorbance spectra (red curves in Figure 4.19 a). The number of pyrene units attached to each SiNC can be estimated from the relative absorbance of the featureless sloping background associated with the SiNCs and the peaked absorption from the pyrene.

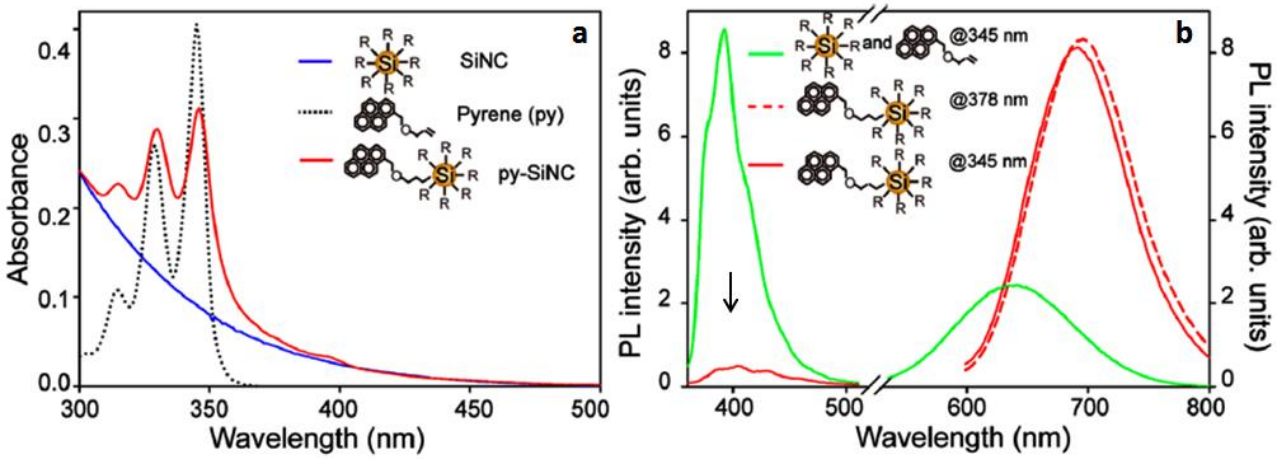

Figure 4.19 a) absorption profile of 3.0 nm diameter **SiNC** (blue line), **Py** (black dotted line), **SiNC-Py** (red line) in air-equilibrated toluene, b) photoluminescence spectra of **SiNC-Py** (solid red line, λ_{ex} = 345 nm; dashed red line, λ_{ex} = 378 nm) and optically matched solutions of free **Py** mixed with **SiNC** in the appropriate ratio (green lines, λ_{ex} = 345 nm) in air-equilibrated toluene. To obtain the PL spectra in (b) the two samples of SiNC-Py photoexcited at 345 and 378 nm are optically matched at the excitation wavelength to enable direct comparison of the emission intensity of the SiNCs when light absorption is dominated by the pyrene moieties or the nanocrystals. In (b) the y-axes on the left correspond to the pyrene-related emission, and the y-axes on the right correspond to the SiNC-related emission.

On the basis of the molar absorption coefficients for Py and 2.6 nm diameter SiNCs, ($\varepsilon_{346\ nm}$(Py) = 4.4 × 10^4 M^{-1} cm^{-1}, $\varepsilon_{400\ nm}$($SiNC_{3.0\ nm}$) = 5 × 10^4 M^{-1} cm^{-1},[64] there are approximately eight and six

[63] Hessel C. M., Reid D., Panthani M. G., Rasch M. R., Goodfellow B. W., Korgel B. A., Chem. Mater. **2012**, 24, 393-401.
[64] Hessel C. M., Reid D., Panthani M. G., Rasch M. R., Goodfellow B. W., Korgel B. A., Chem. Mater. **2012**, 24, 393-401.

pyrene units per nanocrystal for 3.0 nm diameter SiNC-Py made with Py/dodecene ratios of 1:12 (red curve in Figure 4.20 a) and 1:36 (green curve in Figure 4.20 b).

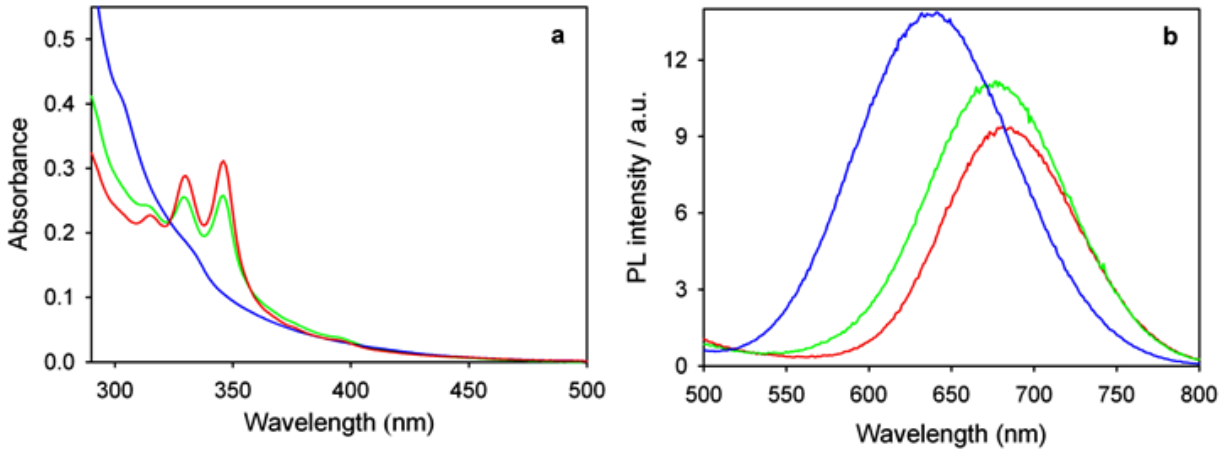

Figure 4.20 (a) Absorbance and (b) photoluminescence spectra (λ_{ex} = 378 nm) of 3.0 nm diameter **SiNC** (blue) and **SiNC-Py** made with pyrene:dodecene molar ratios of 1:12 (red line) and 1:36 (green line) dispersed in air-equilibrated toluene. The solutions are optically matched at the excitation wavelength.

Figure 4.19 b shown the PL spectra of the **SiNC-Py** samples and **SiNCs** mixed with free pyrene. The emission of pyrene at ~400 nm is observed both when it's free in solution and when it's attached to the SiNCs. There is no evidence of **Py** excimer emission, which would occur at a longer wavelength close to 500 nm. The emission of the 3.0 nm nanocrystals was slightly red-shifted from 635 to 680 nm after pyrene passivation (Figure 4.20 b).

To study the influence of the size and chemical surface to optical properties, SiNCs with diameter of 5 nm have also been synthesized.

UV–vis–NIR absorbance and photoluminescence (PL) spectra of toluene dispersions of the 5.0 nm diameter **SiNC** and **SiNC-Py** are shown in Figure 4.21.

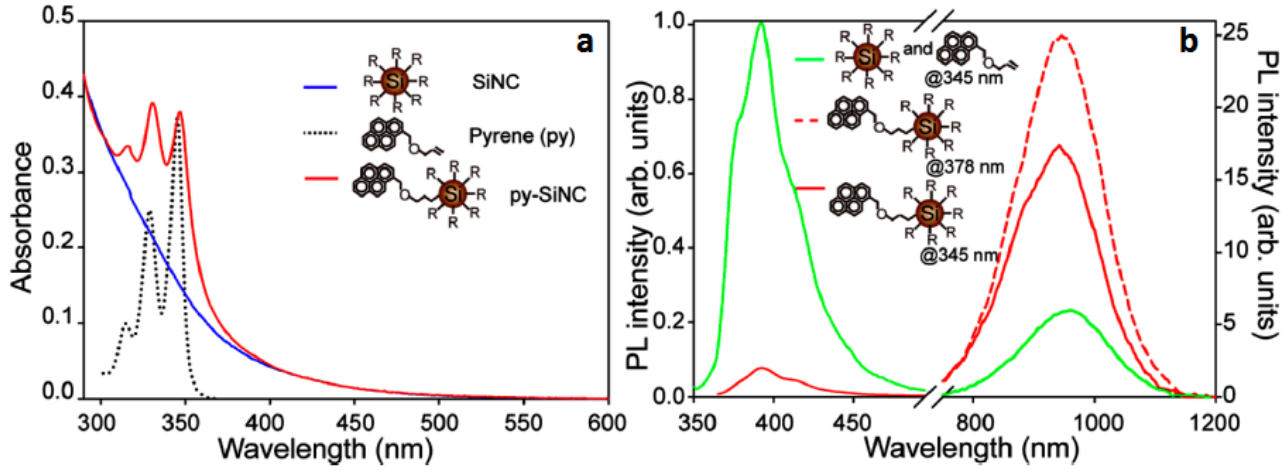

Figure 4.21 a) absorption profile of 5 nm diameter **SiNC** (blue line), **Py** (black dotted line), **SiNC-Py** (red line) in air-equilibrated toluene, b) photoluminescence spectra of **SiNC-Py** (solid red line, λ_{ex} = 345 nm; dashed red line, λ_{ex} = 378 nm) and optically matched solutions of free **Py** mixed with **SiNC** in the appropriate ratio (green lines, λ_{ex} = 345 nm) in air-equilibrated toluene. To obtain the PL spectra in (b) the two samples of SiNC-Py photoexcited at 345 and 378 nm are optically matched at the excitation wavelength to enable direct comparison of the emission intensity of the SiNCs when light absorption is dominated by the pyrene moieties or the nanocrystals. In (b) the y-axes on the left correspond to the pyrene-related emission, and the y-axes on the right correspond to the SiNC-related emission.

The increment of the core size causes a red shift of PL properties. **SiNCs** exhibit photoluminescence emission peak at 970 nm (green line in Figure 4.21 b). In this case, pyrene functionalization does not significantly affect the PL maxima of the **SiNC-Py** (red line in Figure 4.21 b). The estimate number of pyrene units on the basis of the molar absorption coefficients ($\varepsilon_{346\ nm}(Py) = 4.4 \times 10^4\ M^{-1}\ cm^{-1}$, $\varepsilon_{400\ nm}(SiNC_{5.0\ nm}) = 5.3 \times 10^5\ M^{-1}\ cm^{-1}$) is about 60 Py units per nanocrystal on the 5.0 nm **SiNC-Py**.

To selectively photoexcite the SiNC core or the ligand, PL emission spectra were measured with excitation wave-lengths of either λ_{ex} = 378 or 345 nm.

At 378 nm **Py** does not absorb the light while at 345nm the majority of the light is absorbed by pyrene, indeed, pyrene absorbs 67% of the 345 nm light in the case of the 3.0 nm diameter **SiNC-Py**.

To evaluate the entity of energy transfer, the PL spectra of **SiNC-Py** samples in Figure 4.19 b and Figure 4.21 b were measured at the excitation wavelengths of 378 and 345 nm with the same photon absorption by optically matching the **SiNC-Py** dispersions by dilution.

Furthermore, PL spectra were measured for **SiNCs** mixed with free **Py** in the appropriate ratios to match the **SiNC-Py** absorbance profiles (the green curves in Figure 4.19 b and 4.21 d). When **Py** is not attached to the nanocrystals, photoexcitation at 345 nm leads to emission spectra dominated by the 400 nm emission of pyrene, with a lesser contribution of SiNC emission at longer wavelength (green curves in Figure 4.19 b and 4.21 d).

In contrast, photoexcitation of the **SiNC-Py** dispersions with 345 nm light leads predominantly to emission from the nanocrystals with very little pyrene emission. The Py-related emission band is largely quenched for both the 3.0 and 5.0 nm diameter **SiNC-Py** samples, indicative of energy transfer (figure 4.22)

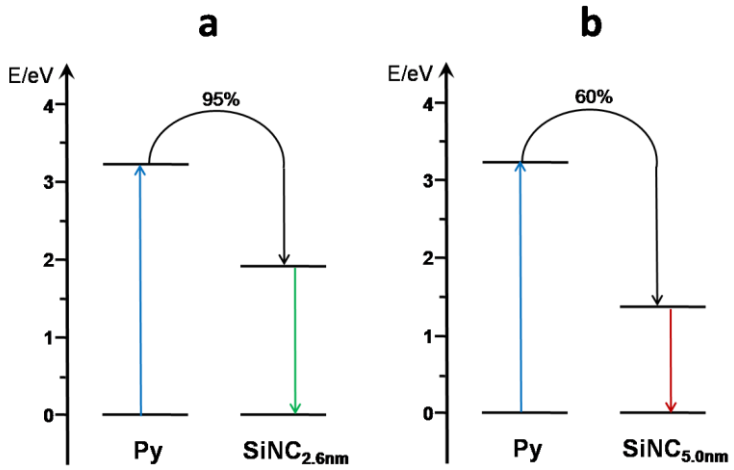

Figure 4.22 Energy level diagram showing the energy transfer processes and the corresponding efficiency occurring in **SiNC-Py** of diameter 3.0 (a) and 5.0 nm (b) upon photoexcitation of the pyrene units.

Photoluminescence excitation (PLE) spectra measured by detecting only the long-wavelength emission from the SiNCs are further consistent with energy transfer between the attached Py moieties and the SiNCs in the **SiNC-Py** samples with the appearance of a peaked pyrene-related absorption band (Figure 4.23).

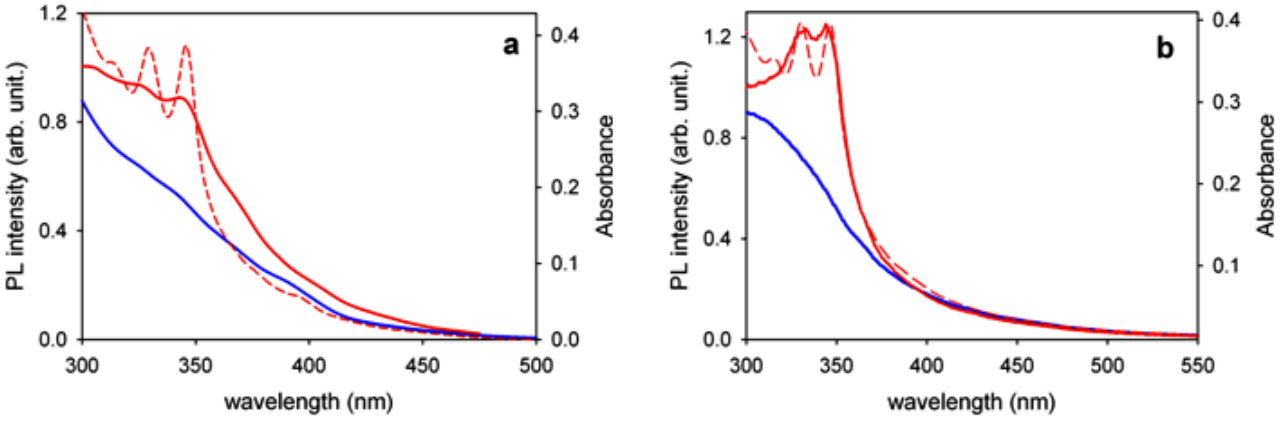

Figure 4.23 Photoluminescence excitation (PLE) spectra of (a) 3.0 nm and (b) 5.0 nm diameter **SiNC-Py** (red solid line) and **SiNC** (blue solid line) recorded with (a) λ_{em} = 660 and (b) 780 nm. For comparison purposes, the absorption spectra of **SiNC-Py** are reported (red dashed line).

The measurement of the lifetime of the Py-related 400 nm fluorescence, confirms the energy transfer from pyrene to SiNCs in the **SiNC-Py** sample.

The characteristic lifetime for emission from the free chromophore is about 18 ns.

The emission intensity decay of **SiNC-Py** at 400 nm cannot be fitted to a monoexponential function; one component is below our instrumental resolution (<0.2 ns), and the second one is ~5 ns (Figure 4.24).

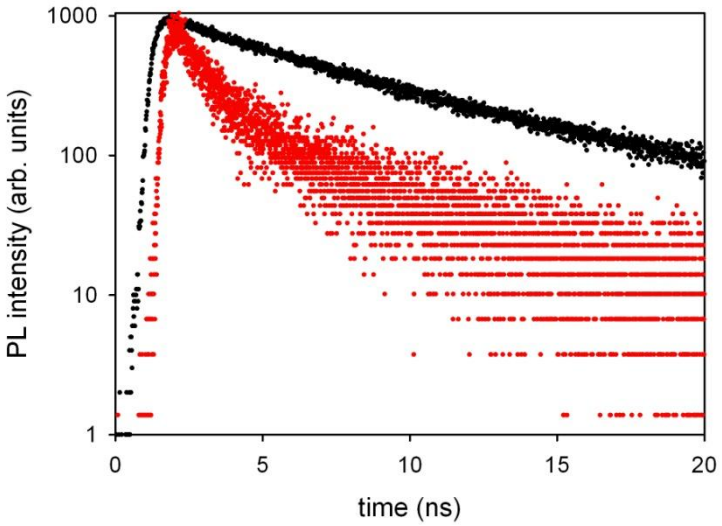

Figure 4.24 Photoluminescence intensity decay at 400 nm (λ_{ex} = 345 nm) of 3.0 nm diameter **SiNC-Py** made with pyrene:dodecene molar ratios of 1:12 (red trace) and Py (black trace) in air-equilibrated toluene.

The shorter lifetimes are consistent with energy transfer from the bound Py to the SiNCs and further confirm that the (limited) PL observed at 400 nm from the **SiNC-Py** sample excited at 345 nm is not due to free pyrene in solution.

The energy transfer efficiency from bound Py to the SiNCs in the **SiNC-Py** was calculated by comparing the SiNC-related PL quantum yields obtained with 345 and 378 nm photo-excitation.

The PL emission quantum yield of the 3.0 nm diameter **SiNCs** was 16% (both in aerated and deaerated solution) with a lifetime of 70 µs (Figure 4.25).

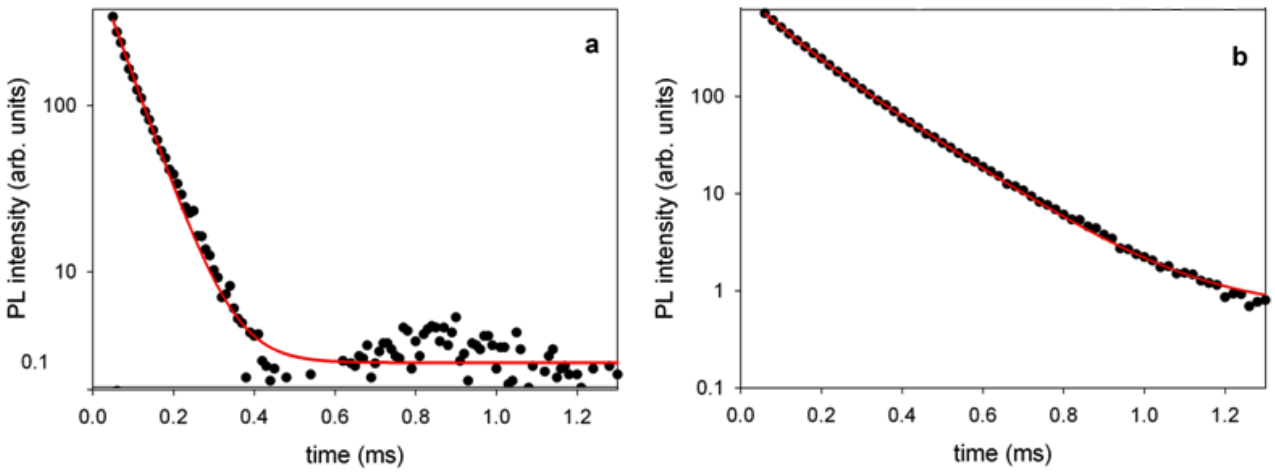

Figure 4.25 Photoluminescence intensity decay at (a) 635 nm and (b) 970 nm for **SiNC** with diameters of 3.0 and 5.0 nm, respectively, dispersed in air-equilibrated toluene. (λ_{ex}=400 nm).

For the 3.0 nm diameter **SiNC-Py**, the SiNC-related PL quantum yields (680 nm emission) were nearly independent of the photoexcitation wavelength, 345 nm (solid red line in Figure 4.19 b, predominantly Py photoexcitation) or 378 nm (dashed red line in Figure 4.19 b, the light was adsorbed only by the SiNC core).

Energy transfer from the pyrene chromophores to the 3.0 nm diameter Si core in the **SiNC-Py** sample took place with >95% efficiency.[65]

The efficiency of energy transfer has been estimated from the spectra reported in Figures 4.19 b and 4.21 b, as detailed in the following:

$$\eta_{en.tr.} = (I_{obs}-I_0)/(I_{100}-I_0)$$

Where:

I_{obs} is the area of the emission spectra observed for the **SiNC-Py** excited at 345 nm (dashed red line in Figures 4.19 b and 4.21 b), in which both pyrene and the Si core absorb light;

I_0 is the area of the emission spectrum observed for the mixture of **SiNC** and **Py** in a proper ratio to match the absorbance spectrum of the previous solution in the entire range (green line in Figures 4.19 b and 4.21 b);

I_{100} is the area of the emission spectra observed for **SiNC-Py** excited at 378 nm (solid red line in 4.19 b and 4.21 b), in which only the Si core is absorbing light, for a solution having the same absorbance at the excitation wavelength of the first case.

I_0 represents the emission intensity expected when energy transfer does not take place and the Si core emission is obtained only by the light at 345 nm directly absorbed by the Si core. I_0 has been corrected to take into account the different emission quantum yield of the Si core upon direct excitation of the silicon core for **SiNC** and **SiNC-Py**, i.e. 0.45 vs 0.40 for 5.0 nm diameter nanoparticles, respectively (Table 4.1).

I_{100} represents the emission intensity expected when energy transfer takes place with 100% efficiency and all the absorbed light results in the Si core emission

[65] Balzani V., Ceroni P., Juris A., Photochemistry and Photophysics: Concepts, Research, Applications; Wiley-VCH: Weinheim, Germany, **2014**, Chapter 6.

Because of the much stronger light absorption of Py compared to that of the SiNCs at 345 nm, Py functionalization led to a nearly 300% brightness enhancement in SiNC PL.

Pyrene emission was also strongly quenched (>90%) in the 5.0 nm diameter **SiNC-Py** sample (red curve, Figure 4.21 b), and the **SiNC** and **SiNC-Py** species exhibited PL quantum yields at 970 nm of 45 and 40%, respectively.

The 970 nm PL emission was insensitive to dioxygen, and the luminescence decays of the SiNC and SiNC-Py were fit to monoexponential functions with lifetimes of 150 and 190 μs, respectively. The emission quantum yield was high compared to that of dye molecules emitting in the same spectral region,[66] for which emission quantum yields higher than 30% have never been reported, to the best of our knowledge, and it is comparable to the value recently reported for PbS and PbSe quantum dots.[67]

On the basis of the relative PL emission spectra for 5.0 nm diameter **SiNC-Py** photoexcited with 345 nm (dashed red curve in Figure 4.21 b) and 378 nm light (solid red curve in Figure 4.21 b), energy transfer from adsorbed pyrene to the SiNCs occurred with 65% efficiency.

With the three-fold enhancement in light absorption due to the adsorbed pyrene, a 40% PL quantum yield, and a 65% energy transfer efficiency from the pyrene to the SiNCs, there was an effective enhancement in NIR PL brightness of 78%.

Table 4.1 summarizes the photophysical properties of **SiNC** and **SiNC-Py** dispersed in air-equilibrated toluene at 298 K along with the model compound **Py** for comparisonspecies studied here.

	d/nm	λ_{ex}/nm	λ_{em}/nm	Φ_{em}[a]	τ/ns[b]
SiNC	**3.0**	**378**	**635**	**0.11**	**70 x 10^3**
SiNC-Py	**3.0**	**345**	**400**	**0.005**	**<0.2, 5**
		378	**680**	**0.08**	**95 x 10^3**
Py		**345**	**400**	**0.06**	**18**
SiNC	**5.0**	**378**	**970**	**0.45**	**150 x 10^3**
SiNC-Py	**5.0**	**345**	**400**	**0.005**	**<0.2, 5**
		378	**970**	**0.40**	**190 x 10^3**

[a]Experimantal error: 10%. [b]Experimental error: 5%.

[66] Wurth C. Pauli, J. Lochmann, C. Spieles, M. Resch-Genger, Anal. Chem. **2012**, 84, 1345–1352.

[67] Semonin O. E., Johnson J. C., Luther J. M., Midgett A. G., Nozik A. J., Beard M. C., J. Phys. Chem. Lett. **2010**, 1, 2445–2450.

4.6 Conclusion

This work demonstrates that SiNCs are a viable scaffold for light-harvesting antenna.

Energy transfer between adsorbed pyrene units and SiNCs occurs with relatively high efficiency, and pyrene functionalization does not deteriorate the SiNC PL properties. These materials represent a family of nanocrystals with significantly enhanced PL brightness as a result of the attachment of light-harvesting antenna that promote light emission from the nanocrystals as a result of energy transfer. The PL brightness of the 3.0 nm diameter nanocrystals is enhanced by nearly 300%. The 5.0 nm diameter SiNC-Py exhibits UV-sensitized NIR luminescence with high emission quantum yield and long lifetime (Table 1), even in the presence of dioxygen.

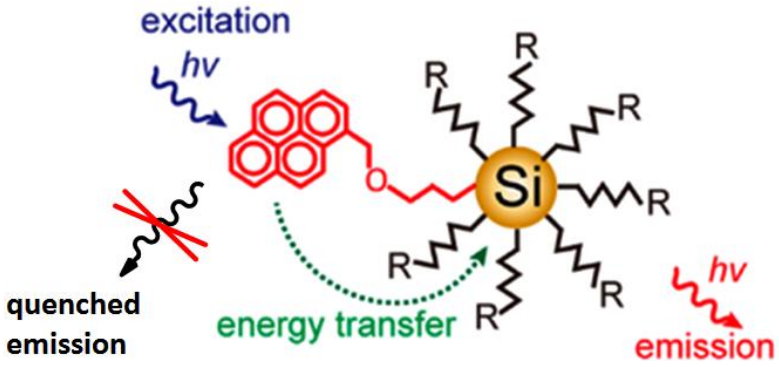

Chapter 5

Interaction between pyrene-functionalized Silicon nanocrystals and carbon allotropes

5.1 Introduction

Here, we study the effect of the distance between the chromophore and the Si nanocrystal core on the sensitized light emission of the Si core.

Silicon nanocrystals with average core diameter of 3 and 5 nm were passivated with dodecene by thermal hydrosilylation and coupled to pyrene (Py) derivative molecules with C_{11} (**SiNC(C_{11})Py**) or C_3 alkyl tethers (**SiNC(C_3)Py**) via a terminal alkene (Figure 5.1). We also studied the electronic interactions of these nanocrystals associated with carbon allotropes: C_{60}, single-walled carbon nanotubes (SWCNTs), and graphene. Additional energy transfer processes were found to occur from the SiNC to these carbon materials.

5.2 Thermal hydrosililation of SiNCs with 1-(allyloxymethyl)pyrene (C_3) and 1-((undec-10-en-1-yloxy)methyl)pyrene (C_{11})

Through the thermal reduction of HSQ and etching with a solution of HF and HCl, hydride-terminated SiNCs have been synthesized as described in the Chapter 4.

The SiNCs were functionalized by thermal hydrosilylation with a combination of ligands: 1-dodecene and pyrene chromophore (Py) binds different alkyl length chains (Figure 1).

To evaluate the influence of the chromophore on optical properties, SiNCs were also passivated with only 1-dodecene (**SiNC**).

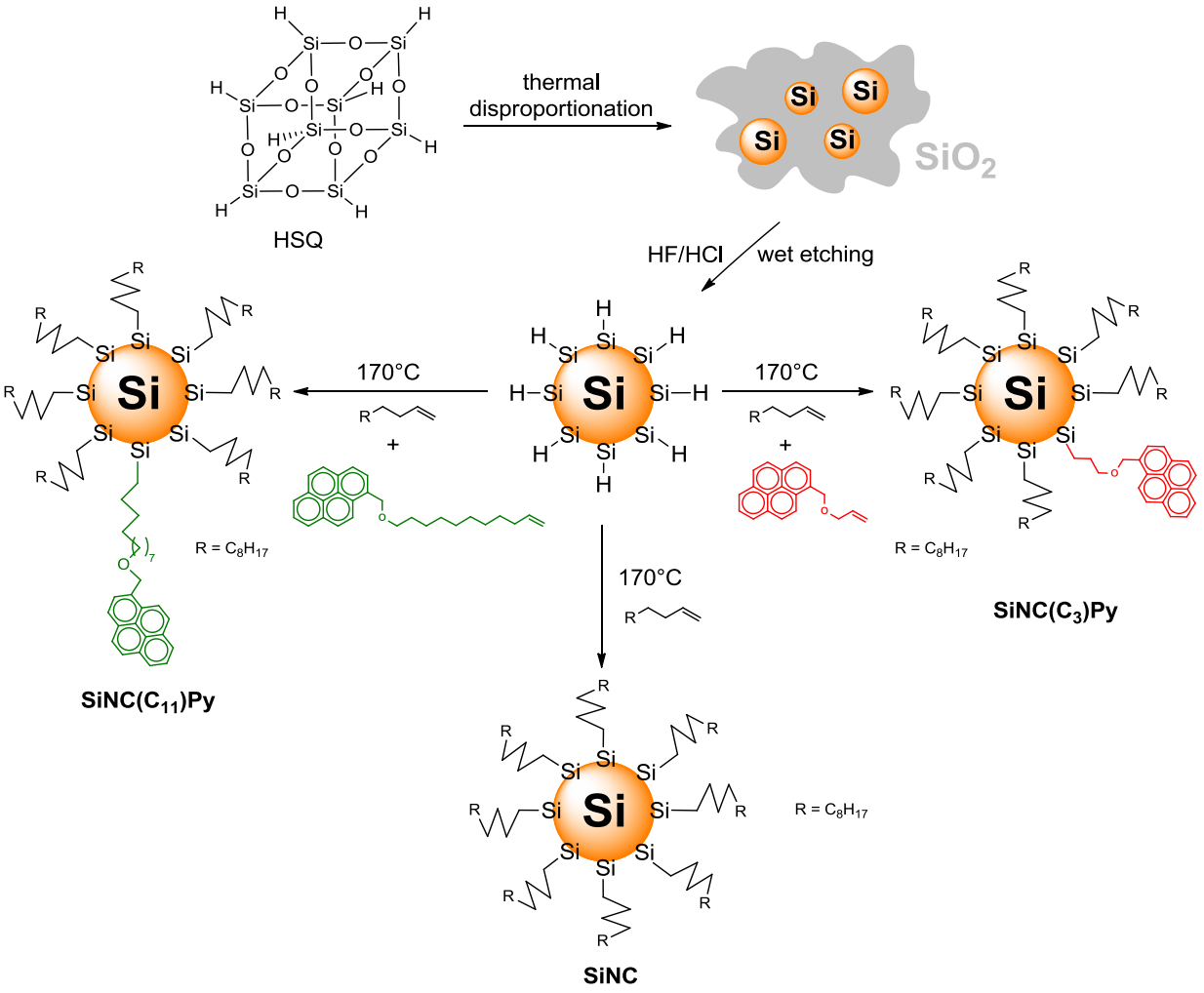

Figure 5.1

5.2.1 Experimental details

Materials: hydrofluoric acid (48% in H_2O), 1-dodecene, 1-pyrenemethanol, sodium hydride, 11-bromide-1-undecene were purchased from Sigma Aldrich.

1-(allyloxymethyl)pyrene (Py) synthesis: Sodium hydride (0.124 g, 5.16 mmol, 1.2 eq) was added to a mixture of 1-pyrenemethanol (1.00 g, 4.30 mmol, 1eq), propargyl bromide (0.645 g, 5.33

mmol, 1.24 eq) in CH_3CN (25 mL) at 70°C. The reaction mixture was stirred vigorously for 24 h at 70°C. After completion of the reaction, three drops of H_2O were added to the reaction mixture to quench the reaction. The mixture was extracted into chloroform (3 x 5 mL). The chloroform layer was dried over $MgSO_4$ and the solvent was removed under reduced pressure to give the crude product. The resulting residue was purified by silica column chromatography (Hexane/ EtOAc 8:2), to give the product as a yellow solid (750 mg, yield = 66 %).

^{1}H-NMR (400 MHz, $CDCl_3$) δ:8.38 (d, J = 9.2 Hz, 1H); 8.23-8.20 (m, 2H); 8.17-8.13 (m, 2H); 8.08-8.03 (m, 4H); 6.21-6.14 (m, 1H); 5.51 (dd, J1 = 1.6 Hz, J2 = 1.6 Hz, 1H); 5.39 (dd, J1 = 1.6 Hz, J2 = 1.6 Hz, 1H); 5.24 (s, 2H); 4.25-4.23 (m, 2H).

^{13}C-NMR (100 MHz, $CDCl_3$) δ:134.9, 131.4; 131.3; 131.2; 130.8; 129.2; 127.6; 127.4; 127.3; 126.8; 125.8; 125.2; 125.1; 124.9; 124.7; 124.5; 123.3; 117.3; 71.2, 70.6.ESI-MS : 232 $[M- C_3H_5]^+$

Synthesis of 1-((undec-10-enyloxy)methyl)pyrene. To a mixture of 1-pyrenemethanol (1.00 g, 4.30 mmol, 1eq), 11-bromide-1-undecene (1.504 g, 6.45 mmol, 1.5 eq) in CH_3CN (25 mL) was added sodium hydride (0.124 g, 5.16 mmol, 1.2 eq) at 80 °C. The reaction mixture was stirred vigorously for 48 h at 70°C. After completion of the reaction, three drops of H_2O were added to quench the reaction. The mixture was extracted (3 × 5 mL) with chloroform. The chloroform layer was dried over $MgSO_4$ and the solvent was removed under reduced pressure to give the solid crude product. The resulting residue was purified by silica column chromatography (hexane/ AcOEt 8:2), to give the product as a yellow solid (yield = 80 %). ^{1}H-NMR (400 MHz, $CDCl_3$) δ: 8.41 (d, J = 9.2 Hz, 1H); 8.24-8.20 (m, 2H); 8.19-8.14 (m, 2H); 8.10-8.04 (m, 4H); 6.02-6.04 (m, 1H); 5.23 (s, 2H); 5.08 (d, J = 17.2 Hz, 1H); 5.03 (d, J = 10.4, 1H); 3.64 (t, J = 6.4 Hz, 2H); 2.13-2.07 (m, 2H); 1.75-1.69 (m, 2H); 1.42-1.40 (m, 4H); 1.53-1.30 (m, 8H). 13C-NMR (100 MHz, $CDCl_3$) δ: 139.0, 131.7; 131.1; 131.0; 130.6; 129.1; 127.3; 127.2; 127.0; 126.6; 125.6; 124.9; 124.7; 124.6; 124.2; 123.3; 114.0; 71.2; 70.3; 33.7; 29.7; 29.4; 29.3; 29.0; 28.2; 26.1. ESI-MS : 407 [M + Na]; 215 $[M- C_{11}H_{21}O]^+$

SiNC, SiNC(C_3)Py and SiNC(C_{11})Py synthesis. The synthetic procedure follows the method developed by Hessel, et al.[68] Generally, 40 mL of Fox-16 (hydrogen silsesquioxane 16 wt%) is dried under vacuum and the resulting white solid is then transferred to a tube furnace and annealed at

[68] Hessel C. M., Henderson E. J., Veinot J. G. C., Chem. Mater. **2006**, 18, 6139-6146.

1100°C (3.0 nm diameter) or 1200°C (5.0 nm diameter) at a heating rate of 18°C/min and held at that temperature for an hour under reducing atmosphere (93% N_2, 7% H_2).

The SiNC/SiO_2 composite is etched with 48% HF and 37.5% HCl (10:1 v/v) in the dark for 4-6 hours and then centrifuged at 8000 rpm for 5 min. The H-terminated SiNCs are then rinsed once with deionized (DI) water, twice with ethanol, and once with chloroform. The nanocrystals are dispersed in 5 mL of 1-dodecene with 490 mg of 1-(allyloxymethyl)pyrene (1:12 pyrene:dodecene molar ratio) to obtain **SiNC(C_3)Py** sample, in 5 mL of 1-dodecene to have **SiNC** and 4 mL of 1-dodecene with 250 mg of 1-((undec-10-en-1-yloxy)methyl)pyrene (1:27 pyrene:dodecene molar ratio) for **SiNC(C_{11})Py**. The initially turbid dispersions are put through three freeze-pump-thaw cycles, and then heated to 170°C under N_2 flow for 12 hours. Over time, the dispersions become optically clear, indicating that passivation of Si nanocrystals has occurred. To purify the nanocrystals, the solutions are transferred to a glass centrifuge tube, spin at 8000 rpm for 5 min and discard the precipitate (poorly capped SiNCs) on the bottom. The supernatant is transferred to another glass centrifuge tube and undergoes many centrifugation/precipitation cycles using toluene/ethanol solvent/antisolvent pair. The final **SiNC**, **SiNC(C_3)Py**, **SiNC(C_{11})Py** samples were dispersed in toluene at a concentration of 3-5 mg/mL until further characterization.

5.3 Material characterization

Transmission electron spectroscopy (TEM) characterization

The nanocrystals were synthesized at either 1100°C or 1200°C to obtain different sizes. The average diameters were determined by TEM of 2.9±0.7 nm and 5.3±2.0 nm, respectively (Figure 5.2).

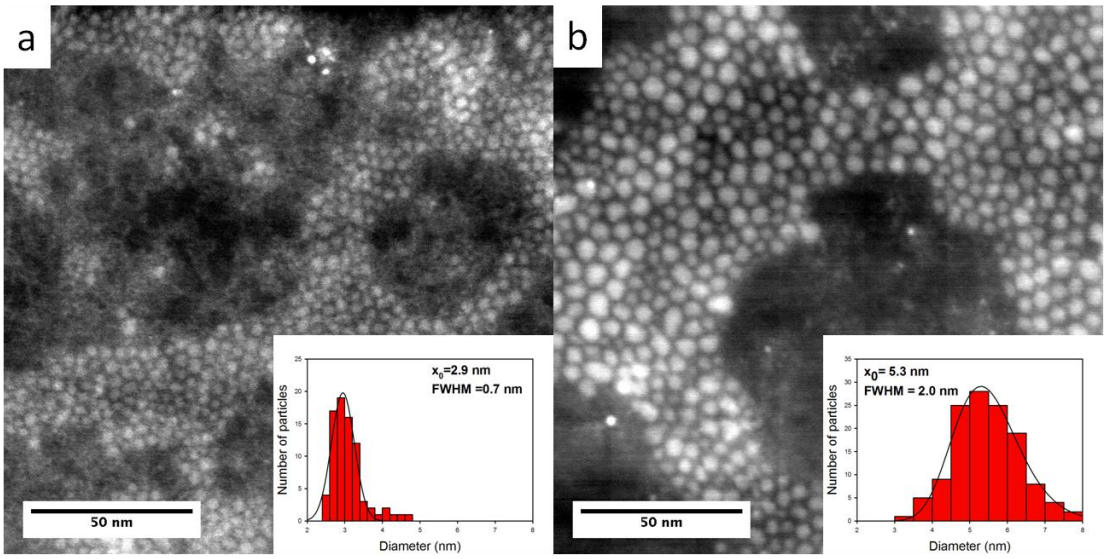

Figure 5.2 STEM-HAADF micrographs of two families of **SiNC(C_{11})Py** nanocrystals, with nominal diameters of 3 nm (a) and 5 nm (b). In the inset the size distribution histograms are obtained by manually measuring the size of the nanocrystals. Histograms are fitted with a Lognormal distribution, and the mean value and the FWHM of the distributions, of 2.9 and 5.3 nm respectively, are reported.

X-ray diffraction (XRD)

Figure 5.3 shows X-ray diffraction of **SiNC(C_{11})Py** of 3 and 5 nm. Both samples present narrow peaks at 28°, 48°, 56° corresponding to reflections from the (111), (220) and (311) crystallographic planes of diamond cubic Si (PDF # 027–1402, a=b=c=5.43088 Å).

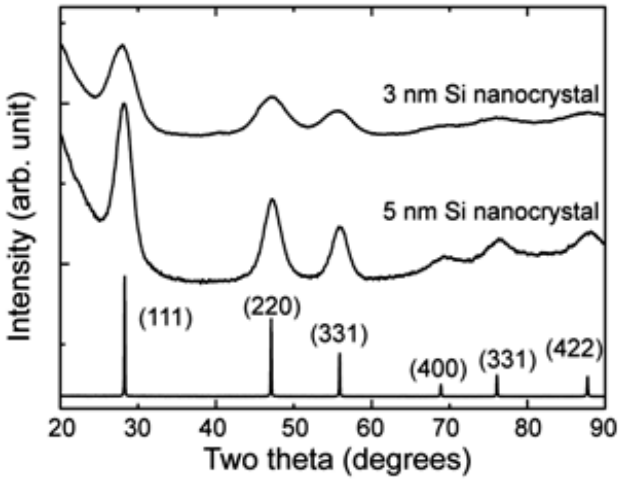

Figure 5.3 XRD (λ=0.154 nm). A reference diffraction pattern is provided for diamond cubic Si in (a) (PDF # 027–1402, a=b=c=5.43088 Å).

X-ray photoelectron spectroscopy

X-ray photoelectron spectroscopy (XPS) confirms the covalent functionalization of **SiNC(C_{11})Py** (3 and 5 nm) with the peak at 102 eV corresponding to the formation of Si-C bonds on the nanocrystals surface (Figure 5.4).

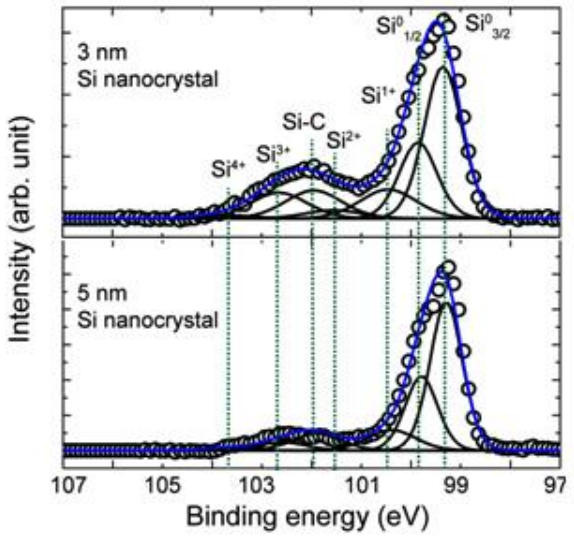

Figure 5.4 XPS of 3 and 5 nm diameter **SiNC(C11)Py**.

FTIR spectroscopy

The FTIR spectrum of **SiNC** (Figure 5.5) shows features due to ν(C–H) stretching at 3000-2850 cm^{-1} and δ(C–H) bending at 1500-1350 cm^{-1}; the presence of the oxygen is evidenced by the strong ν(Si–O) stretching at 1024 cm^{-1}. For **SiNC(C_{11})Py** the covalent attachment of the ligand to the surface is confirmed by the presence of aromatic ν(C–H) stretching at 3100-2890 cm^{-1}, ν(C=C) stretching at 1640 cm^{-1} and δ(C–H) bending at 1480 cm^{-1} and 940-800 cm^{-1}. There is no evidence of ν(Si-H) (ca. 2100 cm^{-1}) consistent with effective functionalization.

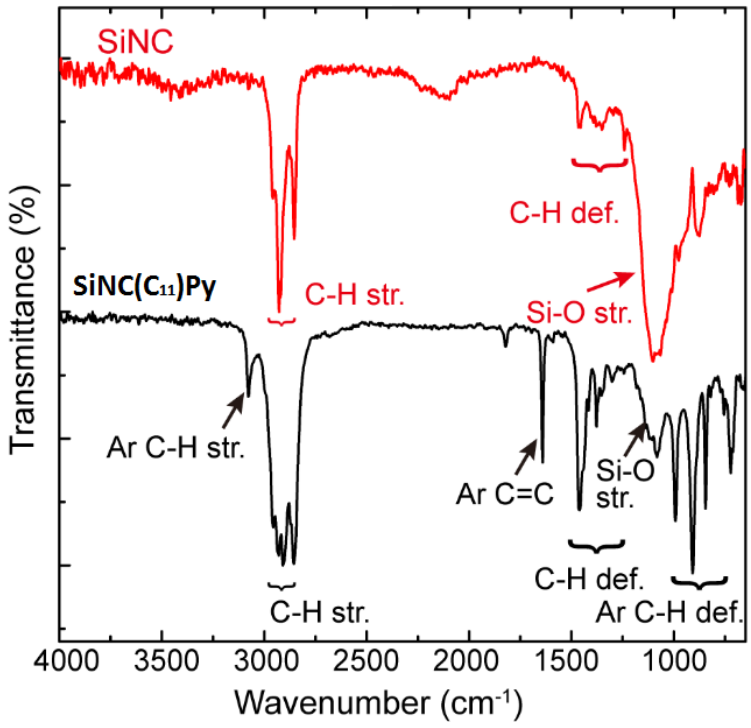

Figure 5.5 FTIR spectra of **SiNC** and **SiNC(C_{11})Py** of 3 nm diameter.

5.4 Results and Discussion

Photophysical measurements The optical properties of silicon nanocrystals functionalized with a combination of ligands **SiNC(C_{11})Py** were compared to those of the sample control **SiNC**and **SiNC(C_3)Py** functionalized with pyrene-short chain (Table 5.1)

Table 5.1 Photophysical properties of **SiNC**, **SiNC(C_{11})Py** and **SiNC(C_3)Py** dispersed in air-equilibrated toluene at 298 K. For comparison, the properties of the model compound **Py** are also reported. The quenching efficiency of the pyrene emission (η_q) and the sensitization efficiency of the Si core emission (η_{sens}) are presented.

	d/nm	λ_{ex} [nm]	λ_{PL} [nm]	Φ_{PL}[a]	τ [ns][b]	η_q	η_{sens}
SiNC	3	420	635	0.16[c]	70×10^3	-	-
SiNC(C_{11})Py	3	345 420	400 700	0.006 0.13	2.0, 11 90×10^3	90%	70%
SiNC(C_3)Py	3	345 420	400 690	0.005 0.11[c]	<0.2, 5 95×10^3	>95%	>95%
Py	-	345	400	0.06	18	-	-
SiNC	5	420	970	0.45	150×10^3	-	-
SiNC(C_{11})Py	5	345 420	400 940	0.006 0.42	3.2, 12 160×10^3	90%	30%
SiNC(C_3)Py	5	345 420	400 970	0.005 0.40	<0.2, 5 190×10^3	>90%	65%

[a]Experimental error: 10%. [b]Experimental error: 5%. For more details. [c]These values are higher than those reported in ref.[69] since the PL quantum yield of the standard was changed from 0.028 to 0.040.[70]

In Figures 5.6 a and 5.6 c the absorption spectra (red line) of **SiNC(C_{11})Py** with diameter 3 and 5 nm is compared with that of **SiNC** (blue line), without **Py** addition. The structured absorption band of **Py** is superimposed on the unstructured SiNC absorption. The ligand **Py** exhibits an absorption maximum at 345 nm. From molar absorption coefficients of Py ($\varepsilon_{345\ nm} = 4.4 \times 10^4\ M^{-1}\ cm^{-1}$) and

[69] M. Locritani, Y. Yu, G. Bergamini, M. Baroncini, J. K. Molloy, B. A. Korgel, P. Ceroni, J. Phys. Chem. Lett. **2014**, 5, 3325.

[70] K. Suzuki, A. Kobayashi, S. Kaneko, K. Takehira, T. Yoshihara, H. Ishida, Y. Shiina, S. Oishi, S. Tobita, Phys. Chem. Chem. Phys. **2009**, 11, 9850.

SiNC ($\varepsilon_{400\ nm}$ = 5 × 10^4 M^{-1} cm^{-1} and 5.3 × 10^5 M^{-1} cm^{-1} for 3 and 5 nm diameter)[71] we estimated 3.5 and 50 pyrene chromophores attached to each 3 nm and 5 nm nanocrystal, respectively.

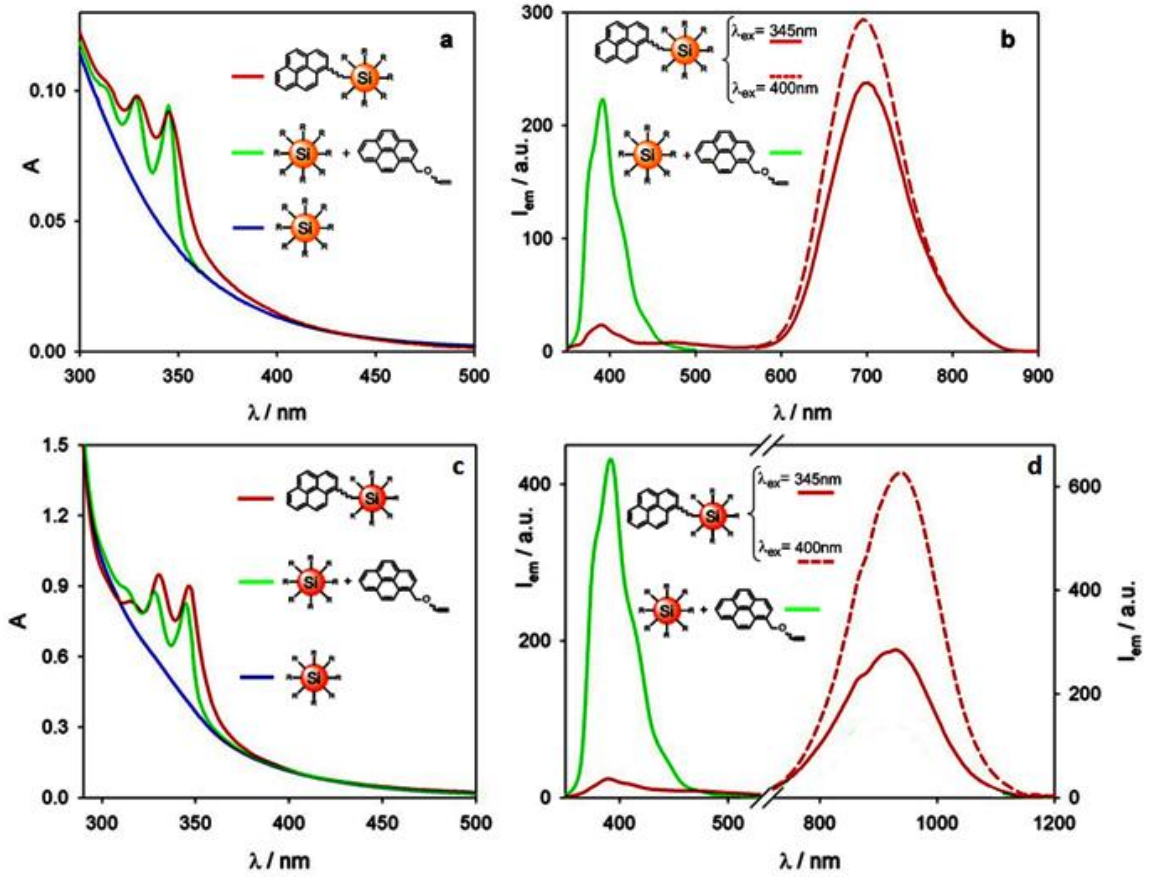

Figure 5.6 Absorbance (left) and PL spectra (right) of 3 nm (a, b) and 5 nm (c, d) diameter **SiNC** (blue line) and **SiNC(C_{11})Py** (red line) in air-equilibrated toluene. PL spectra were recorded for **SiNC(C_{11})Py** with two different excitation wavelengths (solid red line, λ_{ex}=345 nm; dotted red line, λ_{ex}=400 nm) to photoexcite either the pyrene or SiNCs, respectively. The measurements were made with the dispersion concentration adjusted to optically match the amount of absorbed light under each excitation condition. For comparison, the absorbance and PL spectra for a mixture of **SiNC** and **Py** in the proper ratio is shown in dashed black line (λ_{ex}=345 nm).

Exciting at 345 nm in the region where pyrene absorbs, **SiNC(C_{11})Py** present a very weak pyrene emission with maximum at 390 nm (solid red line in Figure 5.6 b and 5.6 d, left): Φ_{PL} = 0.006 compared to 0.06 for Py chromophore in air-equilibrated solution (Table 5.1).

From the comparison of the emission pyrene for **SiNC(C_{11})Py** of 3 and 5 nm with the pyrene emission for an optically matched solution of **SiNC** and free **Py** in a proper ratio (dashed red line in Figures 5.6 b and 5.6 d), results an efficient quenching (η_q = 90%).

Besides, in the emission spectra **SiNC(C_{11})Py** of 3 and 5 nm display a shoulder at 470 nm, which is typical of an excimer emission.[72] The pyrene emission intensity decay can be fitted by a double

[71] M. Rosso-Vasic, E. Spruijt, B. van Lagen, L. De Cola, H. Zuilhof, Small **2008**, 4, 1835.

exponential (Table 5.1), in which the shorter component is assigned to the quenched pyrene monomer, while the longer component to the pyrene excimer. Indeed, the percentage of the longer lifetime increases by recording the emission intensity at 470 nm compared to that at 400 nm. **SiNC(C_3)Py** does not manifest the presence of the excimer emission (Figure 5.7).

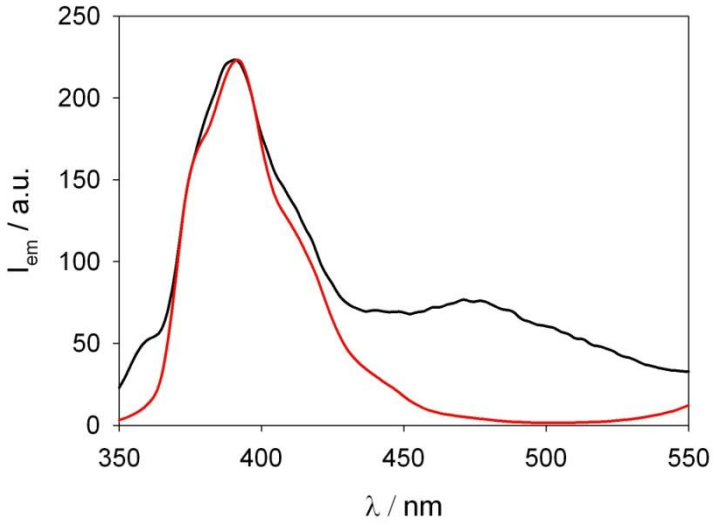

Figure 5.7 Normalized emission spectra of **SiNC(C_3)Py** (red line) and **SiNC(C_{11})Py** (black line) of the pyrene chromophore in toluene solution at room temperature. λ_{ex} = 345 nm.

The pyrene chromophores are embedded within the dodecyl ligand layer on the nanocrystals when linked by the shorter C_3 tether, which eliminates the interaction between pyrene units; whereas, the longer C_{11} tether places the Py units far enough away from the dodecene monolayer that ***Py-Py** interactions become possible.

Photoexcitation of the Si core at 400 nm gives rise to similar PL spectra for both the **SiNC(C_{11})Py** and **SiNC**.

Py does not absorb any light at this wavelength.

In **SiNC(C_{11})Py** of 3 nm a slight decrease of the emission quantum yield (13% compared to 16% for **SiNC**, Table 5.1) is accompanied by a red shift of the emission maximum (Figure 5.8 a) and a slight increase of the luminescent decay lifetime, which is in the range of 90 μs (Table 1).

[72] V. Balzani, P. Ceroni, A. Juris, Wiley-VCH, Weinheim, **2014**, pp. 139–168.

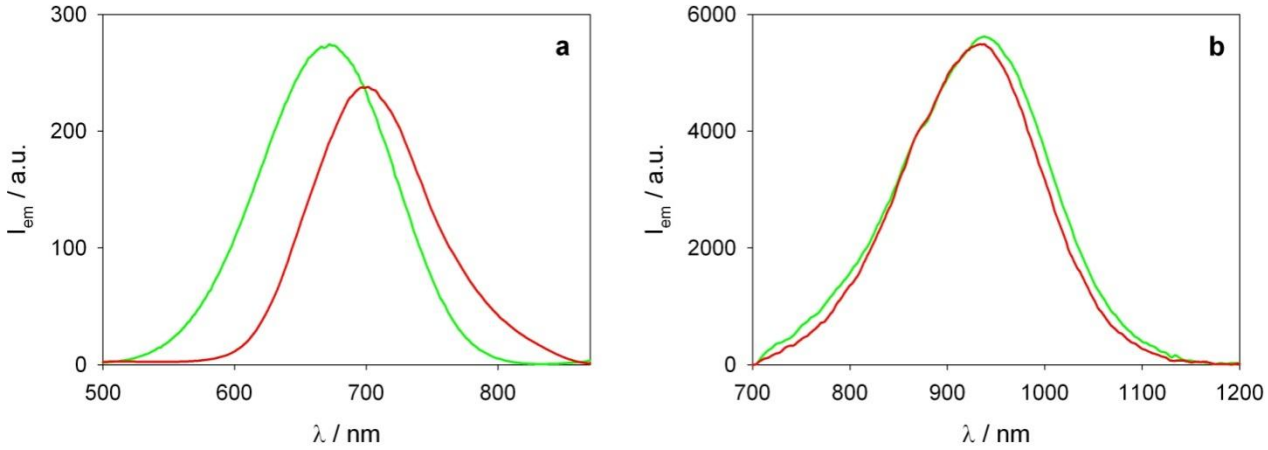

Figure 5.8 Emission spectra of **SiNC** (green line) and **SiNC(C_{11})Py** (red line) of 3 nm (a) and 5 nm (b) dispersed in toluene. The two samples were optically matched at the excitation wavelength of 420 nm.

No difference in the luminescent decay was observed in argon-purged toluene. The lack of quenching by dioxygen is consistent with the previous observations for **SiNC(C_3)Py** nanocrystals.

To evaluate the sensitized emission of the Si core by pyrene, we compared the emission intensity of the silicon core (λ_{max}=700 nm and 970 nm for 3 and 5 nm diameter SiNCs) recorded for two optically matched solutions of **SiNC(C_{11})Py** at the excitation wavelengths of 345 nm, where 50% of the light is absorbed by pyrene units for both 3 nm and 5 nm diameter, and 420 nm, where 100% of light is absorbed by the silicon core.

From the comparison of the spectra in Figures 5.6 b and 5.6 d the sensitization is higher in the case of 3 nm **SiNC(C_{11})Py**. If it is considered that the light is directly absorbed by the Si nanocrystal at 345 nm, the sensitization efficiency was evaluated: 70% and 30% for 3 and 5 nm **SiNC(C_{11})Py**, respectively.

Excitation spectra (Figure 5.9) performed at λ_{em}= 690 nm confirm these results.

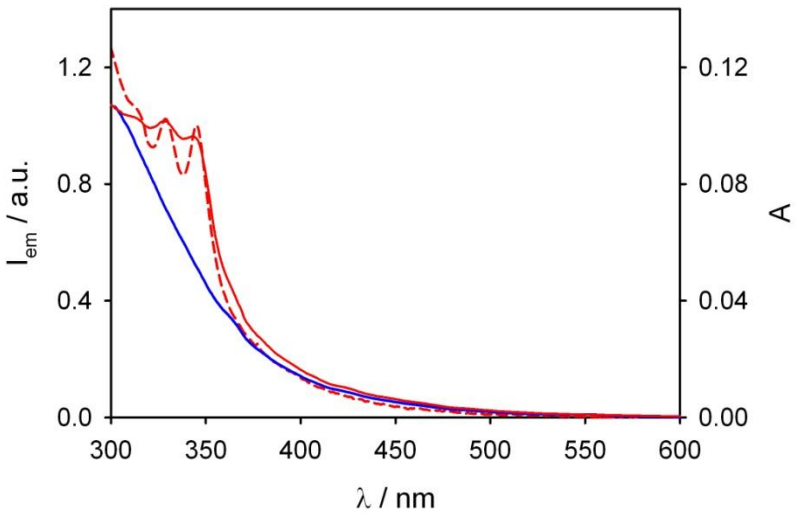

Figure 5.9 Excitation spectra of 3 nm diameter **SiNC(C_{11})Py** (red solid line) and **SiNC** (blue solid line) recorded with λ_{em}= 690 nm. For comparison purposes, the absorption spectrum of **SiNC(C_{11})Py** is reported (red dashed line).

The sensitization efficiency is lower than that observed for the **SiNC(C_3)Py** (Table 1) because of the longer average distance between pyrene and Si core which slows down the energy transfer process. On the other hand, the quenching efficiency of pyrene is only slightly lower than in **SiNC(C_3)Py** because in the case of **SiNC(C_{11})Py**, the radiative decay of the fluorescent pyrene monomer excited state competes, not only with the energy transfer process, but also with excimer formation.

5.5 Interaction of silicon nanocrystals with carbon-based materials

When the tether length is long enough to allow the **Py** units to extend away from the dodecene passivation layer into the solution, it provides the possibility for **Py** interactions with other molecules and surfaces in the surrounding environment. This is not the case when the **Py** units are buried in the ligand passivation layer. The observation of excimer formation for the long-tether **SiNC(C_{11})Py** units indicates that the **Py** is exposed significantly to the surroundings. It is well-known that pyrene interacts strongly with carbon allotropes like carbon nanotubes and

graphene.[73,74] Therefore, a series of tests exposing **SiNC(C_{11})Py** to C_{60}, carbon nanotubes and graphene was performed (Figure 5.10).

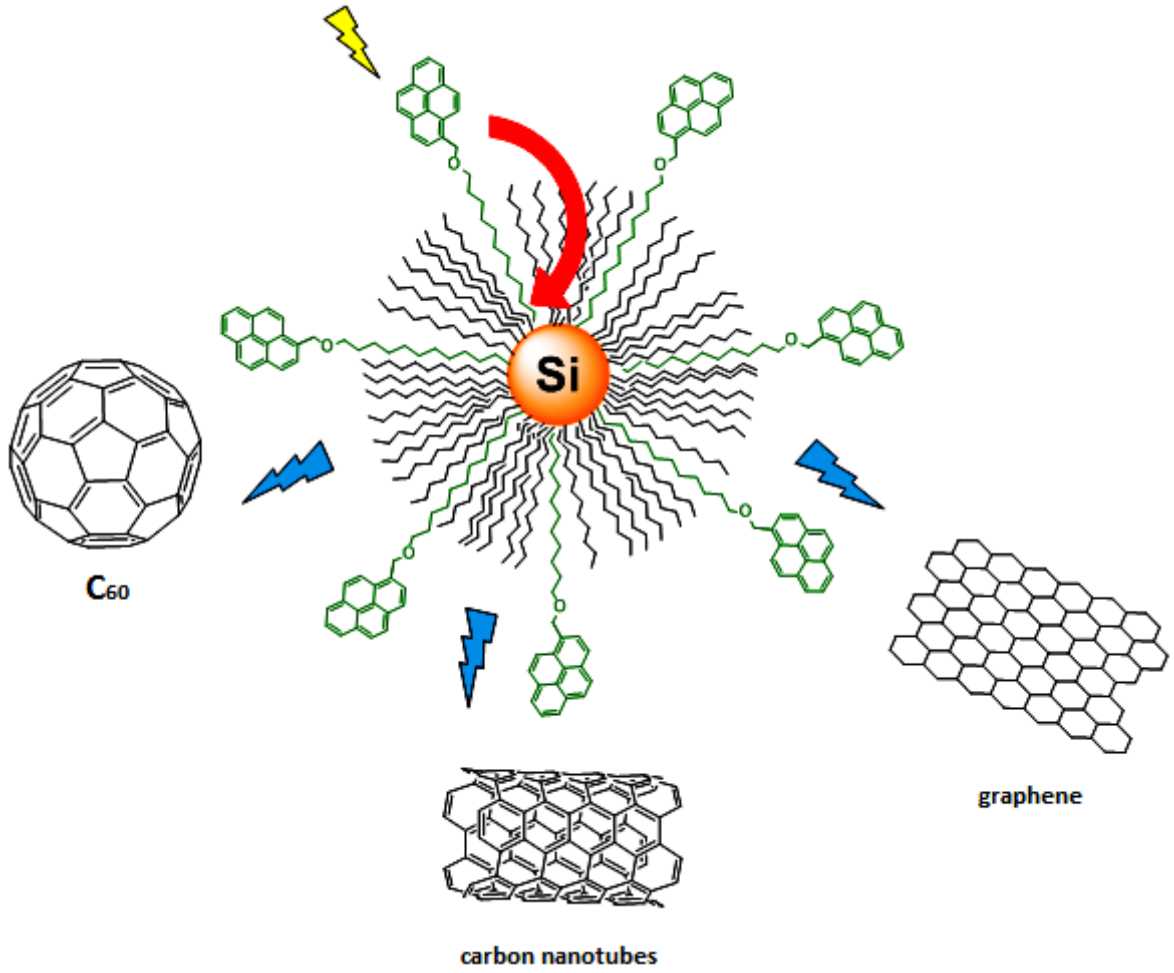

Figure 5.10

[73] X. An, T. Simmons, R. Shah, C. Wolfe, K. M. Lewis, M. Washington, S. K. Nayak, S. Talapatra, S. Kar, Nano Lett. **2010**, 10, 4295.

[74] A. Schlierf, H. Yang, E. Gebremedhn, E. Treossi, L. Ortolani, L. Chen, A. Minoia, V. Morandi, P. Samori, C. Casiraghi, D. Beljonne, V. Palermo, Nanoscale **2013**, 5, 4205.

5.5.1 Interaction of SiNC(C_{11})Py with C_{60}

A toluene dispersion air-equilibrated of 3 nm **SiNC(C_{11})Py** was treated C_{60}.

From previous experiments, it is know that the photoexcitation at 345 nm leads predominantly pyrene light absorption, however, the PL spectrum is dominated by the Si nanocrystals band at 700 nm as a result of energy transfer (Figure 5.6 b). Adding C_{60}, Si nanocrystal PL decreases with a concomitant reduction of the lifetime. Figure 5.11 shows a Stern-Volmer plot of the ratio of the lifetimes in the absence (τ^0) and presence of C_{60} (τ) as a function of C_{60} concentration.

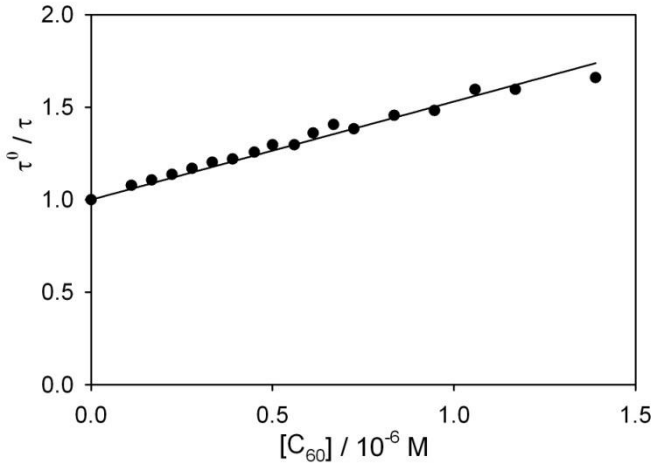

Figure 5.11 Stern-Volmer plot reporting the lifetimes of the Si core emission at 700 nm of **SiNC(C_{11})Py** (diameter 3 nm) dispersed in air-equilibrated toluene in the absence (τ^0) and in the presence of increasing amounts of C_{60} (τ). λ_{ex} = 345nm.

This plot is linear, as expected for a dynamic quenching process:

$\tau^0/\tau = 1 + k_q\tau^0[C_{60}]$

From this equation, the quenching constant (kq) can be evaluated: $k_q = 5.6 \times 10^9\ M^{-1}\ s^{-1}$.

This value is very high and close to the diffusion limit.

To comprehend the mechanism of quenching, we investigated the sensitization of the lowest-energy triplet excited state of C_{60} ($^3C_{60}$) through an excitation of the silicon nanocrystals.

The transient absorption spectrum of $^3C_{60}$ with a maximum at 730 nm[75,76] is superimposed on the transient spectrum deriving from the silicon nanocrystals (Figure 5.12).

[75] R. J. Sension, C. M. Phillips, A. Z. Szarka, W. J. Romanow, A. R. McGhie, J. P. McCauley, A. B. Smith, R. M. Hochstrasser, J. Phys. Chem. **1991**, 95, 6075.

[76] G. Accorsi, N. Armaroli, J. Phys. Chem. C **2010**, 114, 1385.

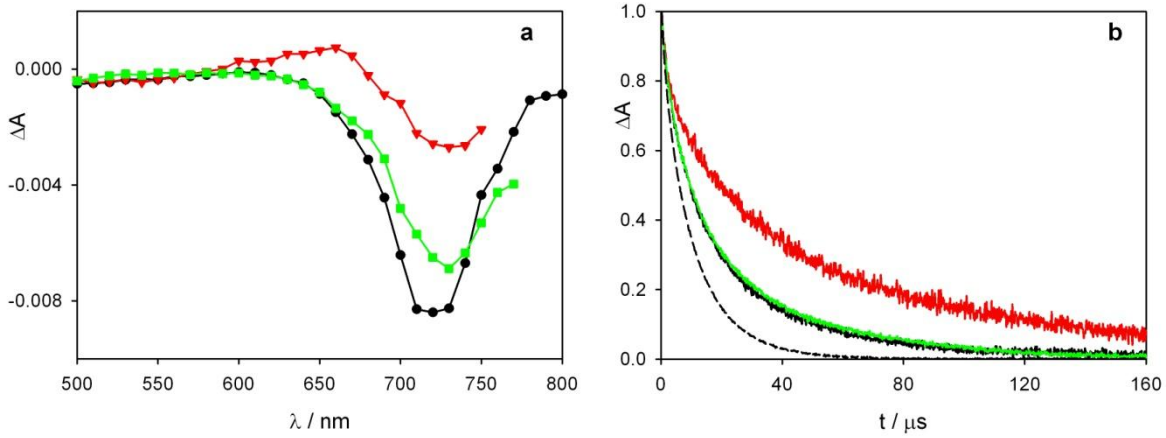

Figure 5.12 (a) Transient absorption spectra of **SiNC(C_{11})Py** (diameter 3 nm) in degassed toluene in the absence (red line) and in the presence of C_{60} 1.5 x 10^{-5} M (black solid line) compared to a degassed toluene solution of C_{60} (1.5 x 10^{-5} M, green line) upon excitation at 532 nm. (b) Normalized transient absorption decays at 735 nm of **SiNC(C_{11})Py** in the absence (red line) and in the presence of C_{60} (black line) compared to C_{60} (green line). The emission intensity decay at 645 nm of **SiNC(C_{11})Py** in the presence of C_{60} (black dashed line) is displayed for comparison purposes.

So we decided to probe the population of $^3C_{60}$ by monitoring the sensitized emission from the lowest-energy singlet excited state of dioxygen $^1O_2$ (Scheme 5.1).

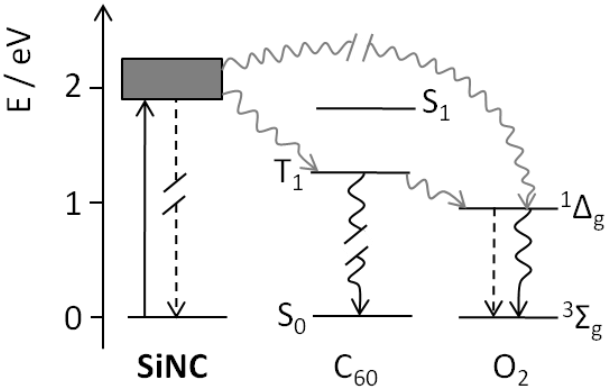

Scheme 5.1 Simplified energy level diagram, showing the energy transfer processes occurring for a sample of **SiNCs** in the presence of C_{60} in air-equilibrated solution. For **SiNCs** a range of energy values for the emitting state is displayed by a rectangle, to take into account particles of different size emitting at different wavelengths.

Indeed, it is known that $^3C_{60}$ sensitizes with unitary efficiency the population of $^1O_2$[77,78] that radiatively deactivates with a maximum at 1270 nm. Figure 5.13 reports the emission band of $^1O_2$

[77] R. R. Hung, J. J. Grabowski, J. Phys. Chem. **1991**, 95, 6073.

obtained for **SiNC(C_{11})Py** dispersed in toluene upon the addition of C_{60} (1.5 x 10^{-5} M) exciting at 420 nm, where light is selectively absorbed by the nanocrystals, compared to that of C_{60} in toluene upon excitation at 350 nm for optically matched solutions at the excitation wavelength.

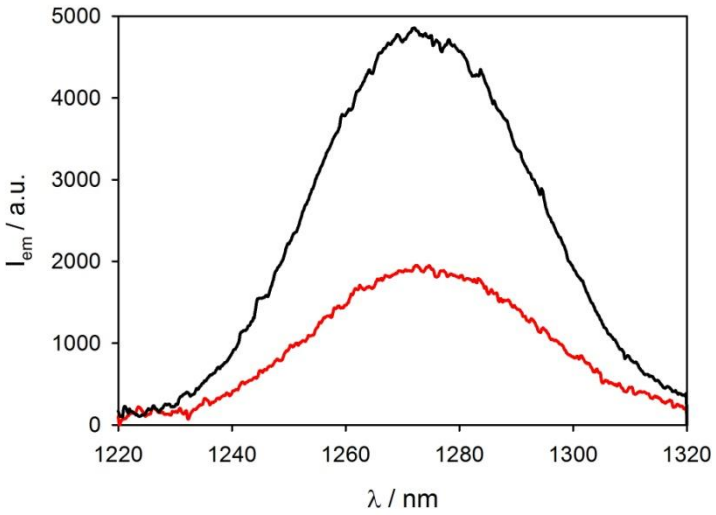

Figure 5.13 PL spectra of $^1O_2$ registered upon excitation at 420 nm of 3 nm diameter **SiNC(C_{11})Py** dispersed in toluene upon addition of C_{60} (1.5 x 10^{-5} M, red line), compared to that of C_{60} (1.5 x 10^{-5} M, black line) in toluene upon excitation at 330 nm for optically matched solutions at the excitation wavelength. For comparison purposes, the tail of the PL spectra of silicon nanocrystals has been subtracted.

The most important results are the following:

- **SiNC(C_{11})Py**, as well as **SiNC**, do not sensitize $^1O_2$ emission, in agreement with the lack of sensitivity to dioxygen of the emission quantum yields of the silicon nanocrystals;

- upon addition of C_{60} to **SiNC(C_{11})Py**, the silicon nanocrystal emission is quenched with an efficiency of ca. 75%;

- a concomitant sensitization of $^1O_2$ emission takes place with efficiency of ca. 40%, as evaluated by the comparison of the emission intensity obtained for the sample containing only C_{60}.

This result demonstrates that energy transfer from the silicon core to C_{60} takes place.

To evaluate the occurrence of a concomitant photoinduced electron transfer between **SiNC(C_{11})Py** and C_{60}, transient absorption spectra in the NIR region were registered, but no signal of C_{60}^- (λ_{max} = 1080 nm)[79] was detected. It is worth noting that the silicon nanocrystals have a transient absorption spectrum extending to the NIR, so we cannot exclude the formation of a small amount of C_{60}^- under our experimental conditions.

---

[78] Y. Rio, G. Accorsi, H. Nierengarten, C. Bourgogne, J.-M. Strub, A. Van Dorsselaer, N. Armaroli, J.-F. Nierengarten, Tetrahedron **2003**, 59, 3833.

[79] T. Nojiri, A. Watanabe, O. Ito, J. Phys. Chem. A **1998**, 102, 5215.

5.5.2 Interaction of SiNC(C_{11})Py with SWCNTs

Adding single-walled carbon nanotubes (SWCNTs) to a sample of **SiNC(C_{11})Py** (3-nm diameter) in air-equilibrated toluene, the emission intensity of the silicon core at 700 nm (Figure 5.14 a) decreases (after correction for the light absorbed and scattered by the SWCNT at the excitation wavelength) with no change of the corresponding lifetime.

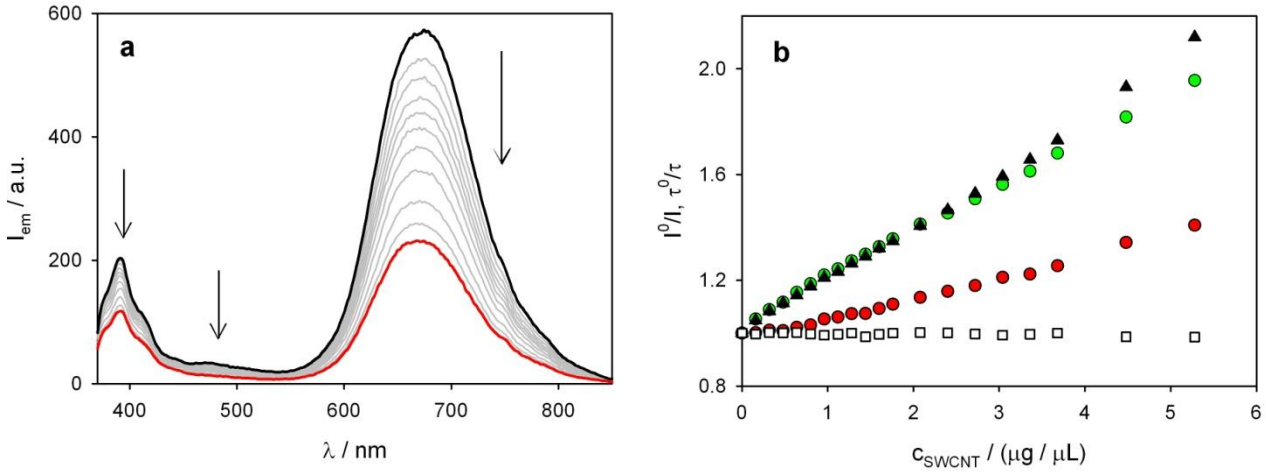

Figure 5.14 (a) PL spectra of **SiNC(C_{11})Py** (λ_{ex} = 345 nm) upon addition of an increasing amount of a 40 μg/ml solution of SWCNT in dichloromethane. (b) Ratio of PL intensities at 390 nm (black circles), 470 nm (empty diamond circles) and 700 nm (black triangles), as well as silicon nanocrystals lifetimes (empty squares) in the absence (I^0, τ^0) and presence (I, τ) of increasing amounts of SWCNTs.

The result is in line with a static quenching,[80] in which the **SiNC(C_{11})Py** and SWCNTs are associated in the ground state. Also the pyrene emission drops upon the addition of SWCNTs.

This can derive from the interaction of the pyrene unit with the carbon nanotube, creating a competitive path to the excimer formation. In particular, the excimer emission band at 470 nm is quenched with the same slope as the silicon nanocrystals emission, while the pyrene monomer emission band at 390 nm is quenched to a lower degree. This experimental finding is consistent with the fact that two opposite mechanisms are active: the pyrene emission is quenched by an interaction with the carbon nanotube, but it is revived by the suppression of the excimer formation.

[80] V. Balzani, P. Ceroni, A. Juris, Wiley-VCH, Weinheim, **2014**, pp. 139–168.

TEM of the adduct formed by SWCNTs and **SiNC(C_{11})Py** further confirms the ground state interaction. The HRTEM and STEM-HAADF micrographs (Figure 5.15) highlight that nanocrystals are preferentially located on the SWCNTs rather than on the carbon film coated copper grid.

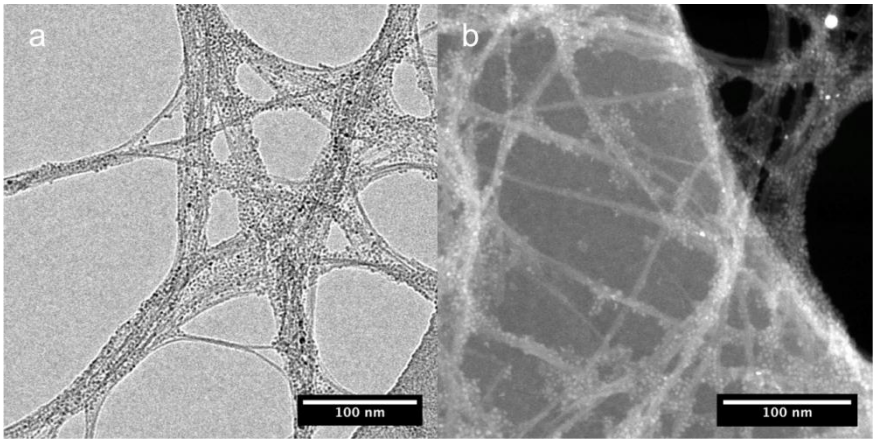

Figure 5.15 (a) TEM micrograph and (b) STEM-HAADF micrograph of SWCNTs coated by **SiNC(C_{11})Py**.

5.5.3 Interaction of SiNC(C_{11})Py with graphene

The interaction of **SiNC(C_{11})Py** (3 and 5 nm diameter) with graphene was evaluated in a different way. The lack of dispersibility of exfoliated graphene in a solvent suitable for **SiNC(C_{11})Py**, complicates the study of solution phase behavior.

Therefore, we immersed a graphene film grown by Chemical Vapor Deposition (CVD) (details on the growth are reported in Ortolani et al.)[81] in a solution of the nanocrystal, and we studied their interaction.

The nanocrystals (Figure 5.16) form a uniformly dispersed monolayer of nanoparticles, without the formation of thick aggregates. The very low thickness of the graphene film, between 1 and 3 layers, allows us to obtain a deeper insight on the crystalline structure of the nanoparticles, by enhancing the contrast for a light element such as silicon, as previously reported by Panthani et al.[82]

[81] L. Ortolani, E. Cadelano, G. P. Veronese, C. Degli Esposti Boschi, E. Snoeck, L. Colombo, V. Morandi, Nano Lett. **2012**, 12, 5207.

[82] M. G. Panthani, C. M. Hessel, D. Reid, G. Casillas, M. José-Yacamán, B. A. Korgel, J. Phys. Chem. C **2012**, 116, 22463.

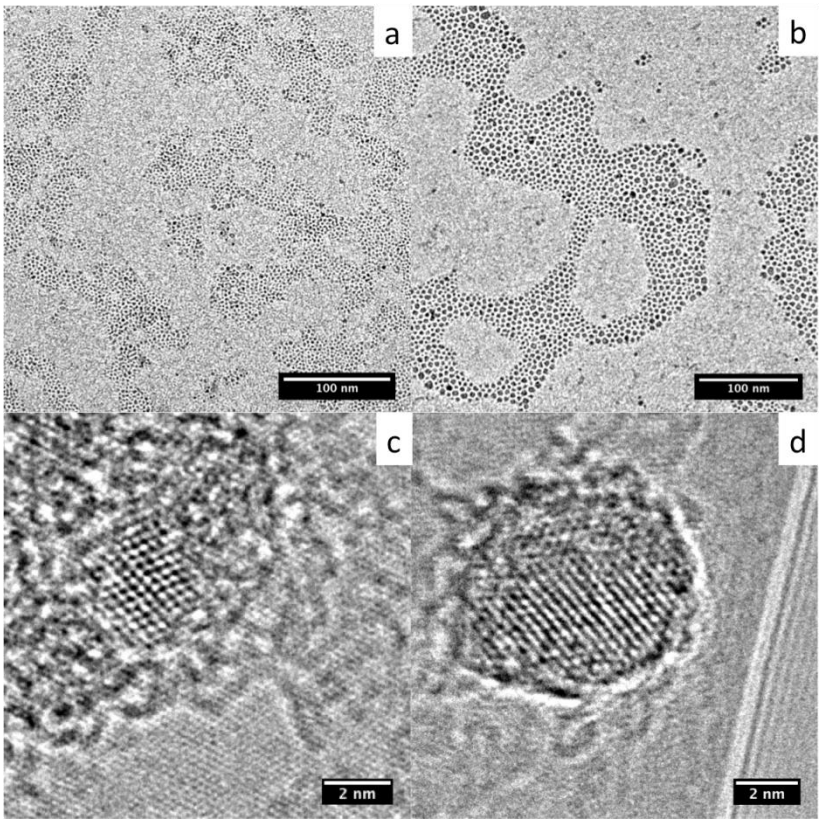

Figure 5.16 Low magnification TEM micrographs of 3 nm (a) and 5 nm (b) **SiNC(C_{11})Py** deposited on CVD graphene. (c,d) High magnification HRTEM image of a supported on graphene, showing the Si (111) lattice fringes at 0.31 nm.

The emission intensity of **SiNC(C_{11})Py** (3 nm diameter) is lower than the graphene layer, as evidenced by both the PL spectrum and the wide-field luminescence image reported in (Figure 5.17).

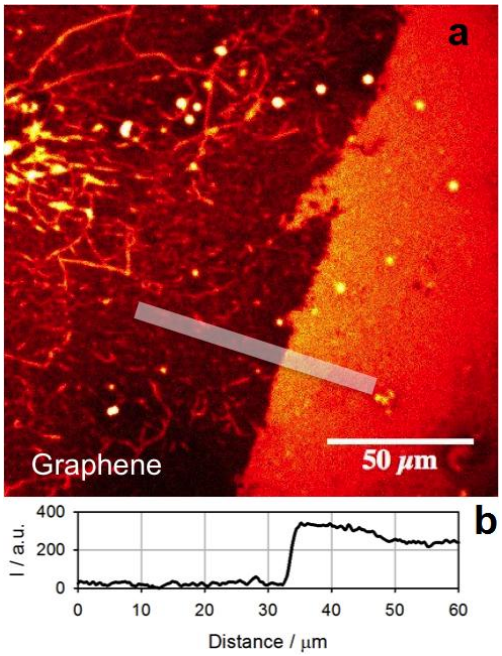

Figure 5.17 (a) Wide-field luminescence microscope image of **SiNC(C_{11})Py** (3 nm diameter) deposited on quartz and graphene coated quartz. The image shows the graphene film edge. (b) Emission intensity profile registered by wide-field luminescence microscopy along the white line in panel (a).

The wide-field image shows luminescent stripes on the graphene that are likely due to breaks in the graphene films. SEM images of **SiNC(C_{11})Py** with diameter of 5 nm (the smallest particles are not visible by SEM) on quartz slides partially covered by CVD graphene (Figure 5.18) show a uniform distribution of the nanocrystals on graphene and quartz.

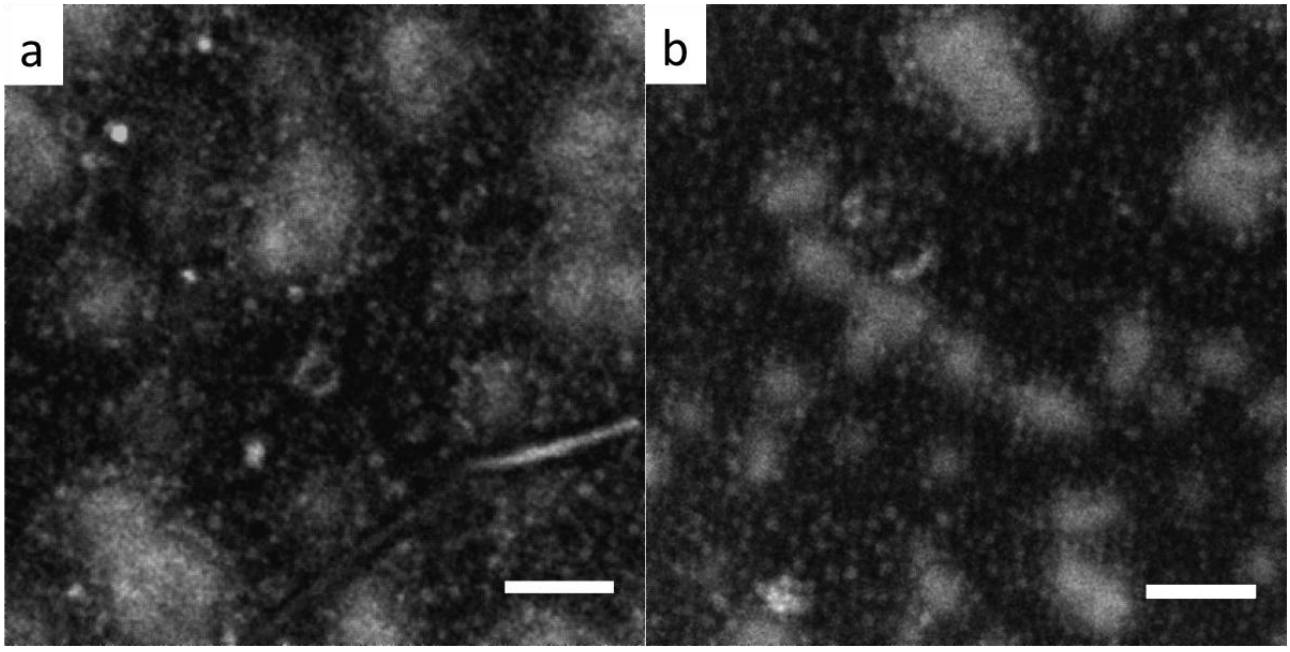

Figure 5.18 SEM micrographs of the **SiNCs** deposited onto the graphene coated area of the Si/SiO_2 wafer (a), with a visible graphene wrinkle, and outside the graphene area, on the pristine SiO_2 layer (b). The nanocrystals are forming a continuous and equally distributed layer (darker areas). Scale bar equal to 50 nm.

Therefore, the different emission intensity registered on quartz and graphene is not due to a different distribution on the two substrates, but it is ascribed to a quenching mechanism. The luminescence lifetimes registered on quartz and graphene are similar, as expected for a static quenching (see previous discussion on SWCNT). The most likely quenching mechanism is energy transfer, as previously reported for CdSe quantum dots.[83]

[83] Z. Chen, S. Berciaud, C. Nuckolls, T. F. Heinz, L. E. Brus, ACS Nano **2010**, 4, 2964.

5.6 Conclusion

The covalent passivation of SiNCs surface allow to exploit the new properties that emerge from the interaction of SiNCs with chromophores.

The chromophores can be exploited as light-harvesting antenna: exciting the pyrene chromophores, energy transfer occurs and sensitized emission of the nanocrystals is observed. The length of the link between the pyrene unit and the silicon core influences the efficiency of this System.

Tethers that are long enough for the pyrene to extend beyond the capping ligand layer into the surrounding solution enable association with molecules and substrates in the surroundings, such as the carbon allotropes studied here: C_{60}, single-walled carbon nanotubes (SWCNTs) and graphene.

Energy transfer process can occur either to or from the Si nanocrystals. Energy is transferred from the organic chromophore to the silicon core in the case of pyrene; whereas, energy flows from the quantum dots to nearby fullerenes to populate their lowest energy triplet excited state. This means that electronic energy harvested by the hybrid **SiNC(C_{11})Py** material can be further exploited by an interaction with external systems.

Chapter 6

Silicon nanocrystals and zinc push-pull tetraphenyl porphyrins

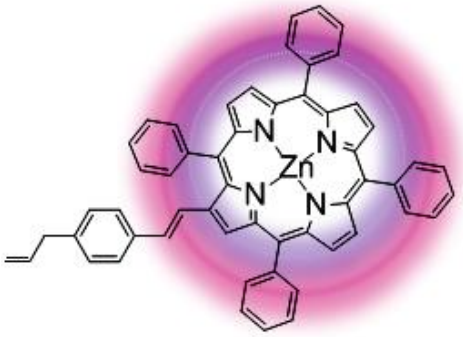

5.1 Introduction

In this work we have studied the influence of zinc tetraphenyl porphyrins (**ZnTPP**) on the optical and chemical properties of silicon nanocrystals.

In particular we have functionalized SiNCs surface by thermal hydrosilylation of terminal alkene present on the **ZnTPP** phenyl ring.

As in previous chapters, two families of SiNCs (3.0 and 5.0 nm) have been analyzed.

6.2 Covalent passivation of SiNCs with ZnTPP

To synthesize SiNCs with diameter 3.0 and 5.0 nm we start from the thermal annealing of HSQ at different temperatures (1100 and 1200°C) followed by HF-etching in the dark as previously described in Chapter 4.

SiNCs were functionalized with a mixed ligands layer of 1-dodecene and ZnTPP to yield **SiNC-ZnTPP** (Figure 1).

To evaluate the influence of chromophore on optical properties, SiNCs were also passivated with only 1-dodecene (**SiNC**).

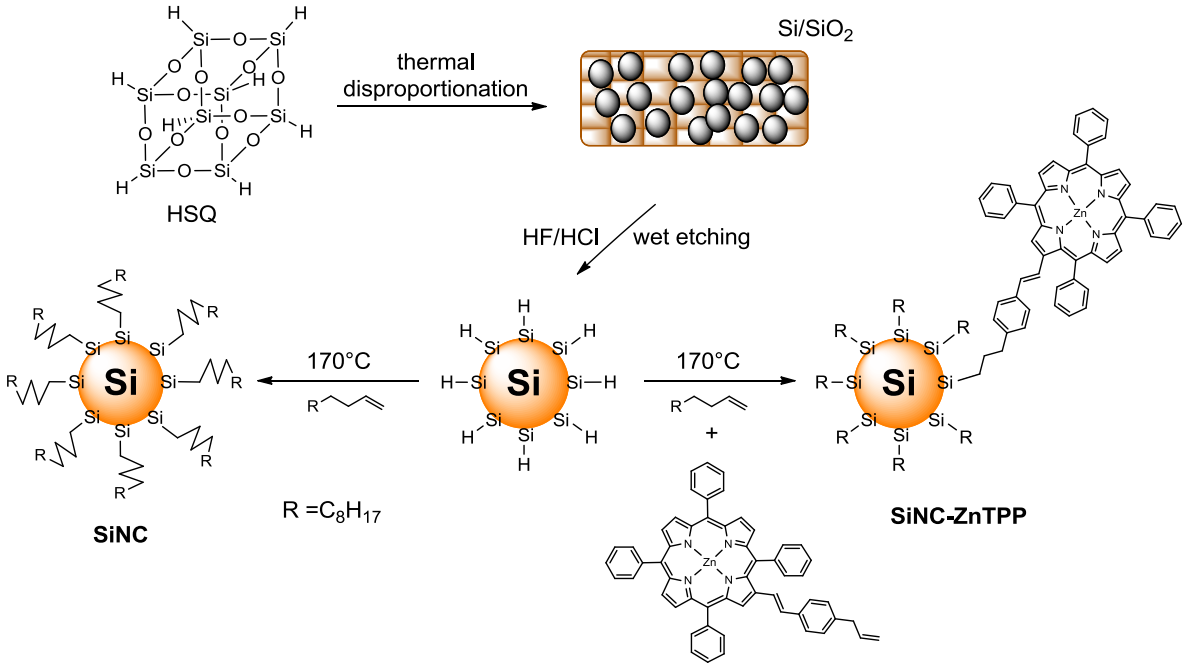

Figure 6.1

6.2.1 Experimental details

SiNC, SiNC-ZnTPP synthesis: the synthetic procedure follows the method developed by Hessel, et al.[84] Generally, 40 mL of Fox-16 (hydrogen silsesquioxane 16 wt%) is dried under vacuum and the resulting white solid is then transferred to a tube furnace and annealed at 1100°C (3.0 nm diameter) or 1200°C (5.0 nm diameter) at a heating rate of 18°C/min and held at that temperature for an hour under reducing atmosphere (93% N_2, 7% H_2).

The SiNC/SiO_2 composite is etched with 48% HF and 37.5% HCl (10:1 v/v) in the dark for 4-6 hours and then centrifuged at 8000 rpm for 5 min. The H-terminated SiNCs are then rinsed once with deionized (DI) water, twice with ethanol, and once with chloroform. The nanocrystals are dispersed in 4 mL of 1-dodecene to have **SiNC** and 4 mL of 1-dodecene with 300 mg of **ZnTPP** (1:50 zinc porphyrin:dodecene molar ratio) for **SiNC-ZnTPP**. The initially turbid dispersions are put through three freeze-pump-thaw cycles, and then heated to 170°C under N_2 flow for 12 hours. Over time, the dispersions become optically clear, indicating that passivation of Si nanocrystals has occurred.

[84] Hessel C. M., Henderson E. J., Veinot J. G. C., Chem. Mater. **2006**, 18, 6139-6146.

Purification of SiNC

To purify the nanocrystals, the solutions are transferred to a glass centrifuge tube, spin at 8000 rpm for 5 min and discard the precipitate (poorly capped SiNCs) on the bottom. The supernatant is transferred to another glass centrifuge tube and undergoes many centrifugation/precipitation cycles using toluene/ethanol solvent/antisolvent pair. The final **SiNC** samples were dispersed in toluene at a concentration of 3-5 mg/mL until further characterization (Figure 6.2).

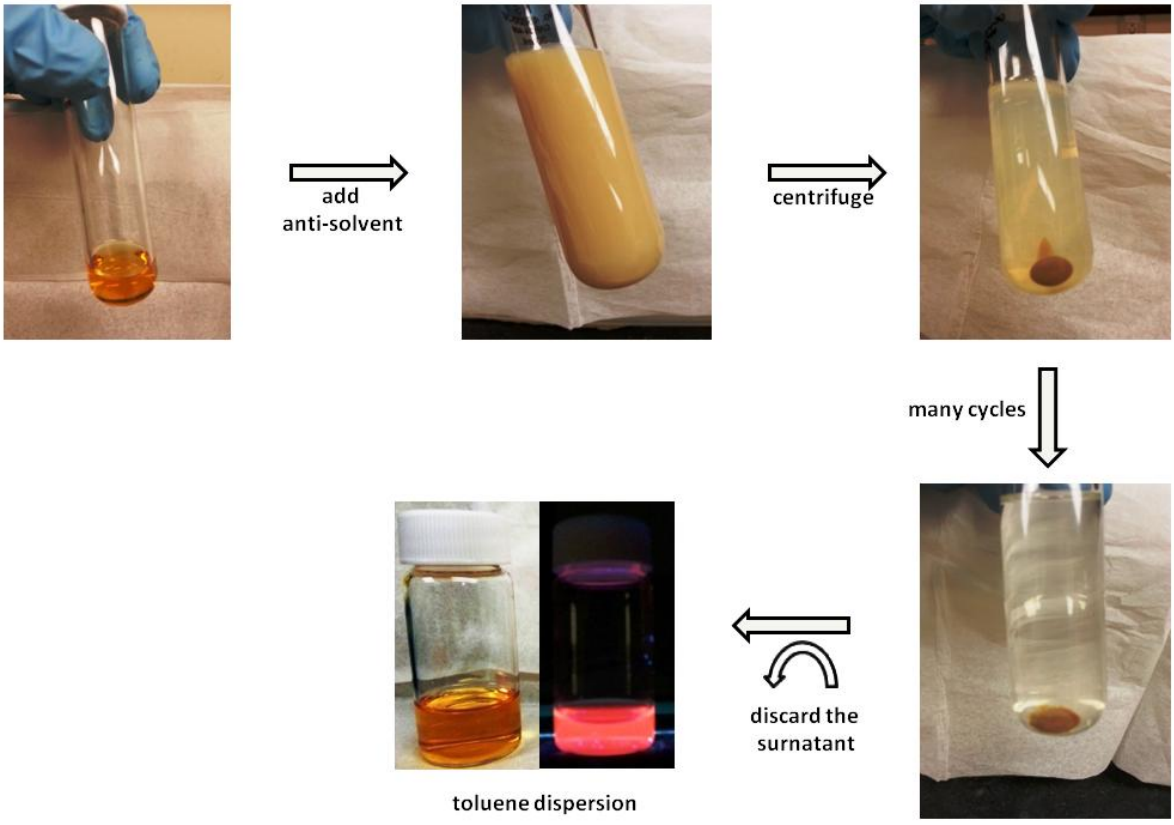

Figure 6.2

Purification of SiNC-ZnTPP

To purify the nanocrystals, the solutions are transferred to a glass centrifuge tube, spin at 8000 rpm for 5 min and discard the precipitate (poorly capped SiNCs) on the bottom. The supernatant is transferred to another glass centrifuge tube and undergoes many centrifugation/precipitation cycles using toluene/ethanol solvent/antisolvent pair. The final **SiNC-ZnTPP** samples were dispersed in toluene at a concentration of 3-5 mg/mL until further characterization (Figure 6.2).

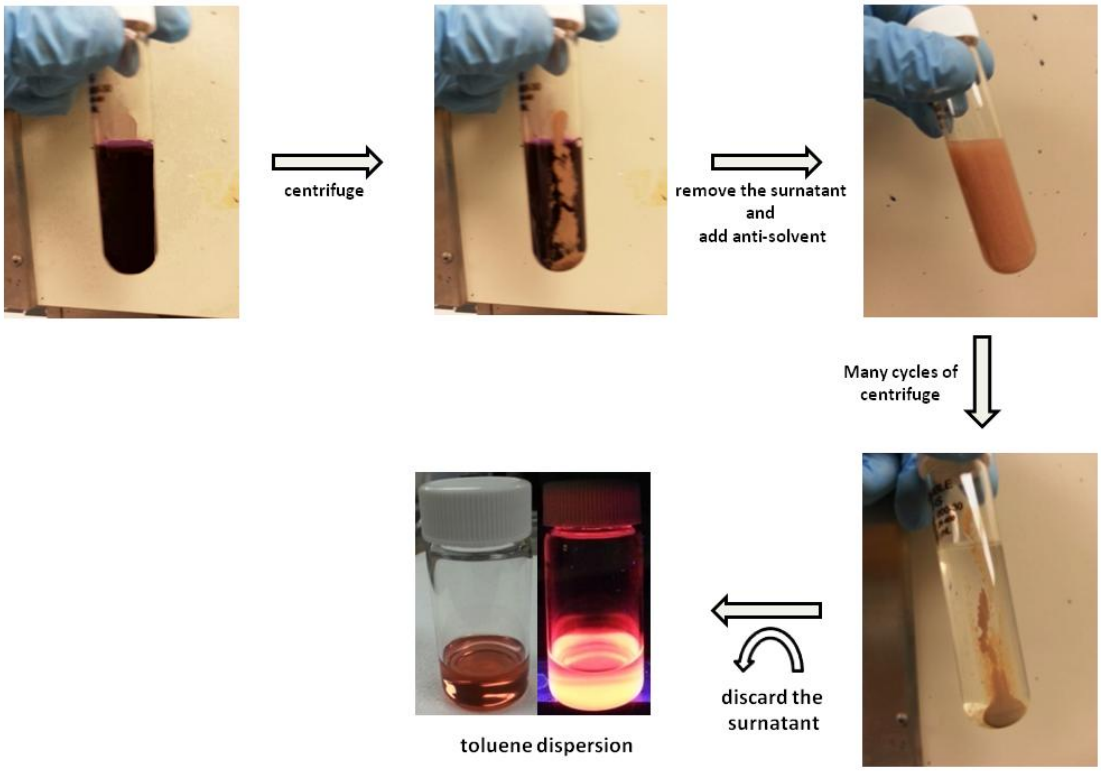

Figure 6.3

6.3 Material characterization

Transmission electron spectroscopy (TEM) characterization

The average Si core diameter of the nanocrystals was determined by TEM.

Figures 6.4-6.5 show TEM images of the 3.0 nm and 5.0 nm diameter **SiNC-ZnTPP** samples used in the studies. The functionalization does not alter the size of SiNCs.

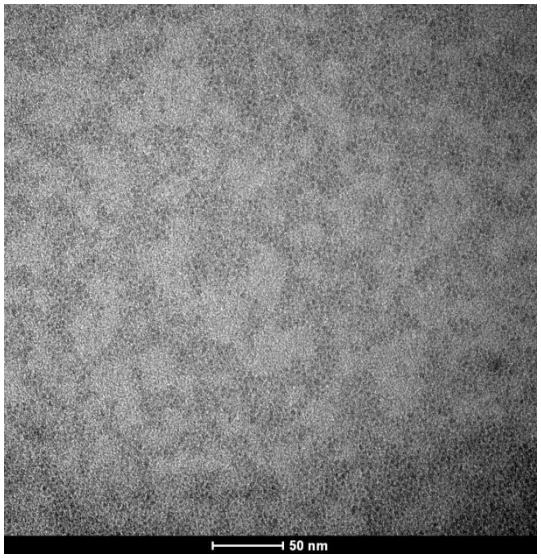

Figure 6.4 TEM image of 3.0 nm diameter **SiNC-ZnTPP**.

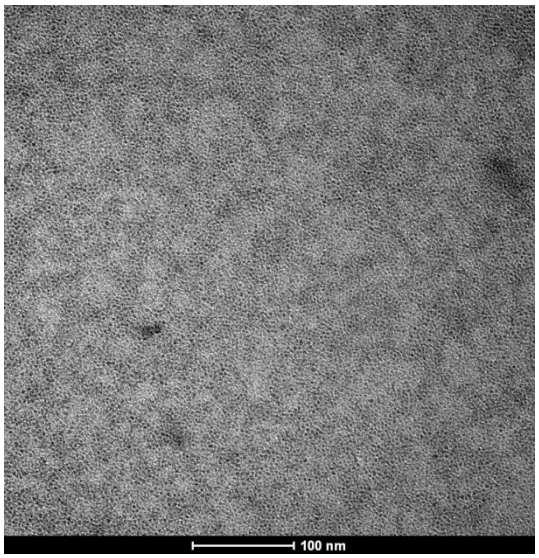

Figure 6.5 TEM image of 5.0 nm diameter **SiNC-ZnTPP**.

6.4 Results and Discussion

Photophysical measurements The optical properties of silicon nanocrystals (3.0 and 5.0 nm) functionalized with a combination of ligands **SiNC-ZnTPP** were compared to those of the sample control **SiNC** and free ligand **ZnTPP** (Table 6.1).

Table 6.1 Photophysical properties of **SiNC** and **SiNC-ZnTTP** dispersed in air-equilibrated toluene at 298 K. For comparison, the properties of the model compound **ZnTPP** are also reported.

	d/nm	λ_{ex}/nm	λ_{em}/nm	Φ_{em}[a]	τ/ns[b]
SiNC	**3.0**	**425**	**700**	**0.09**	**73 x 10^3**
SiNC-ZnTTP	**3.0**	**428**	**655**	**0.035**	**1.2,2.6** **90x10^3**
ZnTTP		**428**	**655**	**0.034**	**2.3**
SiNC	**5.0**	**378**	**922**	**0.45**	**140 x 10^3**
SiNC-ZnTTP	**5.0**	**427**	**649** **906**	**0.011** **0.08**	**1.2** **100 x 10^3**

[a]Experimantal error: 10%. [b]Experimental error: 5%.

The free chromophore **ZnTPP** has a structured absorption band with two peaks at 425 nm (Soret band)[85] and 557 nm (Q band) in Figure 6.6.

[85] Jacques-Louis Soret (**1883**). "Analyse spectrale: Sur le spectre d'absorption du sang dans la partie violette et ultra-violette". Comptes rendus de l'Académie des sciences (in French) 97: 1269–1270.

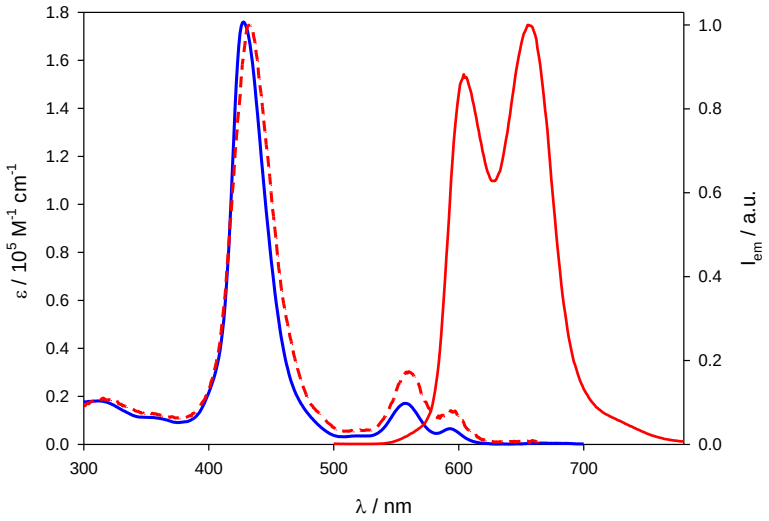

Figure 6.6 Absorption (blue), emission (red, solid, λ_{ex}=425 nm) and excitation (red dashed, λ_{em}=690 nm) spectra of a solution of **ZnTPP** in toluene at RT.

Figure 6.7 shows the comparison of optical properties between **SiNC** and **SiNC-ZnTPP** of 3.0 nm in toluene dispersion.

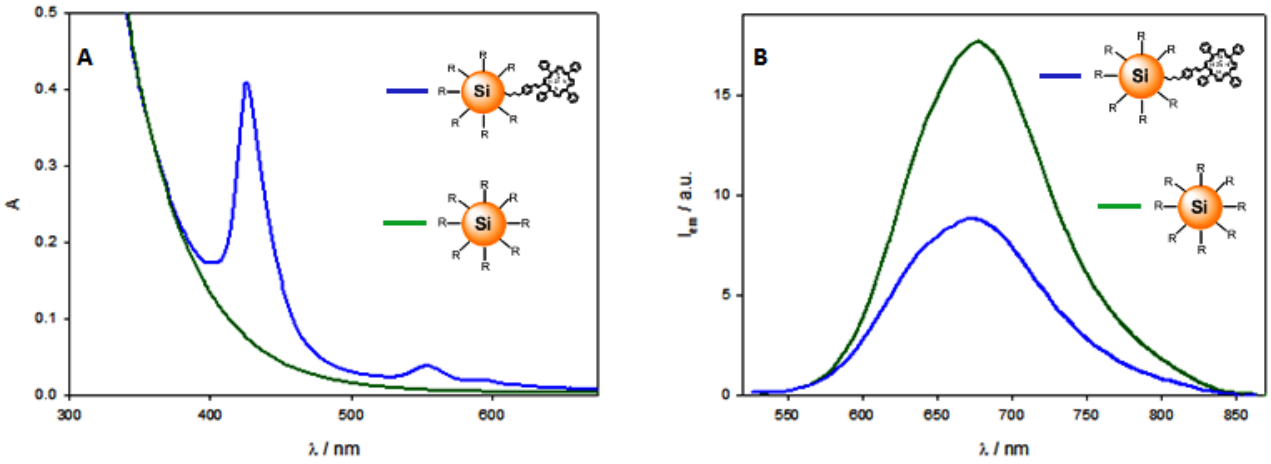

Figure 6.7 Comparison between absorption and emission spectra (λ_{ex}=510 nm, delay 50 µs) of isoabsorbing **SiNp-ZnTPP** (3.0 nm, blue) and **SiNC** (3.0 nm, green).

The sample control **SiNC** (without porphyrin) exhibits an unstructured absorption profile that tails past 500 nm that is characteristic of SiNCs (green curve in Figure 6.7 a).

The contribution of **ZnTPP** is highlighted by the presence of peaks in **SiNC-ZnTPP** absorbance spectra (blue curve in Figure 6.7 a). On the basis of the molar absorption coefficients for **ZnTPP**

and 3.0 nm diameter **SiNC**, ($\varepsilon_{428\ nm}$(ZnTPP) = 1.7 × 10^5 M^{-1} cm^{-1}, $\varepsilon_{400\ nm}$($SiNC_{3.0\ nm}$) = 5 × 10^4 M^{-1} cm^{-1}),[86] there is 1 porphyrin unit per nanocrystal for 3.0 nm diameter **SiNC-ZnTPP**.

In Figure 6.8 there is the absorption and emission spectra of **SiNC** with 5.0 nm with PL maximum at 922nm.

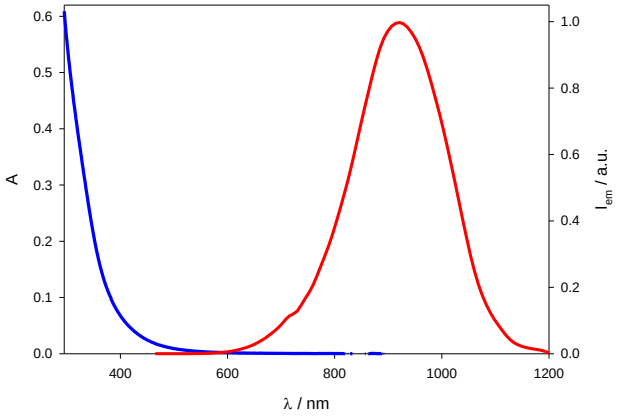

Figure 6.8 Absorption (blue) and emission (red, λ_{ex}=400 nm) spectra of **SiNC** in toluene at RT. Emission spectra were recorded at the same excitation wavelength with two different monochromators (visible: until 720 nm, NIR 700-1200 nm) and then matched together.

Figure 6.9 shows optical measurements of **SiNC-ZnTPP** with diameter 5.0 nm.

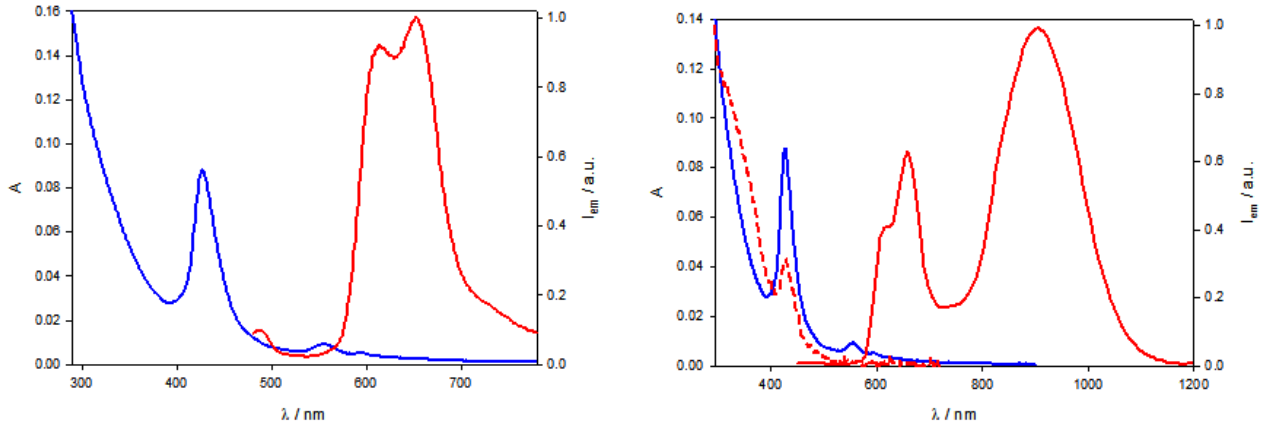

Figure 6.9 Left: absorption (blue) and emission (red, λ_{ex}=425 nm, visible) spectra of a dispersion of **SiNP-ZnTPP** in toluene at RT. Right: absorption (blue), excitation (red, dashed, λ_{em}=950 nm) and emission (visible and NIR, matched, λ_{ex}=425 nm).

[86] Hessel C. M., Reid D., Panthani M. G., Rasch M. R., Goodfellow B. W., Korgel B. A., Chem. Mater. **2012**, 24, 393-401.

In order to investigate the quenching of the porphyrin unit and the energy transfer from the dye to the particle, we added free **ZnTPP** to a dispersion of **SiNC**. This mixture is properly diluted until absorbance at 427 nm (corresponding to the Soret peak of the free **ZnTPP**) is the same of a dispersion of **SiNC-ZnTPP**.

Exciting at the same wavelength, we recorded emission spectra of the two solutions in the visible region, in the same conditions: emission in the visibile region coming from **SiNC-ZnTPP** is partially quenched (integration is 1/3 in respect of the mixed sample), while its emission lifetime decreases from 2.2 ns to 1.2 ns. Similar results were evidenced in a similar experiment, considering isoabsorbing solutions at 558 nm (in correspondence of the lower Q-bands of the porphyrinic unity).

Excitation spectrum recorded for emission at 950 nm shows a peak at 425 nm, pointing out an energy transfer from the **ZnTPP** moiety to the Si nanoparticle (Figure 6.9).

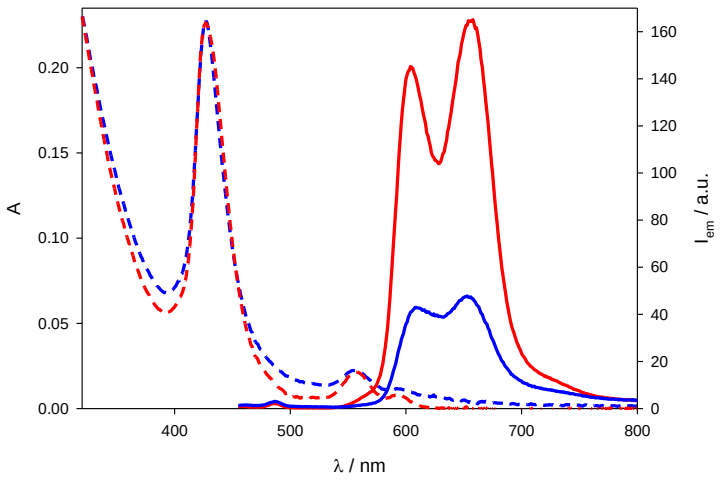

Figure 6.10 Absorption (dashed lines) and emission (solid lines) spectra of a dispersion of **SiNC-ZnTPP(216)** in toluene (blue) and a mix solution of **ZnTPP** and **SiNC** (red line) (λ_{ex}=427 nm).

To evaluate the entity of energy transfer we made the comparison between NIR emission spectra of isoabsorbing dispersion of **SiNC** and **SiNC-ZnTPP**.

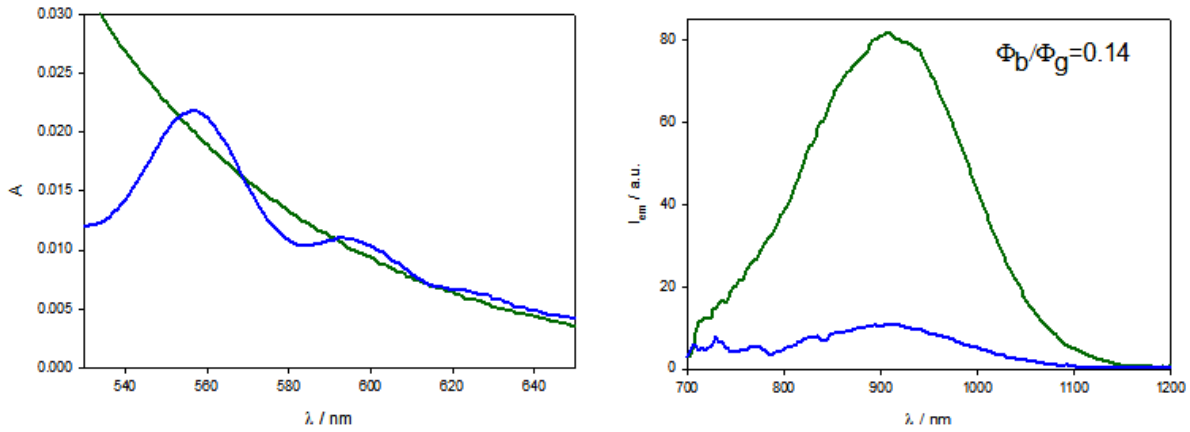

Figure 6.11 Comparison between NIR emission spectra (right) of isoabsorbing (at λ_{ex}=630 nm) dispersion of **SiNC** (green) and **SiNC-ZnTPP** (blue) dispersions: a factor 0.14 was calculated for the silicon core emission quantum efficiency. Left: absorption spectra of the same solutions.

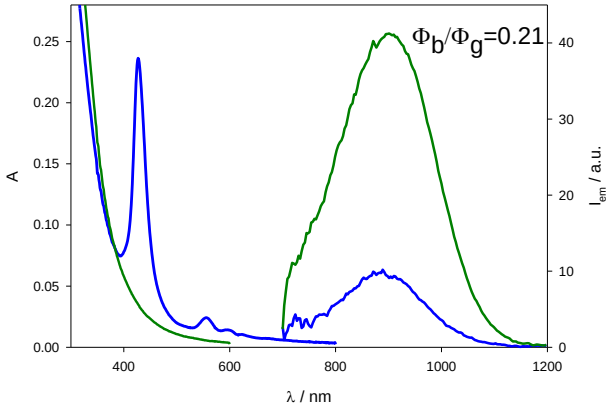

Figure 6.12 Comparison between NIR emission spectra of isoabsorbing (at λ_{ex}=383 nm) dispersion of **SiNC** (green) and **SiNC-ZnTPP** (blue) dispersions: a factor 0.21 was calculated for the silicon core emission quantum efficiency. Left side: absorption spectra of the same solutions.

The energy transfer efficiency was estimated taking into account the different quantum yield of the two types of nanoparticles, **SiNC** and **SiNC-ZnTPP**. Effectively, the quantum efficiency of the Si core drops once the nanoparticle are functionalized with the porphyrine moiety. After exciting selectively at λ_{ex}=630 nm, integration of emission spectra evidenced a ratio of circa 0.14 (Figure 6.11). In a similar experiment, exciting the Si core at λ_{ex}=383 nm (Figure 6.12) we calculated a ratio 0.21 between the two emissions. From these assumptions and considering the NIR emission of an isoabsorbing mixed solution (at λ_{ex}=428 nm, Figure 6.13) we estimated the energy transfer efficiency of 47%.

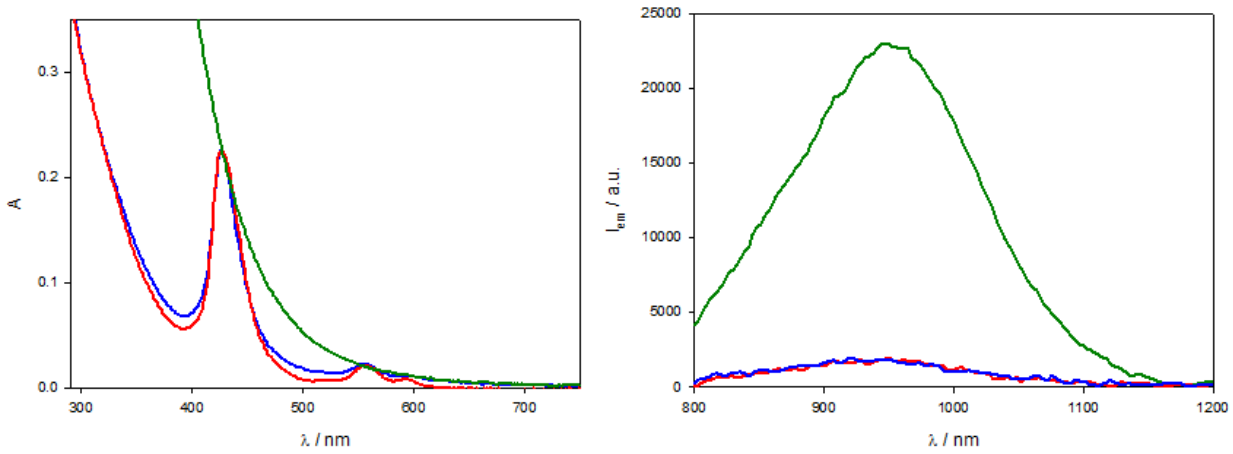

Figure 6.13 Absorption spectra (left) and comparison between NIR emission spectra (right) of isoabsorbing dispersion of **SiNC** (green) and **SiNC-ZnTPP** (blue). Red line refers to the mixing of **SiNC** and **SiNC-ZnTPP**; emission spectra on the right are uncorrected. λ_{ex}=427 nm.

From the molar absorption coefficients the estimate number of phorphyrin units for each SiNCs was 10.

6.5 Conclusion

The present system is under investigation with the aim of increasing the number of chromophores on the silicon nanocrystal surface. In the future we want to replace 1-dodecene with a inert solvent in order to reduce the competition between the ligands for SiNCs surface.

Chapter 7

Silicon nanocrystals with thiadiazole

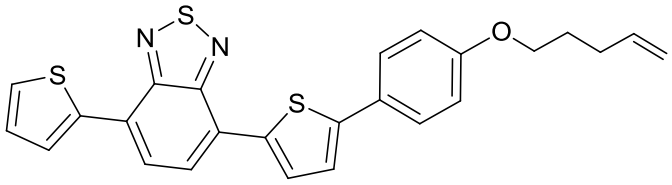

7.1 Introduction

Also the thiadiazole have been tested on SiNCs surface to exploit the properties from interactions between silicon core and ligand.

7.2 Covalent passivation of SiNCs with thiadiazole

SiNCs of different diameters (3.0 and 5.0nm) were functionalized with a mixed ligands layer of 1-dodecene and thiadiazole to yield **SiNC-THP** (Figure 1). We also considered SiNCs passivated with only 1-dodecene (**SiNC**).

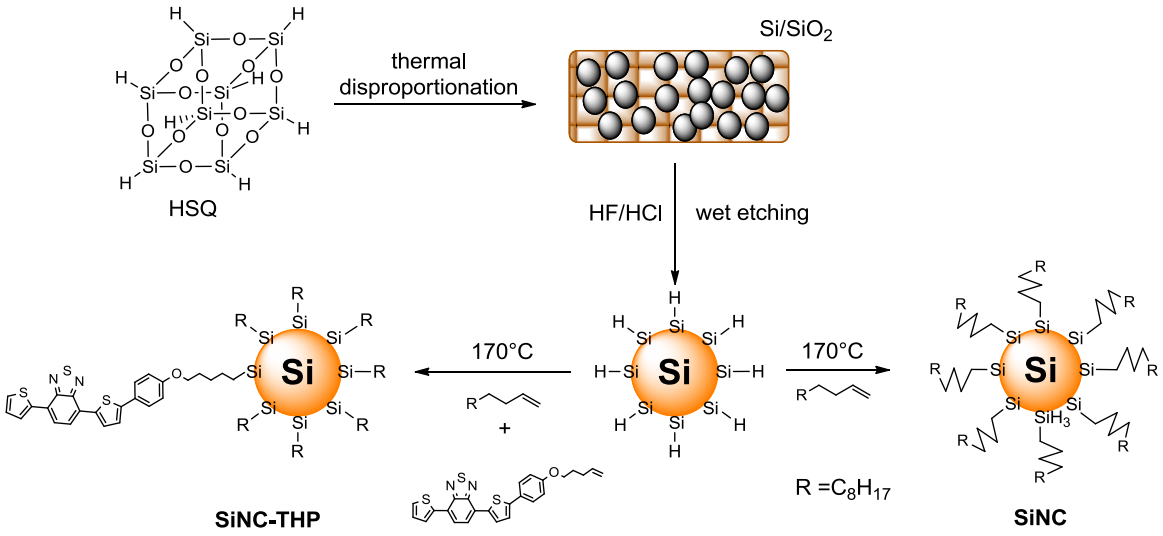

Figure 7.1

7.2.1 Experimental details

SiNC, SiNC-THP synthesis: the synthetic procedure follows the method developed by Hessel, et al.[87] Generally, 40 mL of Fox-16 (hydrogen silsesquioxane 16 wt%) is dried under vacuum and the resulting white solid is then transferred to a tube furnace and annealed at 1100°C (3.0 nm diameter) or 1200°C (5.0 nm diameter) at a heating rate of 18°C/min and held at that temperature for an hour under reducing atmosphere (93% N_2, 7% H_2).

The SiNC/SiO_2 composite is etched with 48% HF and 37.5% HCl (10:1 v/v) in the dark for 4-6 hours and then centrifuged at 8000 rpm for 5 min. The H-terminated SiNCs are then rinsed once with deionized (DI) water, twice with ethanol, and once with chloroform. The nanocrystals are dispersed in 4 mL of 1-dodecene to have **SiNC** and 4 mL of 1-dodecene with 70 mg of **THP** (1:120 thiadiazole:dodecene molar ratio) for **SiNC-THP**. The initially turbid dispersions are put through three freeze-pump-thaw cycles, and then heated to 170°C under N_2 flow for 12 hours. Over time, the dispersions become optically clear, indicating that passivation of Si nanocrystals has occurred.

Purification of SiNC

To purify the nanocrystals, the solutions are transferred to a glass centrifuge tube, spin at 8000 rpm for 5 min and discard the precipitate (poorly capped SiNCs) on the bottom. The supernatant is transferred to another glass centrifuge tube and undergoes many centrifugation/precipitation cycles using toluene/ethanol solvent/antisolvent pair. The final **SiNC** samples were dispersed in toluene at a concentration of 3-5 mg/mL until further characterization.

Purification of SiNC-THP

To purify the nanocrystals, the solutions are transferred to a glass centrifuge tube, spin at 8000 rpm for 5 min and discard the precipitate (poorly capped SiNCs) on the bottom. The supernatant is transferred to another glass centrifuge tube and undergoes many centrifugation/precipitation cycles using toluene/ethanol solvent/antisolvent pair. The final **SiNC-THP** samples were dispersed in toluene at a concentration of 3-5 mg/mL until further characterization (Figure 7.2).

[87] Hessel C. M., Henderson E. J., Veinot J. G. C., Chem. Mater. **2006**, 18, 6139-6146.

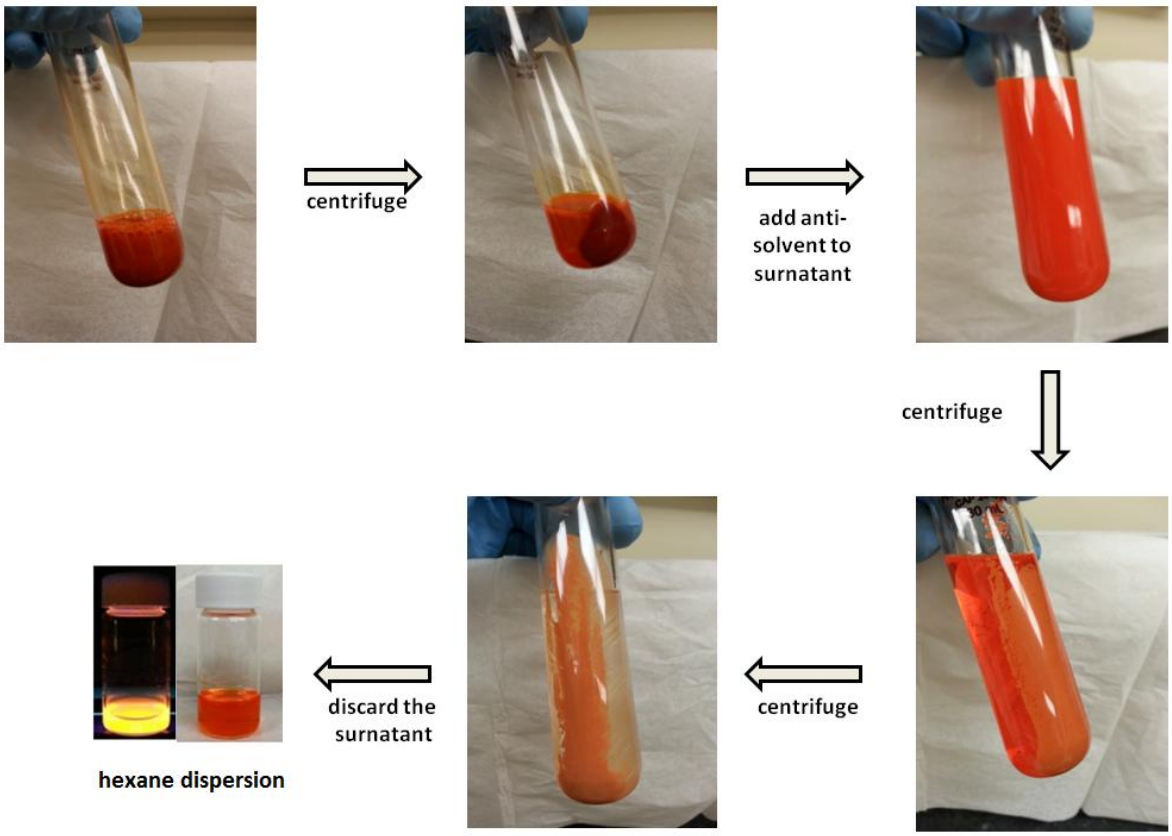
centrifuge
add anti-
solvent to
surnatant
centrifuge
centrifuge
discard the
surnatant
hexane dispersion

Figure 7.2

7.3 Results and Discussion

Photophysical measurements The optical properties of silicon nanocrystals (3.0 and 5.0 nm) functionalized with a combination of ligands **SiNC-THP** were compared to those of the sample control **SiNC** and free ligand **THP** (Table 7.1).

Table 7.1 Photophysical properties of **SiNC** and **SiNC-THP** dispersed in air-equilibrated hexane at 298 K. For comparison, the properties of the model compound **THP** are also reported.

	d/nm	λ_{ex}/nm	λ_{em}/nm	Φ_{em} [a]	τ/ns [b]	η_q	η_{sens}
SiNC	**3.0**	**425**	**647**	**0.086**	**73 x 10^3**	**-**	**-**
SiNC-THP	**3.0**	**378**	**615**	**0.094**	**1.2,7.3**	**88%**	**35%**
THP		**415**	**617**	**0.95**	**8.23**	**-**	**-**
SiNC	**5.0**	**515**	**922**	**0.45**	**140 x 10^3**	**-**	**-**
SiNC-THP	**5.0**	**515**	**649** **906**	**0.011** **0.07**	**0.35,7.5** **100 x 10^3**	**95%**	**80%**

[a]Experimantal error: 10%. [b]Experimental error: 5%.

The free thiadiazole **THP** is a excellent fluorophore with a good emission quantum yield (Φ_{em} = 0.95) as shown in Figure 7.3.

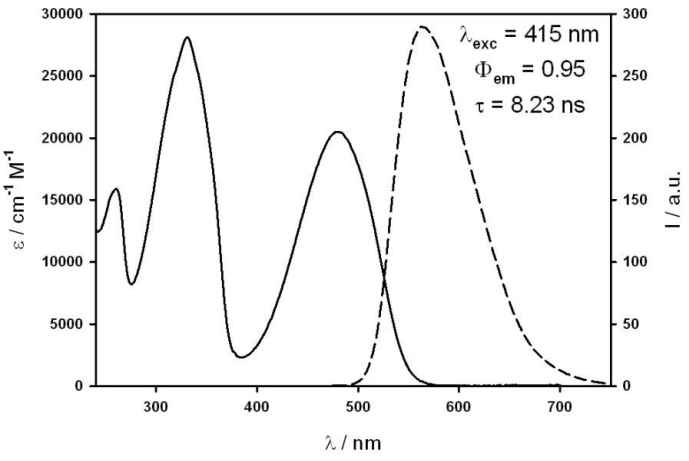

Figure 7.3 Absorption (black solid line), and emission spectra (dashed line, λ_{ex}=415 nm) of a solution of **THP** in hexane at RT.

(Figure 7.4 a) shows the comparison of optical properties between **SiNC** and **SiNC-THP** of 3.0 nm in hexane dispersion.

The sample control **SiNC** (without thiadiazole derivatization) exhibits an unstructured absorption profile that tails past 500 nm that is characteristic of SiNCs (black curve in Figure 7.4 a).

The contribution of thiadiazole is highlighted by the presence of shoulder in the **SiNC-THP** absorbance spectra (red curves in Figure 7.4 a).

As previously described in Chapters 4-6, we made mixing esperiments to evaluate energy transfer from chromophore to SiNCs. There is a quenching of **THP** emission of 88 % (Figure 7.4 b) with energy transfer to SiNCs in **SiNC-THP** sample of 35 % (Figure 7.4 c). The sensitization efficiency was evaluated: 35 % for **SiNC-THP**.

The number of thiadiazole units for each SiNC with d = 3.0 nm is ca. 2.

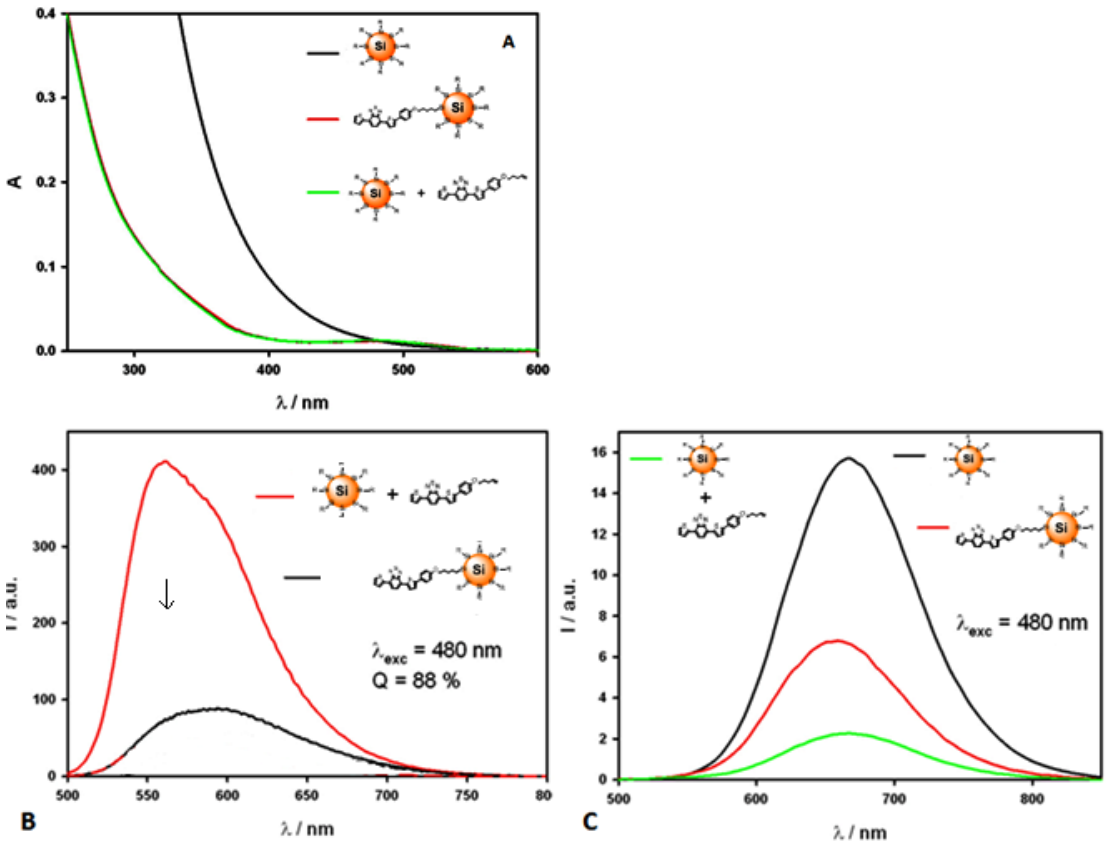

Figure 7.4 a) absorption spectra of **SiNC** (black line), **SiNC-THP** (red line), mixing solution SiNC + THP (green line); b) emission spectra of mixing solution SiNC + THP (red line) and **SiNC-THP** (black line) λ_{exc} = 480 nm; c) compare of emission spectra of **SiNC** (black line), **SiNC-THP** (red line), mixing solution SiNC + THP (green line)) λ_{exc} = 480 nm with delay =50µs.

To study the influence of the size and chemical surface to optical properties, SiNCs with diameter of 5 nm have also been synthesized.

UV–vis–NIR absorbance and photoluminescence (PL) spectra of hexane dispersions of the 5.0 nm diameter **SiNC** and **SiNC-THP** are shown in Figure 7.5 a.

In this case, the quenching of **THP** emission is 95 % with energy transfer to SiNCs in **SINC-THP** sample of 80 %. The sensitization emission is 80%.

The number of thiadiazole units for SiNCs of 5.0 nm is 19.

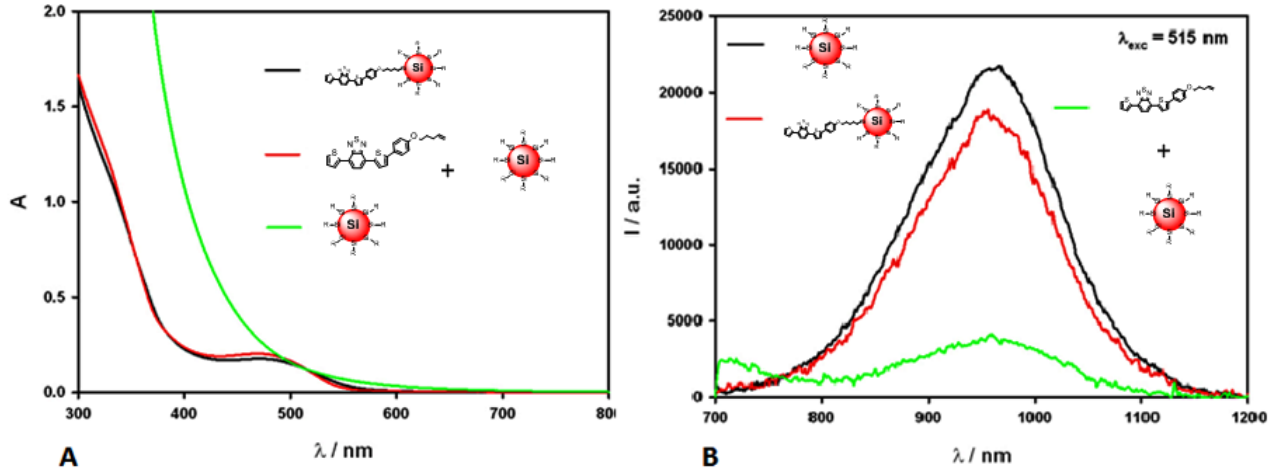

Figure 7.5 a) absorption spectra of **SiNC** (green line), **SiNC-THP** (black line), mixing solution SiNC + THP (red line) and b) emission spectra of **SiNC** (black line), **SiNC-THP** (red line), mixing solution SiNC + THP (green line) λ_{exc} = 515 nm.

Perspectives

This thesis has led to the development of a synthetic method that allows to synthesize silicon nanocrystals with different sizes, narrow size distribution and different chemical properties.

In addition, it has enabled us to achieve a good knowledge of the optical and electronic properties of semiconductor quantum dots.

The resulting SiNCs posses good optical properties and stability to air.

Nevertheless, it is necessary to improve this method in order to:

- increase the coverage of silicon nanocrystal surface;
- reduce the quantity of ligands used in thermal functionalization;
- find different conditions that enable to use hydrophobic and hydrophilic ligands;
- improve the comprehension of electronic processes.

Furthermore, future work will be dedicated to the post-functionalization of a suitable ligand attached to the SiNC surface.

The final purpose is to integrate the nanocrystals in multicomponent systems, to build hybrid materials for the conversion of solar energy into electrical energy.

List of Publications

A. Fermi, M. Baroncini, G. Bergamini, M. Marchini, M. Locritani, P. Ceroni
"A highly luminescent tetramer from a weakly emitting monomer: acid and redox-controlled multiple complexation by CB [7]"
Chem. Eur. J. 2014, 20, 7054-7060.

E. Marchi, M. Locritani, M. Baroncini, G. Bergamini, R. Sinisi, M. Monari, C. Botta, W. Mroz, M. Bandini*, P. Ceroni*, V. Balzani
"Blue and highly emitting [Ir(IV)] complexes by an efficient photoreaction of yellow luminescent [Ir(III)] complexes"
J. Mater. Chem. C, 2014, 2, (22), 4461 – 4467.

M. Locritani, Y. Yu, G. Bergamini, M. Baroncini, J. Molloy, B. A. Korgel*, P. Ceroni*
"Silicon Nanocrystals Functionalized with Pyrene Units: Efficient Light-Harvesting Antennae with Bright Near-Infrared Emission"
J. Phy. Chem. Lett., 2014, 5, 3325–3329.

American Chemical Society LiveSlides presentation to The Journal of Physical Chemistry Letters, title: "Silicon Nanocrystals Functionalized with Pyrene Units: Efficient Light Harvesting Antennae with Bright Near-Infrared Emission" 2014

R. Mazzaro, M. Locritani, J. K. Molloy, M. Montalti, Y. Yu, B. A. Korgel,* G. Bergamini, V. Morandi,* P. Ceroni*
"Photoinduced processes between pyrene-functionalized Silicon nanocrystals and carbon allotropes" Submitted